Kazakh national research technical university named after K.I. Satbayev

UDC 541.64+678.744

AYAZBAYEVA AIGERIM YERLANOVNA

Synthesis and characterization of polyampholyte nano- and microgels based on acrylamide derivatives

8D07108 - Basic processes for the synthesis and production of new organic and polymeric materials / D097

Dissertation for the degree of Doctor of Philosophy (PhD)

Scientific supervisors:
PhD, associate professor Nauryzova Saule Zinagiyevna

PhD Shakhvorostov Alexey Valeriyevich

Foreign scientific supervisor:
PhD, lecturer of the University of Helsinki (Finland)
Aseyev Vladimir Olegovich

Republic of Kazakhstan
Almaty, 2024

CONTENT

LIST OF ABBREVIATIONS AND SYMBOLS

The following designations and abbreviations are used in this thesis:

AA - Acrylic acid

AAm - Acrylamide

AMPS - 2-acrylamido-2-methyl-1-propanesulfonic acid sodium salt

APS - Ammonium persulfate

APTAC - 3-acrylamidopropyltrimethylammonium chloride

DLS - Dynamic light scattering

HLB - Hydrophilic–lipophilic balance

IEP - Isoelectric point

LCST - Lower critical solution temperature

MAA - Methacrylic acid

MB - Methylene blue

MBAA - N,N'-Methylenebis(acrylamide)

MO - Methyl orange

NIPAM - N-isopropylacrylamide

NG - Nanogel

NMR - Nuclear magnetic resonance

SDS - Sodium dodecyl sulphate

SEM - Scanning electron microscope

SMBS - Sodium metabisulfite

TEM - Transmission electron microscope

TGA - Thermogravimetric analysis

VI - 1-vinylimidazole

VPTT - Volume phase transition temperature

UCST - Upper critical solution temperature

INTRODUCTION

Assessment of the current state of the solved scientific problem and its relevance. Polyampholytes are unique macromolecules containing acid/base or anionic/cationic groups in their main or side chains. They can be used to model the behavior of proteins, polypeptides or polynucleotides. Polyampholyte nano- and microgels are three-dimensional macromolecular polymer networks that swell when exposed to a dispersing solvent.

Stimulus-responsive polyampholyte nano- and microgels, which respond adequately to external factors such as temperature, pH, salt composition, solvent, electric or magnetic fields and light radiation, represent tremendous potential for designing "smart" materials in medicine, biotechnology, nanotechnology, catalysis, the oil industry and environmental protection, among others.

Foundation and initial data for the development of the topic. Despite the progress made in synthesis and study of linear and crosslinked polyampholytes, information about polyampholyte nano- and microgels containing hydrophilic and hydrophobic groups in their composition—specifically, thermo- and salt-responsive nano- and microgels - is lacking. This is especially true in the context of controlled-release drug carriers and thickening agents for enhanced oil recovery, dependent on temperature and salt additives.

Justification for the need for research work. Analysis of literature data reveals that polyampholyte nano- and microgels are predominantly pH-sensitive. In contrast, highly charged polyampholyte nano- and microgels, which contain both hydrophilic and hydrophobic groups (thermo- and salt-responsive fragments), remain relatively understudied. This is especially true in the context of their applications in presented model system for controlled drug release and directly as thickening agent in the production of oil.

Information about the scientific and technical level of development, about patent research and conclusions from them. In the course of research work, the primary focus was done on cross-linked polyampholyte nano- and microgels composed of highly charged anionic/cationic and hydrophilic/hydrophobic monomers. The precise control over charge density, charge balance, distance between charges and charge distribution within the macromolecular chain can lead to a significant manifestation of the stimulus-response (or stimulus-responsive) properties of polyampholyte nanogels. It is expected that thermo- and salt-responsive amphoteric nanogels can form a reliable foundation in medicine for developing systems with controlled delivery of biologically active compounds and drugs to targeted organs. Polyampholyte microgels exhibiting temperature and salt sensitivity may also serve as suitable thickening agents in oil reservoirs with high temperatures and salinity.

The aim of the research work is to prepare and study thermo- and salt-responsive polyampholyte nanogels using a combination of hydrophobic monomer - N-isopropylacrylamide (NIPAM), anionic monomer - sodium salt of 2-acrylamido-2-methyl-1-propanesulfonic acid (AMPS), cationic monomer - (3-acrylamidopropyl) trimethylammonium chloride (APTAC) and polyampholyte

microgels from hydrophilic monomer - acrylamide (AAm), anionic monomer - sodium salt of 2-acrylamido-2-methylpropanesulfonate (AMPS), cationic monomer - 3-acrylamidopropyltrimethylammonium chloride (APTAC) for potential applications in the controlled delivery of drugs in the model system and directly as thickening agent for increasing oil production.

The tasks of the research work include:

- synthesis, characterization and properties of polyampholyte nanogels based on NIPAM-APTAC-AMPS obtained via free-radical polymerization;
- analysis of nanogels using NMR and FTIR spectroscopy, SEM, dynamic laser light scattering, zeta potential, TGA and DTA;
- study of thermal and salt sensitivity of nanogels, selection of suitable nanogels for immobilization of model drugs – anionic (methyl orange) and cationic (methylene blue) dyes; study of release kinetics of model drugs from the nanogel matrix in dependence of temperature and salt composition;
- synthesis, characterization and properties of polyampholyte microgels based on AAm-APTAC-AMPS obtained via inverse emulsion polymerization;
- analysis of microgels by FTIR spectroscopy, TEM, dynamic laser light scattering, TGA and DTA;
- use of thermo- and salt-responsive polyampholyte microgels in core flooding experiments as a physical reservoir model to assess the oil-displacing (oil-producing) capacity in reservoir conditions, with a solution salinity of up to 200 g/L.

The objects of study are samples of polyampholyte nanogels based on NIPAM-APTAC-AMPS and polyampholyte microgels AAm-APTAC-AMPS of various compositions.

The subject of the study is synthesis and characterization of polyampholyte nano- and microgels derived from a combination of anionic, cationic, hydrophilic and hydrophobic acrylamide-based monomers to understand and assess their thermal and salt-responsive properties.

The scientific novelty of the results obtained lies in the production of polyampholyte nanogels of various compositions based on NIPAM-APTAC-AMPS, which demonstrate temperature and salt responsivity; polyampholyte microgels of various compositions based on AAm-APTAC-AMPS, which exhibit thermal and salt sensitivity in oil reservoirs. The study of the structure, macromolecular organization, swelling and collapse of nano- and microgels, constructed from highly charged polyampholytes, is contingent on factors such as copolymer composition, microstructure, temperature, ionic strength of the solution and a combination of aqueous-organic solvents. This research enables the development of a novel class of cross-linked structures characterized by stimulus-responsive behavior, self-healing properties, robust adhesion, mechanical flexibility and strength. Long-range Coulomb forces between opposite charges along the polymer chain are the determining factors for conformational and volume-phase changes in highly charged polyampholyte gels.

The scientific, practical and theoretical significance of the study lies in the expansion of our fundamental knowledge about cross-linked polyampholyte nano-

and microgels, consisting of non-ionic and highly charged anionic/cationic and hydrophilic/hydrophobic monomers. The fundamental results obtained can be used in medicine, in particular, for the temperature-controlled release of drugs, and in oil production to increase oil recovery. The results of research can be recommended to domestic and foreign companies engaged in medicine, pharmacy and oil production. On a National scale, the results of research work is of interest in terms of maintaining Kazakhstan's leading position in the world in the field of synthesis and research of synthetic polyampholytes, raising the prestige of Kazakhstan science at the world level, developing public-private partnerships and attracting young scientists and specialists to science. On an international scale, the results of research are of interest to scientists and specialists involved in the theory of polyampholytes, the study of polyampholyte solutions and the development of thermo- and salt-responsive amphoteric nano- and microgels.

The validity and reliability of the results the obtained data were confirmed using selective, accurate and modern analytical methods. To ensure reliability and reproducibility, all experiments were repeated and studied with several methods in parallel to each other.

Relation of the Thesis with research and government programs

The work was conducted in the frame of projects "Synthesis and Study of Thermo- and Salt-Sensitive Polyampholyte Nano- and Microgels" for the period 2020-2022 (AP08855552) and "Development of New Thermal and Salt-Resistant Amphoteric Terpolymers for Enhanced Oil Recovery" for the period 2021-2023 (AP09260574) funded by the Ministry of Science and Higher Education of the Republic of Kazakhstan. It was partly funded by the Horizon 2020 research and innovation program of the European Union Maria Sklodowska-Curie (grant agreement 823883-MSCA-RISE-2018 NanoPol). **The main provisions for defense:**

- results on the development of optimal synthesis conditions for obtaining linear polyelectrolytes and polyampholytes, samples of polyampholyte nano- and microgels with the required physical-chemical, physical-mechanical, rheological, thermal and salt-responsive properties;
- results on the identification and study of polyelectrolyte and polyampholyte nano- and microgels by NMR and FTIR spectroscopy, SEM, TEM, dynamic laser light scattering, zeta potential, TGA and DTA;
- results on the immobilization of model drugs – anionic and cationic dyes (methyl orange and methylene blue) into the matrix of amphoteric nanogels and the determination of the kinetics of the release of model drugs from the matrix of nanogels depending on temperature and salt composition;
- results on the study of the thermal and salt-responsive properties of polyampholyte nano- and microgels, which can be recommended as thickening agents for leveling the injectivity profile of oil reservoirs and increasing oil production;
- results on the use of microgels in core flooding experiments to assess the oil-displacing (oil-producing) capacity in reservoir conditions.

Approbation of work. The dissertation materials were reported and discussed at international scientific-practical conference "Modern aspects of chemical science and chemical education: Theory and Practice" (December 13-14, 2021, Almaty, Kazakhstan), the sixteenth St. Petersburg conference of young scientists with international participation "Modern problems of polymer science" (October 24-27, 2022, St. Petersburg, Russia), XI International Conference on “Times of Polymers (TOP) & Composites” (June 11-15, 2023, Ischia, Naples, Italy).

Publications. The main results of the study are presented in 3 articles published in journals from the list approved by the Committee for Control in the Sphere of Education and Science of the Republic of Kazakhstan, 2 innovative patents of the Republic of Kazakhstan. 2 articles were included in the Scopus and Web of Science database. 3 abstracts of reports were published in proceedings of international conferences.

The volume and structure of the dissertation. The dissertation work is presented on 109 pages of a computer text and consists of an introduction, 3 sections, a conclusion, and a list of used literature from 146 titles, contains 70 drawings, 27 tables.

1 Literature review

1.1 Polyampholyte nano- and microgels

Polyampholytes belong to macromolecules that composed of acid/base or anionic/cationic monomers within their main or side chains. Traditionally, polyampholytes are categorized into three classes: “annealed” (which exhibit pH-dependent behavior), “quenched” (demonstrating pH-independent or highly charged characteristics) and “betainic” (containing betaine or zwitterionic structures) [1-3]. “Annealed” polyampholytes consist of acid-base monomers that are ionized in dependence on pH of the surrounding medium. “Quenched” polyampholytes, composed of highly charged anionic and cationic monomers, maintain their charges irrespective of the pH conditions. “Betainic” (betaine or zwitterionic) polyampholytes are macromolecules, in which each monomer unit contains an equal number of acid-base or anionic/cationic groups [4]. Moreover, zwitterionic polymers also encompass macromolecules that emerge through the pairing of anionic-cationic monomer units without the need for counterions [5, 6].

Linear and cross-linked highly charged polyampholytes exhibit traits such as salt resistance [7], thermal sensitivity, deformation stability [8], self-healing [9, 10], anti-fouling properties [11], self-assembling ability [12] and stimulus sensitivity [13]. These characteristics enable their versatile application in diverse areas such as oil production and transportation [14, 15], as structural biomaterials, carriers and controlled drug delivery [16], energy storage devices, supercapacitors, energy converters, chemomechanical systems [17, 18], etc.

Polyampholyte gels are three-dimensional macromolecular polymer networks that undergo swelling when exposed to a dispersing solvent. Nanogels are cross-linked macromolecular structures with an equivalent diameter ranging from 1 to 100 nm. On the other hand, “microgels” are gel particles with sizes approximately ranging from 0.1 to 100 microns [19-21].

Nano- and microgels encompass the distinctive traits of macromolecules, colloids and surfactants [22]. Similar to macromolecules, they possess soft attributes and rapidly adapt to alterations in solvent quality by adjusting their conformational properties [23, 24]. Like colloids, they have the potential to crystallize at high volume content [25, 26] and akin to surfactants, they adsorb onto diverse surfaces, thereby reducing interfacial tension [27].

Comprehending the structure, macromolecular arrangement, swelling and collapse of nano- and microgels crafted from highly charged polyampholytes hinges on factors such as copolymer composition, microstructure, temperature, ionic strength of the solution and the blend of water and organic solvents. Such understanding paves the way for the development of a novel category of cross-linked structures that exhibit stimulus-responsive characteristics, self-healing capabilities, robust adhesion, mechanical flexibility and strength.

The primary factors influencing conformational and volume-phase alterations in highly charged polyampholyte gels are the long-range Coulomb forces between opposing charges along the polymer chain. For example, highly charged

polyampholytes synthesized at relatively high monomer concentrations introduce a fresh class of gels crosslinked through both potent covalent and delicate ionic bonds. The former contribute to the creation of a rigid mesh structure, preserving the gel's shape, while the latter facilitate stretching, deformation, adhesion, self-healing, memory retention and other vital functionalities.

The distinctive properties of functional nano- and microgels are primarily linked to their permeable and cross-linked architecture, as well as their capacity to swell in diverse solvents and exhibit deformability [28]. Polyampholyte nano- and microgels hold significant interest owing to their remarkable responsiveness to diverse external stimuli, including temperature, pH, ionic strength, solvents, electric or magnetic fields, light radiation, and more. Consequently, they possess considerable potential for designing "smart" materials across domains such as medicine, biotechnology, nanotechnology, catalysis, the oil industry and environmental protection [29-32].

Alterations in external factors frequently result in variations in the size, structure, and interaction characteristics of nano- and microgels. Changes in the gel's volume arise from the interplay between attractive and repulsive forces, the polymer's elastic properties, osmotic pressure, and additional forces like hydrogen bonds, hydrophilic/hydrophobic interactions, and van der Waals forces [33].

1.2 Methods for the synthesis of polyampholyte nano- and microgels

Numerous distinct methods for synthesizing polyampholyte nano- and microgels with controlled properties are documented in the literature. These methods include free-radical polymerization of charged monomers, polymerization in microemulsions, polymerization of anionic-cationic pairs of monomers without counterions, precipitation polymerization, radiation polymerization, polymerization of zwitterionic monomers and polymerization using reversible addition-fragmentation chain transfer (RAFT), a technique that has seen significant development in recent years.

Free radical polymerization is a relatively straightforward method to implement, characterized by its extensive compatibility with diverse functional groups. As a result, it remains a favored choice for numerous laboratory syntheses. Conventional free-radical polymerization continues to find extensive application in the production of nano- and microgels. One drawback of this method is its challenge in precisely controlling the molecular weight, distribution of molecular weights and chain-end structures of the polymer. This limitation prevents its use in obtaining more intricate structural variations [34].

The research presents a description of the preparation of nanogels based on NIPAM and methacrylic acid (MAA) using micellar free radical polymerization [35]. By employing various ratios of NIPAM/MAA, along with a cross-linking agent and a surfactant (sodium dodecyl sulfate, SDS), polyelectrolyte nanogels were successfully synthesized. These nanogels exhibited average sizes that ranged widely, approximately from d~90-650 nm. The study revealed that the ionizable MAA

groups contribute significantly to the pH and electrolyte sensitivity of the nanoparticles. Above the pKa value, electrostatic repulsion between negatively charged COO^- groups emerges as the key factor that prevents particle collapse at temperatures surpassing the phase transition temperature. The nanoparticles demonstrated a distinct bulk phase transition, which could be triggered by denying the negative charges through pH reduction or the introduction of a cationic surfactant. Conversely, below the pKa value, the presence of MAA groups heightened the hydrophobic nature of the particles, as evidenced by a lower phase transition temperature and a more pronounced bulk phase transition.

Presently, free-radical precipitation polymerization remains a pivotal technique for synthesizing thermoresponsive nano- and microgels, distinguished by their versatility, flexibility and scalability [36]. This method enables polymerization in aqueous solutions at relatively low temperatures (60-80°C) and is applicable to a diverse array of monomers - typically acrylamide (such as N-isopropylacrylamide, NIPAM) or N-vinylcaprolactam (N-vinylactam). Furthermore, the introduction of functional groups is achievable by incorporating comonomers, such as acrylic acid (AA), 2-(dimethylamino)ethyl methacrylate (DMAEMA) and acetoacetoxy ethyl methacrylate (AAEM) [37, 38]. The strength of this method encompass its compatibility with a broad spectrum of monomers and its potential to introduce functional groups either through comonomers or post modification.

The synthesis of nano- and microgels through precipitation polymerization demands a meticulous selection of "building blocks" including monomers, cross-linking agents and initiators. The authors [39] detailed the synthesis of copolymer microgels via precipitation polymerization using NIPAM, methacrylic acid (MA) and fumaric acid (FA). The resulting microgels, namely PNIPAM (control sample), poly(NIPAM-co-MA) (with carboxyl groups localized in the core), and poly(NIPAM-co-FA) (with carboxyl groups localized in the crown), were employed as seeds for the polymerization of styrene. The study reveals that the distribution of carboxyl groups within the microgel structure governs the sites of styrene polymerization, thereby influencing the morphology of the composite microgels.

The most prevalent thermoresponsive monomer is N-isopropylacrylamide (NIPAM), which yields poly-N-isopropylacrylamide (PNIPAM). PNIPAM undergoes a coil-to-globule transition in an aqueous environment at 32°C, known as its lower critical solution temperature (LCST). Upon crosslinking these chains into a polymer network, this sensitivity manifests as volumetric collapse due to solvent displacement, primarily water. This temperature-driven transition is referred to as the volume phase transition temperature (VPTT), typically in proximity to the LCST of the corresponding linear polymer [40, 41].

At its cloud point, PNIPAM undergoes a distinctive volume phase transition. This transition involves a shift from a hydrated state, known as the expanded hydrophilic state, to a wrinkled and dehydrated state, referred to as the collapsed structure (Figure 1) [42, 43]. The PNIPAM homopolymer's reversible sol-gel behavior in aqueous solutions can be attributed to the existence of both hydrophilic and hydrophobic groups within the neutral polymer. The switch between hydrophilic

and hydrophobic states is reversible and occurs with changes in temperature, either below or above the lower critical transition temperature (LCST) value of 32°C [44]. Above the LCST, the gel becomes insoluble in the aqueous medium. The LCST is contingent on the critical gel concentration (CGC). When the solvated PNIPAM molecules reach the CGC, they exhibit insolubility in water upon being heated beyond the LCST. The LCST primarily hinges on the hydrogen bonds formed between water molecules and the functional monomeric units' structure within the PNIPAM polymer. Notably, these bonds involve N–H and C=O interactions [45, 46]. Consequently, the incorporation of hydrophilic units typically leads to an elevation of the VPTT, whereas the inclusion of hydrophobic units produces the opposite effect.

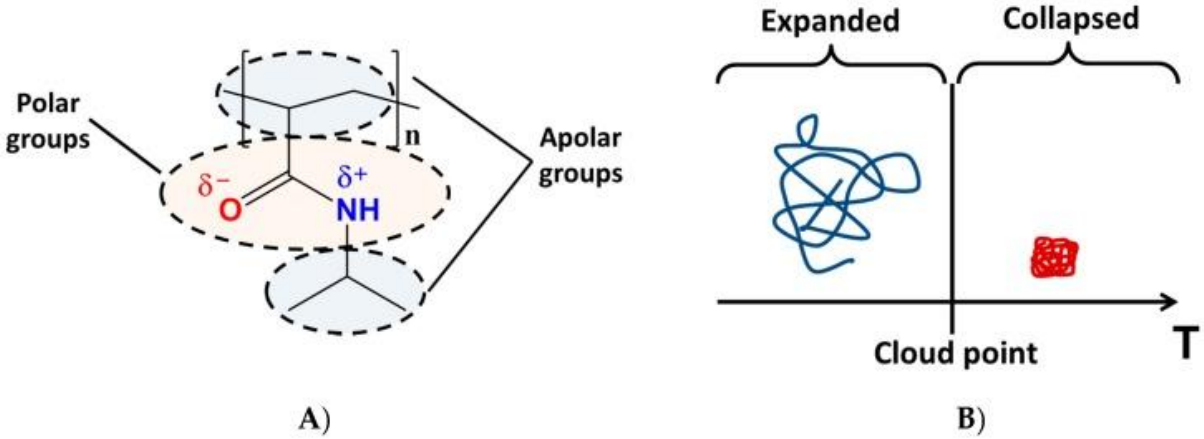

Figure 1 - Chemical formula of PNIPAM (A) and representation of volume phase transition between coil (left) and globular (right) hydrogel conformations (B)

Nanogel synthesis based on NIPAM can be achieved through radical precipitation polymerization [47]. For instance, Truzzolillo et al. successfully produced PNIPAM nanogels with sizes ranging from 240 to 330 nm using N,N-methylenebisacrylamide (MBAA) as a crosslinking agent [48]. In the absence of ionizable groups, the lower critical dissolution temperature (LCST) for NIPAM-based linear homopolymers remains at 32.5–33.0°C [41]. However, when polymerization takes place in the presence of monomers capable of ionization under various conditions or possessing a zwitterionic nature, the resulting nanogels acquire a polyelectrolyte character [49].

Fernandez-Lopez et al. carried out the development of NIPAM-based microgels containing 2% cationic groups through precipitation polymerization, using cetyltrimethylammonium bromide (CTAB) as a cationic surfactant. The study illustrates that alterations in the hydrodynamic radius of the microgels are influenced by both temperature and salt concentration. The anticipated impact arising from the presence of ionogenic groups becomes evident through a shift in the volume phase transition towards higher temperatures, ranging from 33 to 44°C, and conversely, with an increase in the solution's ionic strength. In this scenario, the phase transition temperature shifts towards lower temperatures due to the manifestation of the “salting out” effect [50].

Ahiabu et al. conducted the synthesis of pH and temperature-sensitive microgels, employing NIPAM and various acrylic acid homologues (acrylic acid, methacrylic acid, 2-ethylacrylic acid, 2-butylacrylic acid). These microgels were created through free-radical precipitation polymerization, using MBAA as a crosslinking agent [51]. The resultant microgels underwent characterization using optical microscopy and their responsiveness to changes in temperature and pH was assessed through dynamic light scattering. The research revealed intriguing kinetics behavior among the microgels. Notably, microgels modified with 2-butyl acrylic acid displayed an exceptionally swift response to temperature changes, whereas those modified with acrylic acid exhibited the slowest phase transition kinetics in response to temperature alterations. This observed effect can be attributed to the varying degrees of hydrophobicity of the acid groups. Specifically, heightened hydrophobicity results in a more rapid reaction to fluctuations in the medium's temperature.

Precipitation polymerization stands as a potent technique for creating microgels with potential applications in drug delivery and release. Özbaş et al. successfully synthesized copolymer microgels known as poly(acrylamide-co-N-vinylpyrrolidone-co-2-(diethylamino)ethyl methacrylate) (poly(AAm-co-NVP-co-DEAEMA)). These microgels were used for loading 5-fluorouracil (5-FU) as a model drug. The investigation revealed that the release of 5-FU from the poly(AAm-co-NVP-co-DEAEMA) microgel was notably faster at pH 7.4 compared to pH 5.5 and pH 2.1. This difference was attributed to the increased solubility of 5-FU with higher pH levels [52].

A team of Kazakh researchers, in collaboration with international colleagues, have detailed the synthesis of polyelectrolyte microgels based on NIPAM, coupled with monomers such as AA, 3-acrylamidophenylboronic acid (3-APB), (3-acrylamidopropyl)trimethylammonium bromide (ATMA) and 1-vinylimidazole (VI). These microgels were created alongside a cross-linking agent, N,N-methylenebisacrylamide [53]. Microgels built on 1-vinylimidazole were produced via emulsion polymerization in the presence of cetyltrimethylammonium bromide (CTAB), while the remaining polyelectrolyte microgels were synthesized using precipitation polymerization without surfactants. The resultant microgel particles showcased multi-stimulus-responsive behavior. Microgels composed of NIPAM, 3-APB and CTAB exhibited responsiveness to changes in glucose concentration within the solution. In contrast, NIPAM and VI-based microgels were sensitive to specific metals, particularly copper ions. Microgels containing acrylic acid displayed characteristic thermoresponsive behavior. At low pH levels, the particles underwent collapse, while at high pH values, they exhibited swelling. Microgels with varying VI concentrations demonstrated sensitivity to both temperature and pH alterations. Upon temperature increase, a behavior analogous to microgels containing acrylic acid was observed. The microgel particles underwent continuous compression, causing the LCST to shift towards higher temperatures within the range of 35–45°C.

Despite the numerous opportunities offered by precipitation polymerization for the synthesis of nano- and microgels, certain primary challenges persist [39].

Achieving precise control over the size distribution of nano- and microgels becomes intricate, particularly when employing charged monomers. The distinct reactivity and solubility of these monomers pose difficulties in altering the chemical structure within nano- and microgels. The varying reactivity of monomers and crosslinkers, coupled with the limited array of analytical techniques available for monitoring polymer networks, serves to restrict the capacity for fine-tuning the internal structure and morphology of nano- and microgels [54].

Post modification of microgels provides an avenue for incorporating supplementary chemical functionalities that might not be feasible within the precipitation polymerization process. As an illustration, poly(NIPAM-co-AA) microgels, synthesized with varying AA content, were post-modified using 4'-amino-benzo-12-crown-4-acrylamide ($B_{12}C_4$). This modification led to the creation of microgels capable of serving as molecular recognition receptors, capable of forming host-guest complexes with cyclodextrins (γ-CD). These microgels exhibit a dual role as phase transition activators and adsorbents. They demonstrate an isothermal volume alteration induced by γ-CD, owing to the formation of the γ-CD/$B_{12}C_4$ complex [55].

In recent times, numerous researchers have achieved successful synthesis of nano- and microgels using reversible addition-fragmentation chain transfer (RAFT) polymerization. This method, RAFT polymerization, offers a versatile and controlled approach for polymerization within aqueous solutions, employing a wide spectrum of monomers and readily available initiators. Control over molecular weight and molecular weight distribution in RAFT polymerization stems from the concurrent presence of a relatively small number of growing chains, each with end-of-chain activity. This process operates degeneratively, generating propagating radical chain ends that interact with other molecules [56].

Through RAFT polymerization, the synthesis of reactive cationic poly([2-(acryloyloxy)ethyl]trimethylammonium chloride) (PAETAC) polymers has been achieved. These polymers are subsequently used as emulsion polymerization stabilizers, enabling the production of microgels based on poly(N-vinylcaprolactam) (PVCL) [57].

The authors of the study [58] employed RAFT polymerization to synthesize thermoresponsive nanogels based on poly[poly(ethylene glycol) methyl ether acrylate] and poly-N-isopropylacrylamide (PPEGA-b-PNIPAM), which exhibit a LCST.

Significant attention has been directed towards the synthesis of microgels featuring intricate architecture and morphology, including core/shell [59] or multishell colloids [60]. Within this landscape, thermoresponsive microgels boasting a core/shell configuration are particularly captivating for interactive coatings design. In the authors' study [59], microgels were synthesized, characterized by a core encased in a shell composed of two distinct polymers, each possessing distinct LCST. Notably, the shell exhibited a lower LCST and experienced quicker contraction than the core as temperature increased. Conversely,

during temperature reduction, the core displayed a propensity for swifter expansion, counterbalanced by the restraint exerted by the shell.

The synthesis of covalently bonded nano- and microgels is typically achieved through polymerization within a solution medium. A critical element of this process is conducting the polymerization within a confined space, such as droplets or micelles. The dimensions of these spaces are determined by the desired final product size. Dispersion of organic droplets containing reactive monomers/polymers in an aqueous solution is often referred to as direct emulsion polymerization, categorized as oil-in-water (O/W) emulsion. Conversely, the dispersion of aqueous droplets within an organic medium is termed inverse emulsifying polymerization, classified as water-in-oil (W/O) emulsion. Micelle formation arises from the surfactant's positioning at the oil/water interface [61]. Surfactants play a pivotal role in enhancing the creation and stability of nanodroplets by influencing their size. Through surfactant modulation, nanodroplets can be tailored to form nanogels with diameters below 150 nm [62, 63]. The resultant nanoemulsion boasts an expansive surface area, facilitating the swift and efficient penetration of active components into the dispersed phase. Moreover, the concentration of surfactants can exert an impact on the polymerization reaction. When the surfactant concentration surpasses the critical micellar concentration (CMC), surfactants tend to localize at the oil/water interface, leading to micelle formation that encapsulates monomers. During oil-in-water emulsion polymerization, chemical initiators decompose to generate radicals. Typically, these radicals form outside the micelles and then react with the monomers. These reacted monomers transition into monomeric radicals and infiltrate the emulsion via diffusion. The diffusing monomeric radicals then engage with unreacted monomers, facilitating chain growth [64].

During the emulsion polymerization process for nano- and microgel synthesis, a notable monomer conversion is achieved [65, 66]. Nonetheless, this method does come with drawbacks linked to the substantial surfactant demand and challenges in fully purifying the resultant nano- and microgels. The elimination of surfactants can necessitate supplementary purification steps for the solution, potentially raising the process's cost or introducing unintended impurities into the final product [67].

The synthesis of microgels through inverse emulsion polymerization can be influenced by a variety of factors, including emulsifier and initiator concentrations, stirring speed, surfactant type, and temperature. Characteristics such as particle size distribution, equilibrium swelling and thermal properties of microgels, particularly those based on AAm and 2-acrylamido-2-methylpropanesulfonic acid (AMPS), are contingent upon the concentration of the cross-linking agent, initiator type and temperature [68]. An elevation in the crosslinking agent concentration triggers a reduction in microgel particle size, coupled with a narrower size distribution, decreased swelling capacity, and an increase in the glass transition temperature. Additionally, the hydrophobicity of the initiator also plays a role in influencing particle size, swelling capacity and particle size distribution.

Temperature exerts an impact on the particle size of microgels that are constructed from both hydrophilic monomers (acrylamide and acrylic acid) and

hydrophobic monomers (styrene and methylmethacrylate). This influence is observed within the context of semi-batch emulsion polymerization, employing three distinct surfactants: SDS, Triton-X, and SPAN80. The outcome yields microgel particles characterized by small size, a monodisperse distribution with a narrow spread and a spherical morphology [69].

Shen et al. [70] delved into the hydrodynamic diameters, morphology and swelling degree of a range of pH-sensitive microgels synthesized via inverse microemulsion polymerization, using AAm and AA as base materials. A noteworthy observation is that microgels exhibit elevated swelling coefficients, as well as lower glass transition and thermal decomposition temperatures, as the AA content within the copolymer composition is increased. These properties underscore the pH-sensitive nature of the AAm-co-AA microgels, a characteristic intrinsically linked to the dissociation constant of acrylic acid.

The viscoelastic properties and swelling behavior of thermoresponsive microgels, derived from AAm and AA, are contingent upon the concentration of the crosslinking agent MBAA and acrylic acid. These microgels, synthesized through inverse emulsion polymerization, exhibit a spherical morphology and manifest characteristics akin to colloidal gels in the investigation of rheological properties [71, 72].

In the majority of cases, inverse emulsion polymerization for microgel synthesis involves the utilization of multifunctional vinyl monomers, such as N,N'-methylenebis(acrylamide), as crosslinking agents. Nevertheless, the authors' study [73] diverged from this norm by exploring the effects of cross-linking agents rooted in diglycidyl monomers - specifically, polyethylene glycol diglycidyl ether (PEGDGE) and ethylene glycol diglycidyl ether (EGDGE). The microgels produced from sodium acrylate and 2-acrylamido-2-methylpropane sulfonic acid (AMPS), crosslinked with PEGDGE and EGDGE, exhibited enhanced thickening properties compared to those crosslinked with MBAA.

Landfester et al. [74] undertook the synthesis of polydimethylsiloxane (PDMS) nanogels using polymerization within miniemulsions, resulting in particle sizes ranging from 40 to 1100 nm. They also investigated the impact of surfactant incorporation on the ultimate size and morphology of poly-(N-isopropylacrylamide) nanogels through emulsion polymerization conducted above the lower critical solution temperature (LCST) [75].

Brown et al. developed the synthesis of stimulus-responsive polyelectrolytes and polyampholytes based on NIPAM through classical emulsion polymerization [76]. The monomers employed included NIPAM, sodium 2-acrylamido-2-methylpropanesulfonate (NaAMPS), 2-acrylamido-2-propanetrimethylammonium chloride (APTAC), sodium 3-acrylamido-3-methylbutanoate (NaAMB) and 2-acrylamido-2-methylpropanetrimethylammonium chloride (AMPTAC). Using this approach, they successfully obtained stable amphoteric nanogels with a size of approximately 70 nm. The authors highlight that by employing varying combinations of surfactants during the polymerization process, it's feasible to regulate the hydrophobic-lipophilic balance (HLB), a factor crucially impacting the

stability of the inverted emulsion throughout synthesis. Consequently, the fusion of microemulsion polymerization with a well-selected array of monomers possessing polymerizable groups of similar reactivity leads to the creation of homogeneous composition copolymers. These copolymers, characterized by well-defined structures, serve as excellent candidates for studies in the field of physics.

Unlike the synthesis of polyampholyte nano- and microgels, which involves the incorporation of both positively charged and negatively charged monomers, leading to challenges in pH control during the synthesis process, the situation is notably different for zwitterionic microgels [77]. With zwitterions, the presence of equal amounts of positive and negative charges within a single molecule renders them electrically neutral. Consequently, the stages of synthesis involving polywitterions are not pH-dependent, simplifying the pH control aspect.

Zwitterionic nanogels were described in the work [78]. The researchers were able to synthesize monodisperse microgel particles based on NIPAM, acrylic acid and dimethylaminopropyl methacrylamide (methylenebisarylamide crosslinker) that undergo a reversible volume change in response to changes in pH and temperature. Aqueous dispersions of zwitterionic microgels demonstrate the minimum value of the hydrodynamic diameter at the isoelectric point. In addition, the study describes the controlled uptake and release of ionic and non-ionic surfactants from these microgel particles.

1.3 Application of stimuli-responsive nano- and microgels for controlled drug delivery

“Smart” polymer systems have captured the interest of researchers for their potential in drug delivery to specific organs. The adaptable porosity, composition, colloidal stability and elasticity of nano- and microgels offer notable benefits in enhancing the delivery of diverse drugs [79]. Achieving controlled release of the active substance from the polymer matrix can be attained through the manipulation of external factors, including temperature, pH, ionic strength of the solution, redox potential and more [80].

Nanogels offer several advantages over other drug delivery systems, making them a superior choice for various applications:

- control over particle size and surface properties: nanogels allow precise control over particle size and surface properties. This control helps prevent rapid clearance by phagocytic cells, enabling both passive and active drug release strategies;
- targeted and sustained drug release: nanogels facilitate controlled and sustained drug release at the intended target site. This characteristic enhances therapeutic effectiveness while minimizing side effects;
- enhanced drug loading capacity: nanogels exhibit relatively high drug loading capacities without the need for chemical reactions. This aspect is crucial in maintaining the potency of the loaded drug;

- effective penetration: the small size of nanogels enables them to reach even the smallest capillary vessels. They possess the ability to penetrate tissues through both paracellular and transcellular pathways, ensuring efficient drug delivery [81];
- biocompatibility and biodegradability: nanogels boast high levels of biocompatibility and biodegradability, reducing concerns related to their impact on living systems.

Overall, nanogels represent a promising drug delivery system due to their ability to address multiple challenges associated with drug administration, leading to improved therapeutic outcomes.

The scheme of the release of the drug from the nanogel is shown in Figure 2 [82].

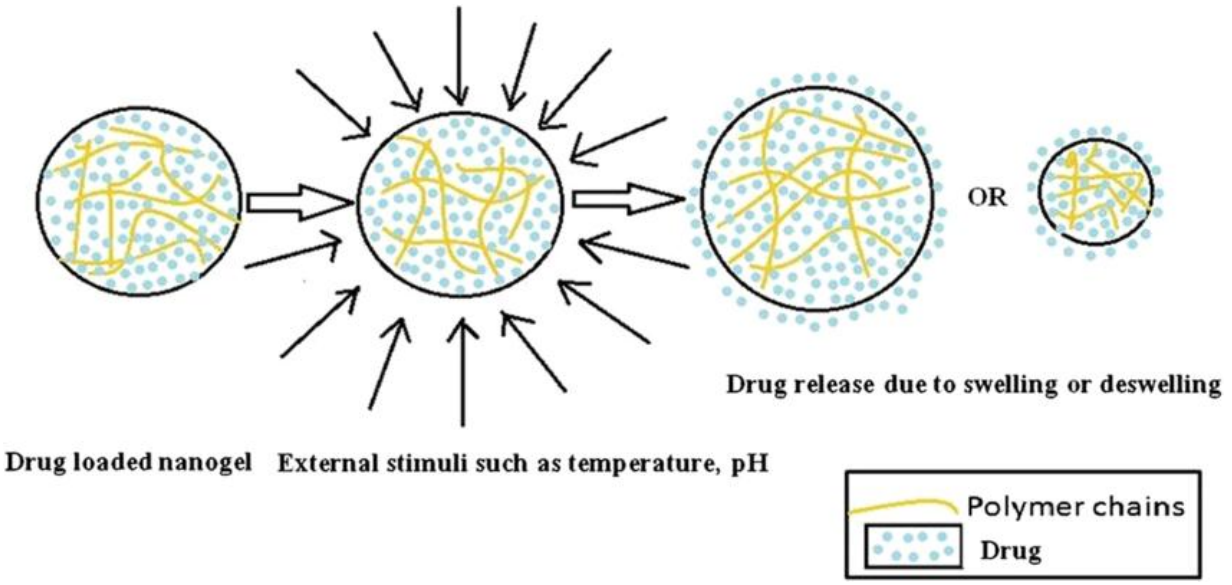

Figure 2 - Drug release from the nanogel

The utility of nanogels as drug carriers relies on the presence of specific functional groups within their structure. These functional groups exert a significant influence on drug transport and release dynamics. Moreover, certain functional groups can be conjugated with drugs or antibodies to facilitate targeted drug delivery. With a typical size range of 20–200 nm, nanogels possess the ability to impede rapid renal clearance, contributing to their effectiveness as drug carriers [83].

Various temperature-responsive nanostructures hold the potential to release drugs within the elevated temperature conditions of affected tissues, yielding enhanced therapeutic outcomes. This attribute is particularly advantageous when paired with external hyperthermia techniques, especially in addressing conditions like cancerous tumors. Thermoresponsive materials exhibit a structural transformation in response to temperature changes, facilitating a controlled release of encapsulated pharmaceutical agents. During hyperthermia treatment, an elevated temperature range of approximately 40–45°C induces several physiological effects, including heightened blood flow, increased vascular permeability, reduced DNA and protein synthesis, modified functional expression of molecular markers, and altered

growth factor binding affinity. Compositions based on poly(N-isopropylacrylamide) (PNIPAM), known for their lower critical solution temperature (LCST) behavior, stand out as promising and widely used examples within the realm of thermoresponsive systems. This characteristic makes them a prime candidate for advanced drug delivery strategies [84-86].

PNIPAM has garnered substantial attention in research due to its water solubility and its lower critical solution temperature (LCST) that closely aligns with human body temperature (around 36.5–37.5°C) [87]. PNIPAM finds extensive application in various biomedical fields, with drug delivery and tissue engineering being the most extensively studied areas. These applications are followed by its using in stem cell research, microfluidic devices, biosensors, and bioimaging. The unique thermoresponsive properties of PNIPAM make it a versatile and promising material for advancing innovations in medical and biological contexts.

Hollow thermoresponsive nanoparticles based on PNIPAM are achieved by decomposing the crosslinked core formed by N,N-bis(acryloyl)cystamine (BAC), while the shell consists of non-degradable NIPAM [88]. The inclusion of the negatively charged monomer 2-acrylamido-2-methyl-1-propanesulfonic acid (AMPS) in the nanoparticle synthesis facilitated the incorporation of the anti-inflammatory enzyme kinase 2 (MK2)-inhibiting cell-penetrating peptide (KAFAK). The developed formulation, housed within the hollow nanoparticles, demonstrated effectiveness in delivering a therapeutically active dosage to bovine cartilage explants. It achieved this by mitigating the anti-inflammatory response in interleukin-6 (IL-6) expression after being stimulated with interleukin-1 beta (IL-1β). This innovative thermoresponsive hollow nanoparticle system presents a robust platform for the targeted delivery of peptide therapeutics, especially within highly proteolytic environments such as osteoarthritis.

In the study [89], the authors demonstrated the potential disintegration of microparticles composed of PNIPAM through the using of near-infrared (IR) irradiation on gold nanorods. This process resulted in the release of drugs. The researchers effectively established stable and uniform dispersions of gold nanorods, which were functionalized with polyethylene glycol, within PNIPAM cylinders having a diameter of 140 μm. Upon irradiation with an IR laser, these composite structures underwent contraction, forming micrometer-sized indentations at the site targeted by the laser. The rate of this contraction surpassed what could typically be achieved through external thermal stimulation. Furthermore, the composite gels demonstrated a controlled release of a model drug when they were in a swollen state without irradiation. However, under the influence of irradiation, the drug release process was dramatically accelerated. The composite gels exhibited rapid drug release within just 60 seconds, specifically within a range of 300 μm around the irradiated spot. This innovative approach could have significant implications for achieving controlled and on-demand drug release applications.

Nanogels synthesized from dendritic polyglycerol (dPG) in combination with two thermoresponsive polymers, namely, poly(glycidyl methyl ether-co-ethyl glycidyl ether) (p(GME-co-EGE)) and poly(N-isopropylacrylamide) (pNIPAM),

hold promise for the treatment of severe skin diseases. These thermoresponsive nanogels exhibit the capacity to encapsulate significant quantities of therapeutic agents like dexamethasone and tacrolimus, which are commonly employed for addressing skin-related conditions. A comprehensive characterization was conducted to understand the cellular uptake, intracellular localization, and toxicological properties of these produced nanogels. The investigation was carried out using primary normal keratinocytes (NHK) and spontaneously transformed aneuploid immortal keratinocytes from adult skin. Through laser scanning confocal microscopy, it was observed that the fluorescently labeled nanogels efficiently penetrated into the cells, with their primary localization occurring within lysosomal compartments. This research highlights the potential of these nanogels as carriers for dermatological treatments, providing insights into their cellular behavior and intracellular fate [90].

Comonomers frequently paired with NIPAM include 2-hydroxyethyl methacrylate (HEMA), a hydrogel renowned for its utilization in contact lens production [91]. The study [92] detailed the synthesis of a triblock copolymer comprising NIPAM, HEMA and dimethyl-γ-butyrolactone acrylate (DBA), wherein a poly(ε-caprolactone) (PCL) derivative acted as the copolymerization initiator via the ATRP method. DBA was chosen to enhance the hydrophilicity and degradability of NIPAM within bodily fluids. Notably, DBA can hydrolyze into AA. In cases where the hydrolyzed PNIPAM triblock copolymer contains 4% or more AA content, poly-(NIPAM-co-HEMA-co-AA) demonstrates a lower critical temperature for expansion (LCST) above 37°C, rendering it stable within the body for drug delivery. The inclusion of PCL as an initiator is thought to play a role not only in breaking down side chains but also in disrupting the main chain of the copolymer. In vitro assessments were conducted to evaluate the response of hydrogels of different stiffness levels, both with and without incorporated collagen, to the introduction of cardiospheric origin cells (CDC) into myocardial tissue. This research delves into the potential applications of the developed hydrogels for controlled cell delivery and tissue engineering, considering varying physical properties and cellular interactions.

Dual-stimulus responsive nanogels have garnered significant attention within the biomedical domain owing to their unique attributes and adaptability. A notable example involves nanoparticles combining PNIPAM and chitosan, which exhibit sensitivity to both pH and temperature. Research outcomes have unveiled an accelerated drug release mechanism within acidic microenvironments, particularly those influenced by cancerous tumors, coupled with temperature elevation. In vitro investigations have validated the biocompatibility of these nanoparticles and their enhanced uptake when functionalized with K237 peptides. Consequently, a marked, specific cytotoxic impact has been demonstrated in contrast to normal cells. This innovative approach holds considerable promise for targeted drug delivery and cancer therapy due to its ability to harness the pH and temperature characteristics of tumor microenvironments [93].

Dadfar et al. [94] elucidate the synthesis of hydrogels with dual thermo- and pH-sensitivity, using a semi-interpenetrating polymer network consisting of NIPAM, pH-responsive N-ethylmaleamic acid (NEMA) and sodium alginate. N,N-methylenebisacrylamide serves as the crosslinking agent in this process. These hydrogels exhibit remarkable responsiveness to changes in both temperature and pH, even in the presence of substantial amounts of the pH-sensitive monomer. The hydrogel matrix efficiently encapsulates the model drug doxorubicin hydrochloride (DOX). Notably, in vitro experiments focusing on drug release kinetics reveal rapid and efficient DOX release in conditions mimicking the tumor environment (phosphate-buffered saline, pH 6.5, 37°C) or endosome/lysosome conditions (pH 5.5, 37°C), in contrast to conditions simulating the human physiological milieu (pH 7.4, 37°C). This demonstrates the potential of these smart hydrogels for targeted drug delivery, with the ability to respond to the specific microenvironments encountered in tumor tissues and intracellular compartments.

In the study, researchers investigated temperature- and pH-sensitive nanogels composed of NIPAM and acrylic acid for their potential as a versatile vehicle for topical drug delivery, using caffeine as a representative permeant model [95]. The influence of the pH regulator, citric acid, within the nanogel system was also examined. Caffeine loading was conducted in deionized water at two distinct temperatures: 2-4°C and 25°C, over a period of 3 days. The results demonstrated that caffeine loading into the nanogel was notably higher at the lower temperature range (2-4°C) compared to room temperature, with respective values of 334 mg/g and 267 mg/g. A similar loading pattern was observed for the control nanogel composed of PNIPAM. The increased drug loading at lower temperatures is attributed to the hydrophilic characteristics of the PNIPAM polymer network, particularly at temperatures below its lower critical solution temperature (LCST). In vitro diffusion studies were carried out across porcine skin epidermis at 32°C for a saturated caffeine solution, as well as for nanogels based on PNIPAM-AA and PNIPAM. The in vitro permeability data of the PNIPAM-AA nanogel (saturated at 2-4°C) indicated a substantial enhancement in caffeine delivery through the epidermis, with an approximately 3.5-order increase compared to caffeine-saturated solution alone. These findings underscore the potential of the temperature- and pH-sensitive nanogels, specifically the PNIPAM-AA nanogel, as an effective platform for enhancing drug permeation and delivery across the skin. Such multi-responsive nanogels offer promise for the development of advanced topical drug delivery systems.

In the study by Sharma et al. [96], the researchers focused on the synthesis and characterization of poly(N-isopropylacrylamide)-co-poly(acrylic acid) (pNIPAM-pAA) nanogels with dual responsiveness to stimuli. These nanogels were designed to exhibit temperature and pH sensitivity, and their sizes were controlled in a precise manner, ranging from 130 to 400 nm. This tunability was achieved by adjusting the surfactant concentration and the reaction temperature during the synthesis process. The study also explored the potential of pNIPAM-pAA nanogels as a drug delivery platform. Loading and release studies were conducted using a

model protein drug, cytochrome C (Cyt C), at temperatures above the VPTT in an acidic environment. This allowed for the investigation of the nanogels' ability to efficiently load and release the drug under specific conditions. Furthermore, the researchers evaluated the biocompatibility of the pNIPAM-pAA nanogels using an ex vivo human whole blood model. They quantified inflammatory responses during exposure to the nanogels, aiming to assess their compatibility with biological systems. This comprehensive study contributes to the understanding of dual-responsive nanogels and their potential applications in drug delivery. The ability to precisely control their size and responsiveness makes these nanogels promising candidates for various biomedical applications.

The research described the synthesis and characterization of pH- and temperature-responsive copolymers based on N-isopropylacrylamide (NIPAM) and propylacrylic acid (PAA) using the reversible addition-fragmentation chain transfer (RAFT) polymerization method. The copolymers were designed with varying PAA content, ranging from 0 to 20 mol.% [97]. At physiological pH (pH 7.4) and with 5 wt.% PAA content, the polymer remained soluble even at temperatures exceeding 50°C. However, at lower pH values (around pH 5.5 and below), the polymer displayed a unique behavior. It existed as a liquid at 20°C, but as the temperature increased, it underwent a sol-gel phase transformation, forming a physical gel at 37°C. The incorporation of the hydrophobic monomer, butyl acrylate, into the random copolymer altered its properties. This change raised the gelation pH to greater than 6.0 at 37°C. The hydrogel's potential for drug delivery was explored through drug loading studies. Basic fibroblast growth factor bioactivity was preserved even after the hydrogel was stored for 40 hours. Additionally, the hydrogel exhibited sustained release of vascular endothelial growth factor, dependent on pH, for at least three weeks. This research demonstrates that the synthesized hydrogel has the ability to undergo a sol-gel phase transformation in response to changes in pH and temperature. These properties make it suitable for controlled drug delivery applications, where the hydrogel can dissolve gradually as it delivers drugs to the target site, coinciding with the return of the ischemic site to its physiological pH.

The behavior of pH-sensitive nanogels is primarily linked to their ionizable groups, which can undergo deformation due to ionization or deionization in response to pH changes. Certain scientific studies have indicated that the microenvironment of tumor tissues (pH 6.5–7.2) and tumor cells (pH 4.5–5.0 in lysosomes and pH 5.0–6.5 in endosomes) is more acidic compared to the physiological pH of 7.4 in the bloodstream and normal tissues [98]. Nanogels sensitive to pH, derived from methacrylic acid (MAA) and methyl ester (ME), maintain their swollen state under normal pH conditions while exhibiting high permeability. When the pH is lowered, leading to deionization of MAA and ME, the nanogels undergo contraction, entrapping the hydrophobic fluorescent indicator oligothiophene (TF) and the hydrophilic drug DOX. Furthermore, an enhanced release of DOX is observed at pH 5.5, potentially owing to the increased shrinkage of pH-sensitive nanogels and the protonation of DOX [99].

Nanogels responsive to both temperature and UV-radiation are discussed in [100]. A novel nanogel composed of poly(N-isopropylacrylamide [PNIPAM]-co-chlorophyllin) was developed with dual control over temperature and UV exposure through surfactant-free emulsion polymerization. The incorporation of hydrophilic chlorophyllin into the PNIPAM backbone yielded a poly[NIPAM-co-CHLN] nanogel with a well-defined size distribution (D~180 nm), as verified by atomic force microscopy and transmission electron microscopy. This nanogel exhibited a lower critical solution temperature of approximately 35°C. During the phase transition, the nanogel size decreased significantly under UV light (50 nm), in contrast to the size change induced by temperature (90 nm). The non-uniform collapse phenomenon was attributed to the temperature gradient established from the gel surface towards the core, where a dense PNIPAM layer was enveloping it. Challenges impeding the release of the anti-cancer drug 5-fluorouracil (5-FU) were effectively surmounted by light irradiation due to the drug's substantial diffusion coefficient.

1.4 Application of stimuli-responsive nano- and microgels in oil recovery

With the increasing number of mature oil fields reaching their final operational stage, the necessity for developing more efficient enhanced oil recovery (EOR) technologies has become evident. Elevated water cut levels in wells result in unfavorable outcomes such as corrosion, scale accumulation and a reduction in the efficiency of oil production [101]. Technologies using cross-linked microgels in oil production is one of the newest and most promising areas that is gaining momentum every year (Figure 3) [102]. This is attributed to the straightforwardness of the process, remarkable selectivity during treatment, adaptability to reservoir conditions and the assured effectiveness when the appropriate candidate-wells are chosen.

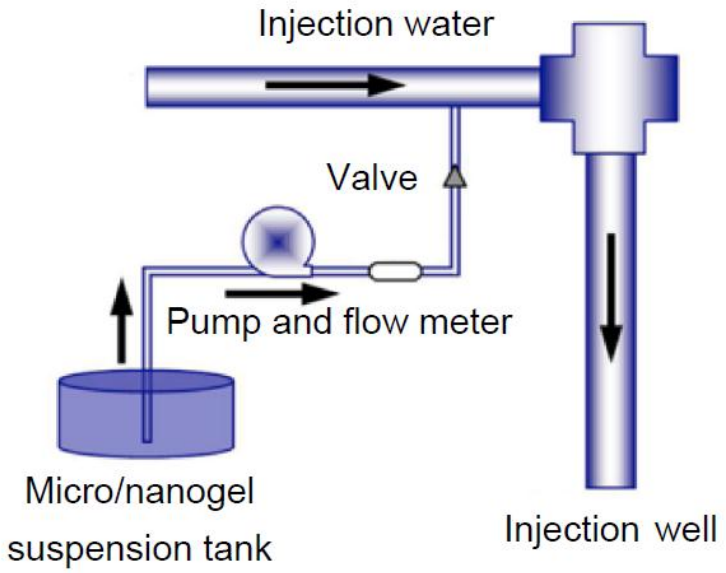

Figure 3 - Micro/nanogel injection facilities

The various types of microgels employed in oil production include microspheres, thermo- and pH-sensitive microgels, pre-formed hydrogel particles and colloidal-dispersed gels [103]. Microgels have garnered significant interest owing to their distinctive properties, which encompass characteristics from three compound categories: colloidal substances, surfactants and polymers. These microgels exhibit distinct attributes from each class, including structural integrity, softness, deformability and permeability, etc. [22].

Microgels containing hydrophilic groups can be used as thickening agents due to their capability to form non-Newtonian fluids and enhance rheological properties [104].

Microgels employed for enhanced oil recovery are acquired through the following primary methods: synthesis of bulk gels and subsequent mechanical grinding, precipitation polymerization and inversion (inverse) emulsion polymerization [105]

The simplest method to prepare microgels - mechanically grinding of bulk gel. The sizes of the resultant particles can vary by at least 10 times, thereby tailoring the resulting product to distinct reservoir properties.

When microgels are produced through precipitation polymerization, the synthesis involves three components: monomer, crosslinker and initiator. The polymerization process advances through a radical mechanism [106]. At the polymerization temperature (50–70°C), the water-soluble initiator (a compound based on peroxide or persulfates) decomposes into free radicals. Once microgel particles attain a critical size, they stabilize and electrostatic repulsion prevents particle coagulation [107].

The most commonly used method in microgel production is inverse emulsion polymerization, which enables the generation of particles of varying sizes and offers numerous modifications. Depending on conditions such as emulsifier concentration, stirring speed, initiator and dispersant concentrations, inverse emulsion polymerization can manifest as suspension polymerization, polymerization in micro- and nanoemulsions. This method facilitates the production of microgels with diverse particle sizes. While all types of emulsions use the same reagents - hydrocarbon solvent, water and surfactant - the distinction among these methods lies in the thermodynamic stability of the emulsions, influencing particle sizes [105]. The benefits of inverse emulsion polymerization encompass temperature regulation during the reaction, production of granular product without requiring a grinding process, ease of drying the product and resulting microgels possessing substantial water absorption capacity [108].

The primary stages in the synthesis of microgels through the inverse emulsion polymerization method are as follows:

- selection of the continuous phase (typically organic solvent, such as mineral oil or refined kerosene);
- choosing an emulsifier mixture;
- opting for a blend of comonomers and a crosslinking agent that define the physicochemical characteristics of the microgels;

- selection of the initiator (for example, ammonium persulfate and sodium sulfite) [109].

The choice of an emulsifier mixture stands as the pivotal step in inverse emulsion polymerization. The emulsifier mixture's hydrophilic-lipophilic balance (HLB) should align with that of the organic solvent (continuous phase). Commonly employed emulsifier combinations for microgel synthesis via inverse emulsion polymerization include TWEEN60, TWEEN80, SPAN80 and others [110].

The structure of a microgel synthesized through inverse emulsion polymerization comprises the subsequent components: polymer chain network, crosslinking agent and functionalized fragments incorporated within the polymer backbone.

Polyacrylamide (PAM) microgels stand as one of the most economical and environmentally friendly polymers extensively employed in oil production. This preference is attributed to their remarkable viscosity-enhancing attributes and their capacity to gel and flocculate in the presence of crosslinking agents [111, 112].

Microgels based on polyacrylamide were synthesized through free-radical inverse emulsion polymerization using diesel fuel as the continuous phase and investigated in the study [113]. MBAA was employed to achieve a cross-linked structure, while a blend of TWEEN60 (polyethylene glycol sorbitan monostearate) and SPAN80 (sorbitan monooleate) served as emulsifiers for the emulsion polymerization process. The absorption capacity was evaluated based on alterations in particle diameter. The absorption capability of the resulting microgels was ascertained, initially with an average diameter of the samples was 50 nm, which expanded to several μm upon swelling. It was observed that the employed emulsifiers, when used in conjunction with an extra surfactant or NaOH, significantly reduced the oil/water interface and stress during microsphere injection. This reduction led to an increase in residual oil and yielded approximately 20% additional oil in core experiments.

The crosslinked elastic polyacrylamide microspheres with MBAA exhibit an average diameter of approximately 12.05 μm. Following a 3-day swelling period, the particle size increases to 25 μm dependent to the temperature. In a saline solution (15–20 g/L), the particle size measures around 16–17 μm. Experiments involving sand pack core flooding have demonstrated that the optimal fit ratio (microsphere diameter to pore size ratio) ranges between 1.35 and 1.55 [110]. Nevertheless, the synthesis of microgels based on acrylamide and acrylic acid through inverse emulsion polymerization, without cross-linking agents, enables the attainment of a particle swelling degree fivefold greater than their initial size (5 μm). The resulting microgels also verified their capacity to redistribute injected water flows within the lower permeable zone of the reservoir [114].

Swelling and viscoelasticity stand as two crucial properties of polymeric microspheres for regulating the injectivity profile of a formation [115]. The impact of monomer concentrations, a crosslinking agent, and an initiator on the storage modulus (representing the elasticity of polymer microspheres) and the loss modulus (reflecting the viscosity of polymer microspheres) was investigated in [116].

Microspheres based on AAm, AA and 2-acrylamido-2-methyl propane sulfonic acid (AMPS), synthesized via emulsion polymerization using aviation kerosene as the oil (or continuous) medium, along with SPAN80 and TWEEN60 dissolved within, exhibit the capability to swell several hundred times their original size upon contact with water. These microspheres can effectively influence water profiles in mature oil fields, either fully or partially.

In the synthesis of low-elastic polymeric microspheres derived from acrylamide, acrylic acid and 2-acrylamido-2-methylpropane sulfonic acid (AMPS) via inverse emulsion polymerization, aviation kerosene served as the continuous phase, while the emulsifier was composed of a combination of SPAN80 and TWEEN60. The microgels exhibited an elastic modulus of 23.6 Pa, a parameter responsible for particle deformability and injectability. Flooding experiments were conducted on cores of varying porosities, revealing that the microgels possess a notably high efficiency in selectively controlling profiles within remote heterogeneous reservoir zones [117, 118].

Nanogels synthesized from AAm and 2-acrylamido-2-methyl-1-propane sulfonic acid (AMPS) with a monomer ratio of AAm:AMPS=80%:20% were created using inverse emulsion polymerization [119]. Cyclohexane (>98%) was employed as the continuous phase, with SPAN80 and TWEEN85 acting as emulsifiers during polymerization. The integration of ionic groups into polymeric materials enhances their resistance to salts. AMPS, classified as a vinyl monomer, demonstrates commendable thermal stability and robust salt resistance, attributed to its ionized sulfonate groups [120]. Furthermore, AMPS vinyl structure yields high molecular weight polymers, an advantageous trait for studies concerning enhanced oil recovery. Owing to their elevated molecular weight, favorable thermal characteristics and enduring stability (up to 50 days), poly(AAm-co-AMPS) nanogels exhibit promising potential for deployment as agents for enhanced oil recovery, particularly within demanding reservoir conditions.

Cross-linked polymer microspheres, which are degradable and synthesized through inverse emulsion polymerization of AAm, 2-methyl-2-acrylic amide propyl sulfonic acid (AMPS) and alpha-methyl styrene (HM), can serve a dual purpose. Initially, they can function as a conformance control agent, effectively obstructing regions characterized by high absorption levels. Subsequently, these microspheres can be employed as polymers for oil displacement, facilitating enhanced oil recovery [121]. Microsphere degradation was investigated using SEM and viscosity experiments. The results illustrated a degradation progression, transitioning from initial swelling to eventual degradation into a linear polymer form. Furthermore, core experiments have indicated that these microspheres possess the capability to mitigate formation heterogeneity, making them suitable for deployment as compliance control agents.

A novel category of microgels, designed to fluoresce under ultraviolet irradiation, has been developed for the purpose of detecting them within reservoir fluids. These microgels are synthesized through inverse suspension polymerization, involving using of specific fluorescent comonomers, such as acryloyloxy coumarin

[108, 122], allyl-rhodamine B (RhB) [122, 123], oxyfluorescein [122]. Fluorescent monomers do not significantly affect the properties and particle size of microgels, since their concentration is rather low.

The pH-sensitive microgel variant exhibits a low viscosity under low pH conditions, with viscosity rising as pH increases. pH-sensitive microgels find application in controlling conformance within remote reservoir zones. The process involves injecting microgels into a low pH environment, allowing small particles to penetrate and traverse the bottomhole zone. Throughout this procedure, the acid from the microgel reacts with the minerals in the rocks, resulting in a pH increase. Consequently, the microgels undergo swelling and subsequently obstruct high-permeability zones situated deeper within the reservoir. This pH sensitivity is achieved by incorporating comonomers with carboxyl functional groups, such as acrylic acid [124].

An elevation in pH initiates the hydrolysis of carboxyl groups within polyacrylate networks, prompting the repulsion of charged groups from each other. Consequently, polymer chains extend, leading to microgel swelling. To ensure the microgel's penetration into the deep formation zone, it is imperative to pre-flush the formation using acids during treatment. Acetic acid is particularly effective for pre-flushing purposes. Subsequently, the microgel is introduced into the formation, followed by the final treatment stage, postflooding. It's noteworthy that the higher the mineralization of water, the lower the pH of weak acids, consequently diminishing the capacity of microgels to swell [125].

Hence, stimuli-responsive nano- and microgels exhibit potential as versatile soft polymeric materials with numerous applications, such as stabilizers, sensors, catalysts, selective sorbents, carriers for targeted drug delivery and thickening agents for oil production. These gels consist of cross-linked polymer chains that undergo swelling in the presence of a solvent. Micro- and nanogels prove to be valuable subjects for scientific investigation.

2 Experimental part

2.1 Materials and Methods

Polyampholyte terpolymers, nano- and microgels were synthesized using the following chemicals: the monomers, N-isopropylacrylamide (NIPAM, 97% purity), acrylamide (AAm, 99% purity), 2-acrylamido-2-methylpropanesulfonic acid sodium salt (AMPS, 50 wt.%) and (3-acrylamidopropyl) trimethylammonium chloride (APTAC, 75 wt.% in water). N,N'-methylenebisacrylamide (MBAA, 99% purity) was used as the crosslinking agent. Ammonium persulfate (APS, 98% purity) and sodium metabisulfite (SMBS, 97% purity) - as polymerization initiators. Surfactants - sodium dodecyl sulfate (SDS, 99% purity), sorbitan monooleate (SPAN80, HLB=4.3) and polyethylene glycol sorbitan monooleate (TWEEN80, HLB=15). Isooctane (i-C8) was used as the organic medium. Sodium chloride (chemically pure) was used to prepare saline solutions of nano- and microgels. Further material - dialysis tubing cellulose membrane (12-14 kDa). All were purchased from Sigma-Aldrich Chemical Co., and used without further purification.

2.2 Synthesis of copolymers based on NIPAM-APTAC and NIPAM-AMPS

Copolymers based on NIPAM-APTAC and NIPAM-AMPS were synthesized via conventional redox initiated free radical copolymerization at 60°C for 4 h. The required amounts of monomers (NIPAM, APTAC or AMPS) listed in Table 1 were dissolved in deionized water at room temperature in a 50 mL beaker under constant stirring. After that, the solution of monomers was filtered through a 5 μm syringe filter and purged with argon for 15-20 min to remove the dissolved oxygen. Then, the solution was carefully transferred to round bottom flask and dry powders of APS and SMBS were added. The flask was immersed in a water bath with periodical shaking of the mixture. Later, the flask was removed from the water bath and cooled down to room temperature. Obtained polymer solutions were dialyzed against distilled water for 72 h and then freeze-dried.

Table 1 - Synthetic protocol of NIPAM-APTAC and NIPAM-AMPS copolymers

The initial composition of monomers, mol. %			NIPAM, g	APTAC, g	AMPS, g	H_2O, mL	APS, mg	SMBS, mg	Yield, wt. %
NIPAM	APTAC	AMPS							
90	10	0	2	0.541	-	21.65	22.4	44.8	87
90	0	10	2	-	0.9	21.4			91

2.3 Synthesis of amphoteric terpolymers based on NIPAM-APTAC-AMPS

Amphoteric terpolymers based on NIPAM-APTAC-AMPS were synthesized via conventional redox initiated free radical copolymerization at 60°C for 4 h. Briefly, the desired composition of the monomers was dissolved in deionized water at room temperature in a 50 mL beaker under constant stirring. After that, the solution of monomers was filtered through a 5 μm syringe filter and purged with argon gas for 15-20 min to remove the dissolved oxygen. Then, the solution was carefully transferred to round bottom flask and dry powders of APS and SMBS were added. The flask was immersed in a water bath with periodical shaking of the mixture. Later, the flask was removed from the water bath and cooled down to room temperature. Obtained polymer solutions were dialyzed against distilled water for 72 h and then freeze-dried. Synthetic protocol of NIPAM-APTAC-AMPS terpolymers is given in Table 2. As is seen, the yield of the terpolymers is enough high and varied from 80 to 93 wt.% [126].

Table 2 - Synthetic protocol of NIPAM-APTAC-AMPS terpolymers

The initial composition of monomers, mol. %			NIPAM, g	APTAC, g	AMPS, g	H_2O, mL	APS, mg	SMBS, mg	Yield, wt. %
NIPAM	APTAC	AMPS							
90	5	5	2	0.135	0.225	21.8	22	37	89.3
90	7.5	2.5	2	0.406	0.225				80
90	2.5	7.5	2	0.135	0.675				93

2.4 Synthesis of nanogels based on NIPAM-APTAC and NIPAM-AMPS

Polyampholyte nanogels were synthesized via conventional redox initiated free radical copolymerization in the presence of a crosslinking agent at 80°C for 4 h under inert atmosphere with constant stirring of the solution. The required amounts of monomers (NIPAM, APTAC and (or) AMPS), MBAA and SDS listed in Table 3 were dissolved in deionized water with constant stirring. Further, the required amount of APS/SMBS redox system was added to the solution and stirred until complete dissolution. The solution with dissolved monomers, crosslinking agent, surfactant and redox system was transferred to a round bottom flask and heated on a water bath. The resulting solutions of nanogels of the indicated compositions were dialyzed against deionized water for 14 days to remove unreacted residues [127].

Table 3 - The amount of monomers, initiator, crosslinking agent and surfactant for the synthesis of nanogels based on NIPAM-APTAC and NIPAM-AMPS

The initial composition of the monomers, mol. %			NIPAM, g	APTAC, g	AMPS, g	H_2O, mL	APS, mg	SMBS, mg	MBAA, g	SDS, g	Yield, %
NIPAM	APTAC	AMPS									
90	10	0	0.83	0.225	-	97	50	10	0.111	0.35	90
90	0	10	0.815	-	0.367	97.5	30			0.23	72

2.5 Synthesis of nanogels based on NIPAM-APTAC-AMPS

Polyampholyte nanogels were synthesized via conventional redox initiated free radical copolymerization in the presence of a crosslinking agent at 80°C for 4 h. NIPAM, APTAC, AMPS, MBAA and SDS were dissolved in deionized water at room temperature in a 100 mL beaker under constant stirring. The resulting solution was then filtered through a 5 μm syringe filter and purged with argon for 15-20 minutes in order to remove dissolved oxygen. The solution was then carefully transferred to a stoppered round bottom flask, and dry powders of APS and SMBS were added. The flask was immersed in a water bath of 80°C under constant stirring. After 4 hours, the flask was removed from the water bath and cooled to room temperature. The resulting nanogel solutions were subjected to dialysis in distilled water for 14 days. Ratios of NIPAM-APTAC-AMPS nanogels are given in Table 4. As can be seen, the yield of nanogels varies from 67 to 88 wt.% [128].

Table 4 – The amount of monomers, initiator, crosslinking agent and surfactant for the synthesis of nanogels based on NIPAM-APTAC-AMPS

The initial composition of the monomers, mol. %			NIPAM, g	APTAC, g	AMPS, g	H_2O, mL	APS, mg	SMBS, mg	MBAA, g	SDS, g	Yield, %
NIPAM	APTAC	AMPS									
90	5	5	0,735	0,099	0,165	98	30	10	0,111	0,23	70
90	7.5	2.5	0,735	0,149	0,082		20			0,35	88
90	2.5	7.5	0,735	0,049	0,248		30			0,23	67

2.6 Synthesis of microgels based on AAm-APTAC-AMPS

Synthesis of microgels based on AAm, APTAC and AMPS was carried out via inverse emulsion polymerization in a 100 ml reactor equipped with a mechanical stirrer and reflux condenser in an argon atmosphere. To prepare the organic phase, isooctane (continuous phase) was mixed with SPAN80 and TWEEN80 (HLB=5-7).

To prepare the aqueous phase, AAm, APTAC, AMPS (used as the dispersed phase) and MBAA were dissolved in deionized water at room temperature with constant stirring. To obtain an emulsion, the aqueous phase was added dropwise to the organic phase, then the emulsion was stirred on a homogenizer for 10 min at a speed of 10 thousand rpm. Next, the resulting water-in-oil emulsion was heated on a water bath to 80°C in the presence of an initiator, APS, and stirred at a speed of 800 rpm for 3 hours.

Then, the resulting emulsion was precipitated in 200 ml of cold methanol, centrifuged at 1000 rpm and washed several times with cold methanol. The residue after precipitation was dissolved in distilled water and freeze-dried to obtain a purified dry microgel [129].

2.7 Fourier-transform infrared spectroscopy (FTIR) of terpolymers, nano- and microgels

The functional groups of terpolymers, nano- and microgels were characterized using Fourier-transform infrared spectroscopy, performed using a Cary 660 FTIR (Agilent, USA) equipped with pike MIRacle ATR accessory (Attenuated Total Reflection mode). Before performing the measurement terpolymers, nano- and microgel samples were freeze-dried for 24 h until moisture was completely removed. The spectra were measured in the wavenumber range of 500 to 4000 cm^{-1} at room temperature.

2.8 Thermogravimetric analysis (TGA) of terpolymers, nano- and microgels

The thermal decomposition of terpolymers, nano- and microgels was investigated using a LabSys Evo (Setaram, France) under a nitrogen atmosphere in a temperature range of 25 to 500°C, with a heating rate of 10°C min^{-1}. The TG curve made possible the determination of the initial decomposition temperature and the residual mass percentage. Further, the maximum thermal decomposition temperature of terpolymers, nano- and microgels was calculated using the differential peaks of the DTA curve.

2.9 ^{1}H NMR spectroscopy of terpolymers and nanogels based on NIPAM-APTAC-AMPS

^{1}H NMR spectra were recorded on a JNN-ECA 400 spectrometer (JEOL, Japan) at a frequency of 399.78 MHz, using D_2O as a solvent. The temperature was varied from 20 to 55°C at intervals of 5°C. For each temperature, the sample was allowed to stabilize for 10 min prior to measurement. Chemical shifts were measured relative to residual proton signals from the deuterated solvent.

2.10 The weight average molecular weight M_w, the number average molecular weight M_n and the polydispersity index (PDI) of the NIPAM-APTAC-AMPS terpolymers

The values of M_w, M_n and PDI for NIPAM-APTAC-AMPS terpolymers measured by gel-permeable chromatography using Viscotek GPC/SEC systems (Malvern Instruments, UK) in aqueous solution.

2.11 Determination of the average hydrodynamic size and zeta potential of terpolymers based on NIPAM, APTAC and AMPS

The average hydrodynamic size (R_h) and zeta-potential (μ) of the terpolymers in aqueous and saline solutions were measured using dynamic light scattering (DLS) on a Zetasizer Nano ZS90 (Malvern Instruments, UK). The particle size was measured in a 0.1wt.% solution of terpolymers with μ = 0.001, 0.005, 0.01, 0.05, 0.1, 0.5 and 1 M NaCl. Zeta-potential of the terpolymers was measured as a function of polymer concentration (0.01-0.1 wt.%) at 25°C.

2.12 Determination of the average hydrodynamic size and zeta potential of nanogels based on NIPAM, APTAC and AMPS

The average hydrodynamic size (R_h) and zeta-potential (μ) of nanogels in aqueous and saline solutions were measured using dynamic light scattering (DLS) on a Zetasizer Nano ZS90 (Malvern Instruments, UK). The particle size was measured in a 0.1wt.% solution of nanogels at a range of 25 to 50°C at intervals of 5°C and with μ = 0.001, 0.1 and 1 M NaCl. Zeta-potential of the nanogels was measured first in an aqueous solution with 0.1wt.% at 25°C, and then in a 0.001 M NaCl solution, which was heated from 25 to 60°C at intervals of 5°C.

2.13 Determination of the average hydrodynamic size of microgels based on AAm-APTAC-AMPS

The average hydrodynamic size (R_h) of the AAm-APTAC-AMPS microgels in isooctane solution was measured using dynamic light scattering (DLS) on a Zetasizer Nano ZS90 (Malvern Instruments, UK). The particle size was measured in isooctane solution of microgels.

2.14 Determination of phase transition temperatures of nanogels based on NIPAM, APTAC and AMPS

Aqueous and saline solutions of nanogels are transparent at temperatures below the LCST; at room temperature (25°C). When the temperature is above the LCST, the solution becomes milky white and the transmittance decreases as the nanogels dehydrate and become more hydrophobic, thus less soluble in water. The VPTT, of nanogels in aqueous and saline solutions, with ionic strength (μ), equal to

0.001, 0.01, 0.1, 0.5 and 1 M NaCl, were determined by observing changes in the transmittance of the solution after changing the temperature. The phase transition temperature was determined as the minimum on the differential curve. The experiments were carried out using a concentration of 0.1 wt.% at $\lambda = 700$ nm and a 0.5°C min^{-1} heating rate over a temperature range of 25-60°C.

2.15 SEM data of nanogels based on NIPAM-APTAC-AMPS

In order to determine the surface morphology, 0.1 wt.% solution of nanogels were preliminarily dried at 25°C, and then analyzed using a MIRA 3 LMU scanning electron microscope (Tescan, Czech Republic).

2.16 TEM data of microgels based on AAm-APTAC-AMPS

The morphology of microgel particles were determined using JEM-1230 (JEOL, Japan) transmission electron microscopes. For TEM imaging, a carbon coated copper grids were glow discharged prior to use. The dilute dispersions (5 μL) were placed on the freshly prepared grids.

2.17 Immobilization of dyes within the matrix of charge-imbalanced amphoteric nanogels

Immobilization of anionic dye, methyl orange (MO), and a cationic dye, methylene blue (MB), into the matrix of nanogels was performed as follows. 2.5 mL of 1 mM MO solution and 2.5 mL of 0.4 wt.% $NIPAM_{90}$-$APTAC_{7.5}$-$AMPS_{2.5}$ nanogel were poured to a 50 mL flask. Distilled water was then added up to the required volume. The final concentration of MO and $NIPAM_{90}$-$APTAC_{7.5}$-$AMPS_{2.5}$ nanogel in the flask was $5 \cdot 10^{-2}$ mM and 0.1 wt.%, respectively.

The MB immobilization is identical to the procedure described above: 2.5 mL of 1 mM MB and 2.5 mL of 0.4 wt.% $NIPAM_{90}$-$APTAC_{2.5}$-$AMPS_{7.5}$ nanogel were poured into a 50 mL flask; the required amount of water was added obtaining $5 \cdot 10^{-2}$ mM MB and 0.1wt.% $NIPAM_{90}$-$APTAC_{2.5}$-$AMPS_{7.5}$ nanogel [130].

2.18 Measurement of the interfacial tension of microgels based on AAm-APTAC-AMPS

For determination of the optimal surfactant concentration, interfacial tension (IFT) was measured at 25°C using a KRUSS tensiometer SDT (Germany).

2.19 Measurement of the viscosity of microgels based on AAm-APTAC-AMPS

The viscosity of the microgels was measured with a Brookfield rotational viscometer (Brookfield AMETEK DV2TLV, USA) using spindles LV-1 and LV-2

(rotation speed 100 rpm) at a shear rate of 7.32 s^{-1} and room temperature. The shear rate 7.32 s^{-1} has been accepted by petroleum engineers as standard to allow direct comparison of solutions in chemical flooding [131]. In reality, 7.32 s^{-1} is the shear rate value that a fluid will experience at a flow rate of 0.3 m/day in porous media with a permeability range of 0.6-0.8 Darcy. Therefore, a shear rate of 7.32 s^{-1} was specifically selected for amphoteric microgels to evaluate their behavior in a porous medium.

2.20 Core flooding experiments to evaluate the applicability of microgels for oil recovery in a model oil reservoir

The core flooding experiment was carried out at the core flooding apparatus "УИК-С (2)" (Russia) and using a piston pump, epoxy core holder equipped with 2 pressure transducers taking readings at the inlet and center of the core.

The core flooding experiments were performed in the following sequences:

1 - Vacuuming the core;
2 - Saturating with brine;
3 - Injection of around 6 pore volumes of crude oil to displace brine;
4 - Injection of around 3 pore volumes of brine to displace oil;
5 - Injection of 3 pore volumes of 2,500 ppm microgel suspension;
6 - Aging the model for 24 h;
7 - Post-flush with brine.

Steps from 3 to 7 were done at 0.5 cm^3/min and 25°C. It should be noted that the microgel was injected at conditions very close to residual oil saturation in the core.

3 Results and discussion

3.1 Synthesis and characterization of anionic and cationic copolymers based on NIPAM-APTAC and NIPAM-AMPS

Linear copolymers of various compositions [NIPAM]:[APTAC] = 90:10 mol.% and [NIPAM]:[AMPS] = 90:10 mol.%, were synthesized via conventional redox initiated free radical copolymerization (Figure 4).

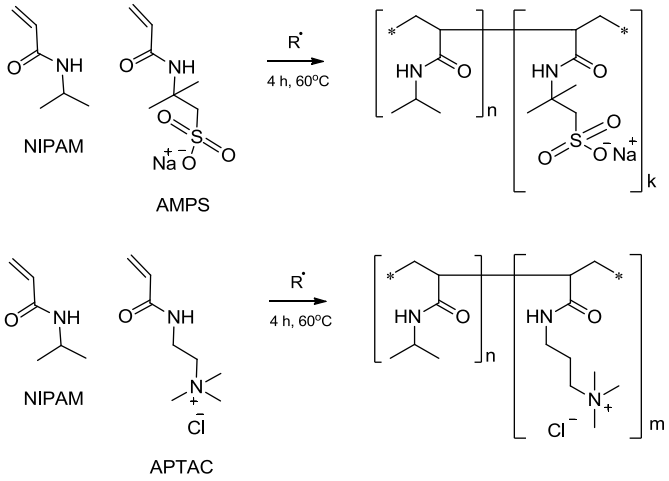

Figure 4 - Schematic representation of free-radical copolymerization of NIPAM-APTAC and NIPAM-AMPS monomers

Figure 5 shows FTIR spectra of the NIPAM-APTAC and NIPAM-AMPS copolymers.

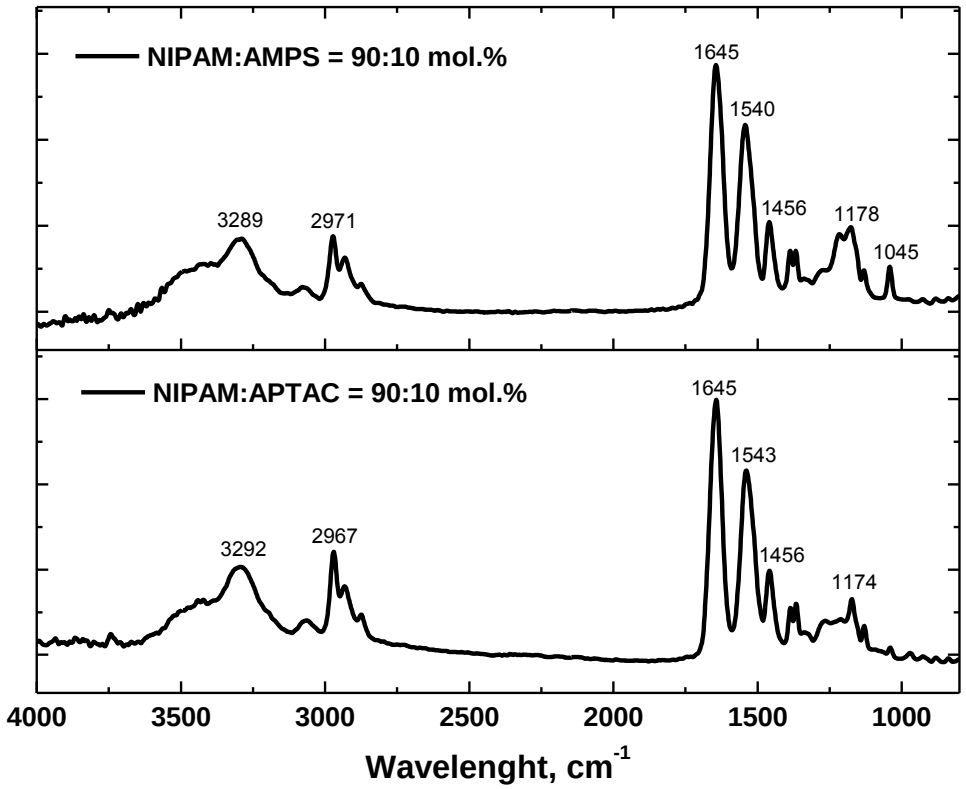

Figure 5 - FTIR spectra of NIPAM-APTAC and NIPAM-AMPS copolymers

The broad absorption band in the region of 3290–3500 cm^{-1} corresponds to the secondary and tertiary amine groups, and the absorption bands in the region of 2800–3000 cm^{-1} correspond to the asymmetric and symmetric vibrations of CH groups. Intensive peaks at ν =1640 and 1540 cm^{-1} belong to N-substituted groups (amide I and amide II). The S=O groups containing in AMPS fragments are detected at ν =1040 cm^{-1}.

Figure 6 shows the results of thermogravimetric (TGA) and differential thermal (DTA) analysis. The dry copolymers show 5% mass loss between 25 and 150°C. This additional weight loss is, however, hard to assign to loss of water alone because the TGA and DTA data do not show a clear step in this temperature range. The mass loss up to 200-300°C may be a result of evaporation of residual water and beginning of the copolymers decomposition. Complete thermal decomposition of NIPAM-APTAC and NIPAM-AMPS copolymers takes place at the interval of temperature between 409 and 415°C.

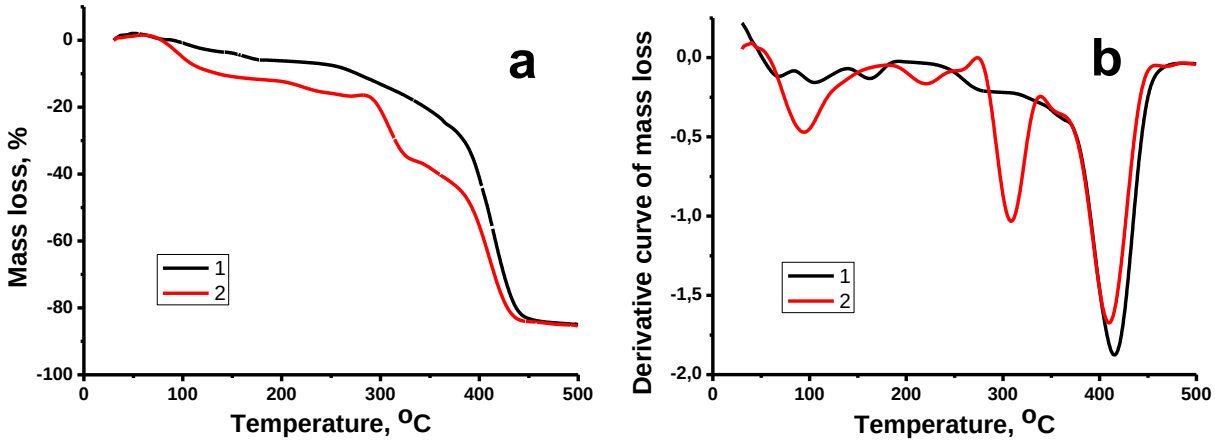

Figure 6 - TGA thermograms (a) and differential curves (b) of anionic and cationic copolymers: 1 –NIPAM:APTAC=90:10 mol.%, 2 – NIPAM:AMPS=90:10 mol.%

Zeta potentials NIPAM-APTAC and NIPAM-AMPS copolymers in aqueous solutions were measured as a function of polymer concentration (Figure 7). The copolymer [NIPAM]:[APTAC]=90:10 mol.% with the excess of positively charged APTAC monomer independently on the polymer concentration (0.01-0.1 wt.%) has ζ=+30±10 mV. The copolymer [NIPAM]:[AMPS]=90:10 mol.% with the excess of negatively charged AMPS monomer slightly depends on concentration (0.01-0.1 wt.%) and has ζ= –54±3 mV.

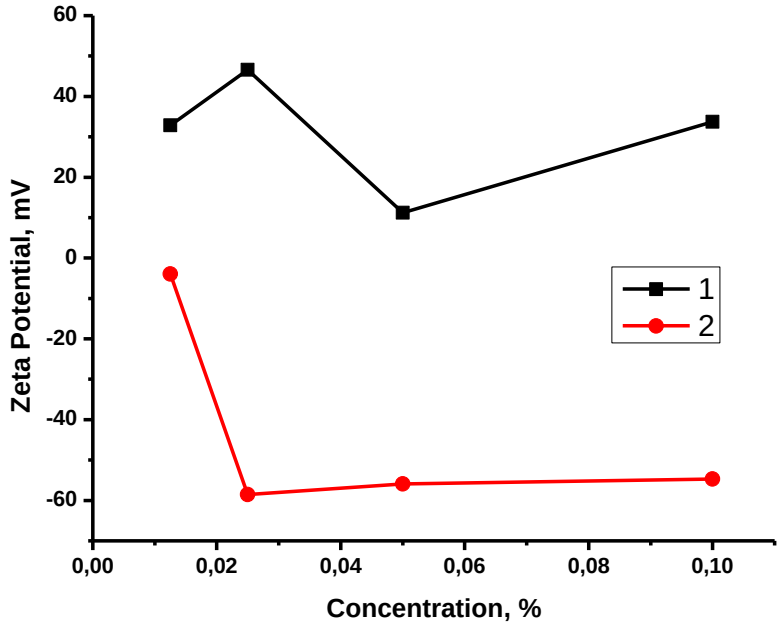

Figure 7 - Zeta potentials of copolymers: 1 –NIPAM:APTAC=90:10 mol.%, 2 – NIPAM:AMPS=90:10 mol.%

3.1.1 Study of the thermo- and salt responsive properties of cationic NIPAM-APTAC and anionic NIPAM-AMPS copolymers in aqueous and saline solutions

The average hydrodynamic size (R_h) and the VPTT of positively charged copolymer [NIPAM]:[APTAC]=90:10 mol.% in deionized (DI) water and in NaCl solutions (μ = 0.001; 0.005; 0.01; 0.05; 0.1; 0.5; 1M NaCl) are presented in Figures 8 and 9.

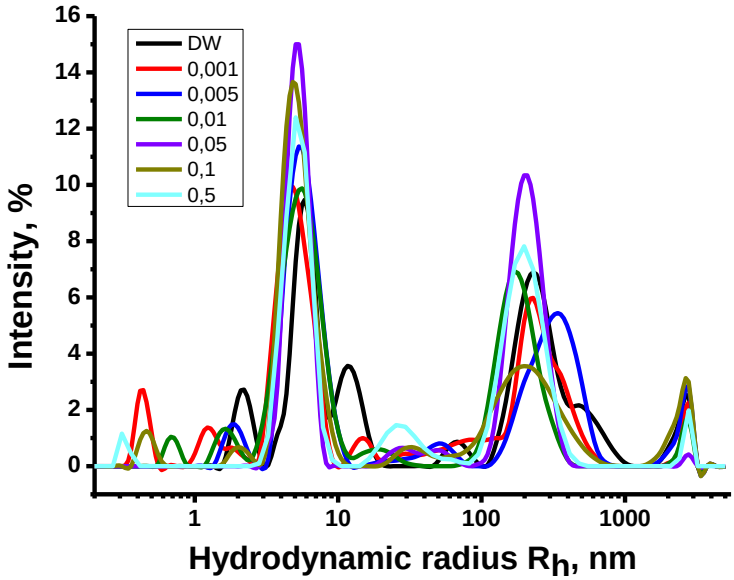

Figure 8 - The effect of the μ on the average hydrodynamic size of [NIPAM]:[APTAC]=90:10 mol.% at 25^0C

The average hydrodynamic size of the cationic copolymer NIPAM-APTAC has a bimodal distribution and lies in the ranges of 4-6 nm and 160-340 nm (Figure 8).

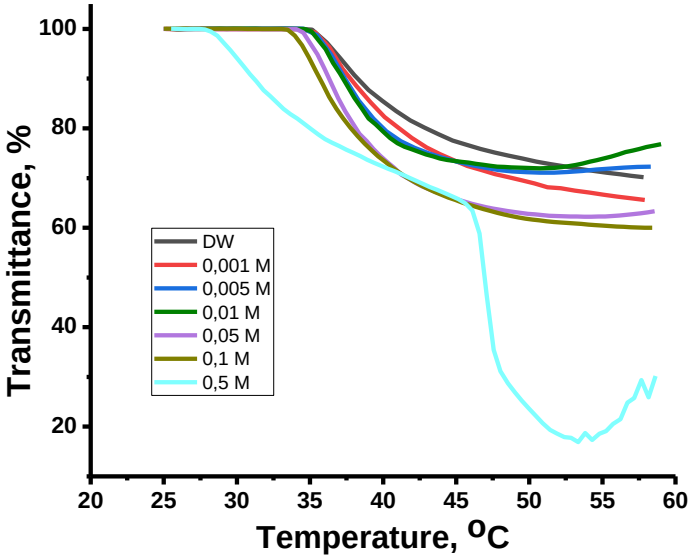

Figure 9 - Temperature dependent phase behavior of terpolymer [NIPAM]:[APTAC]:=90:10 mol.% at various μ

The VPTT of the cationic copolymer [NIPAM]:[APTAC]=90:10 mol.% in DI water is 37.1°C (Table 5). Increasing the ionic strength (μ) to 0.001-0.005M shifts VPTT towards higher values. At μ above 0.1M, the low molecular weight salt shields the charge of the terpolymer, which leads to the recovery of the thermal behavior of pure PNIPAM. At μ=0.5M, fractures are observed on the turbidity curve and a decrease in transparency in the range of 45-50°C, further heating causes precipitation of polymer chains due to the "salting out" effect (Figure 10). In 1M NaCl solution terpolymer is insoluble.

Table 5 - The effect of the ionic strength (μ) on the phase transition temperature of NIPAM-APTAC and NIPAM-AMPS

Terpolymer	Ionic strenght μ, mol·L^{-1} (NaCl)							
	0	0.001	0.005	0.01	0.05	0.1	0.5	1.0
	Volume phase transition temperature (VPTT), °C							
[NIPAM]:[APTAC]=90:10 mol.%	37.1	37.2	37.4	37.1	36.5	35.4	41.7	-
[NIPAM]:[AMPS]=90:10 mol.%	35.2	35.1	34.9	34.9	34.1	33.4	51.5	-

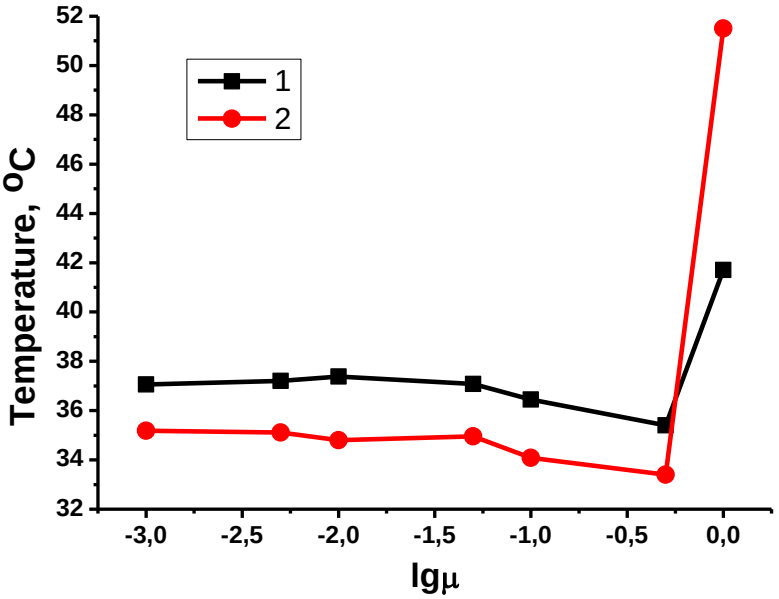

Figure 10 - Temperature dependent phase behavior of NIPAM-APTAC and NIPAM-AMPS copolymers at various ionic strength (μ), where curve 1 - [NIPAM]:[APTAC]=90:10 mol.%; curve 2 - [NIPAM]:[AMPS]=90:10 mol.%

The R_h and VPTT of negatively charged copolymer [NIPAM]:[AMPS]=90:10 mol.% in deionized (DI) water and in NaCl solutions at various μ are presented in Figures 11 and 12.

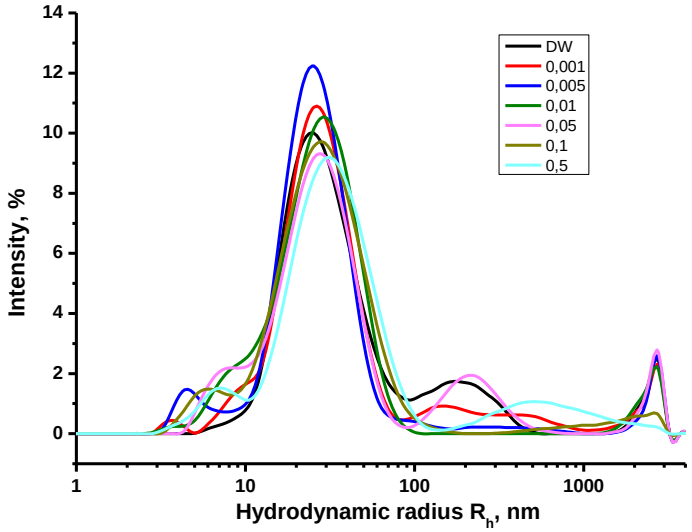

Figure 11 - The effect of the μ on the average hydrodynamic size of [NIPAM]:[AMPS]=90:10 mol.% at 25°C

The average hydrodynamic radius of R_h macromolecules at various μ is about 20-30 nm, also peaks are observed in the region of 180 and 210 nm in DI water, 0.001 and 0.05 M NaCl solution (Figure 11).

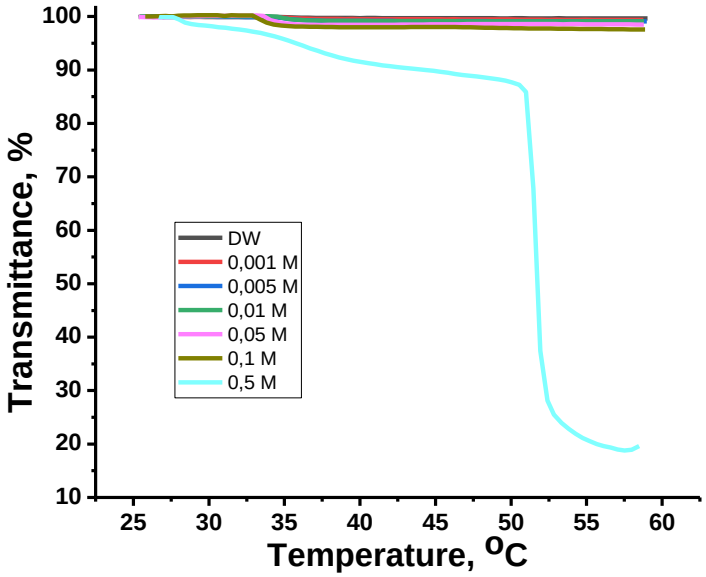

Figure 12 - Temperature dependent phase behavior of anionic copolymer [NIPAM]:[AMPS]:=90:10 mol.% at various μ

Since the copolymer [NIPAM]:[AMPS]=90:10 mol.% is an anionic polyelectrolyte, the addition of salt leads to shielding of the electrostatic repulsion of uniformly charged groups. The copolymer is insoluble in 1 M NaCl solution. For μ in the range of 0.001–0.1 M, the transmittance practically does not change. An increase in μ to 0.05 M leads to a shift in VPTT towards lower temperatures, with the addition of 0.1 M NaCl, the VPTT of the copolymer increases and is equal to 34.9°C (Table 5). With a further increase in ionic strength to 0.05 and 0.1 M, VPTT decreases and amounts to 34.1 and 33.4°C, respectively. At μ=0.1 M, the VPTT value is practically equal to the LCST of pure PNIPAM (~33°C), which is explained by the shielding of electrostatic repulsion between negatively charged AMPS groups and, consequently, the phase behavior and solubility of the copolymer [NIPAM]:[AMPS]=90:10 mol.% is determined by NIPAM90 fragments. At μ=0.5 M, the turbidity curve has breaks and shifts VPTT towards 51.5°C, and precipitation of the copolymer is observed due to the "salting out" effect (Figure 10).

3.2 Synthesis and characterization of polyampholyte linear terpolymers based on NIPAM-APTAC-AMPS

Linear terpolymers of various compositions [NIPAM]:[APTAC]:[AMPS] = 90:5:5; 90:7.5:2.5; 90:2.5:7.5 mol.%, were synthesized via conventional redox initiated free radical copolymerization (Figure 13). The resulted terpolymer samples have randomly distributed charged units along the macromolecular chain [76].

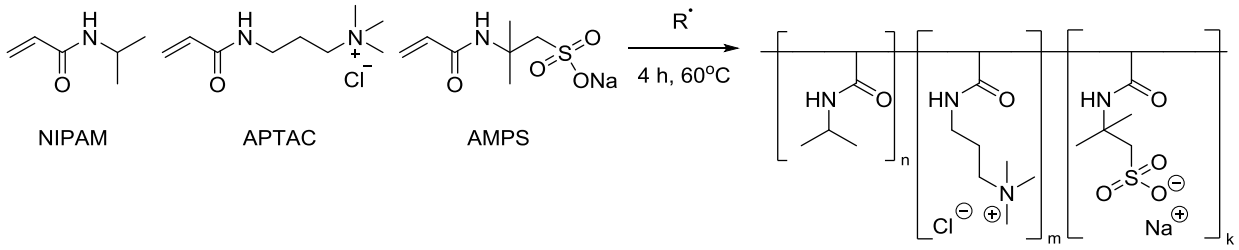

Figure 13 - Schematic representation of free-radical copolymerization of NIPAM, APTAC and AMPS monomers

Figure 14 shows FTIR spectra of the NIPAM-APTAC-AMPS terpolymers. The wide absorption band in the region of 3200-3500 cm^{-1} corresponds to the secondary and tertiary amine groups, the absorption bands in the region of 2800-3000 cm^{-1} correspond to the asymmetric and symmetric vibrations of the CH groups. The absorption bands at 1650 and 1530 cm^{-1} belong to the vibrations of the N-substituted groups, i.e. to amide I and amide II, respectively. The absorption band at 1450 cm^{-1} is characteristic for deformation vibrations of the CH groups. The absorption band in the region of 1040 cm^{-1} corresponds to the fluctuations of the S=O groups containing in the AMPS moieties.

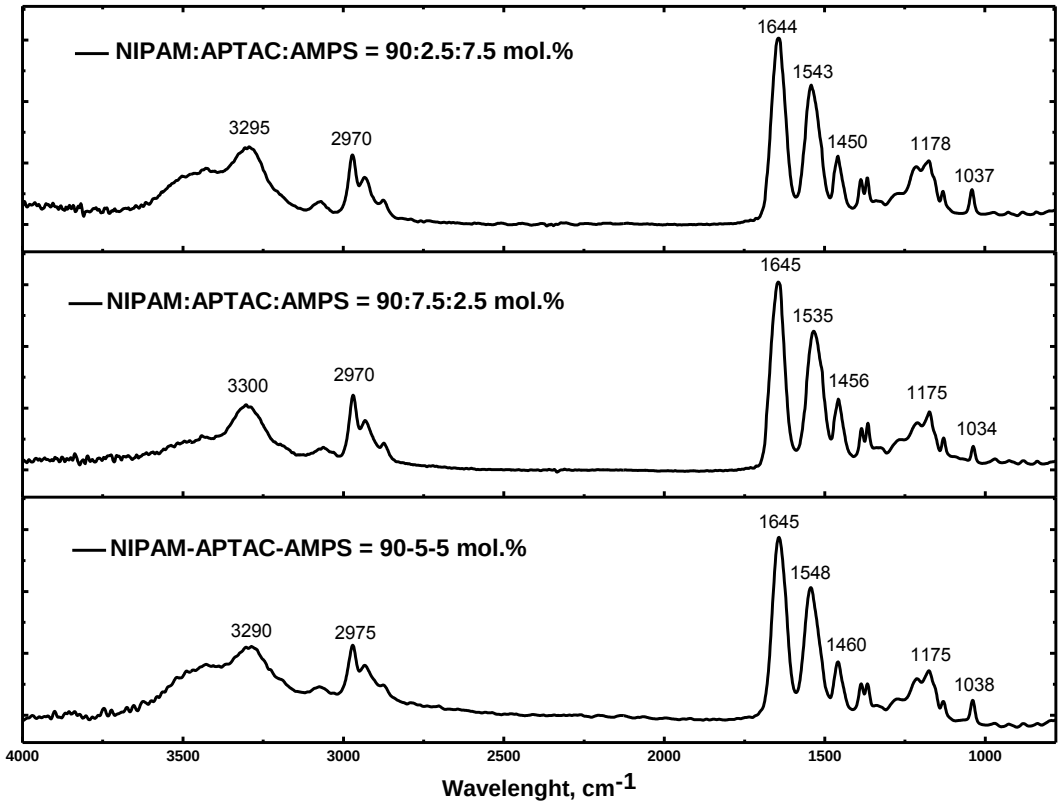

Figure 14 - FTIR spectra of NIPAM-APTAC-AMPS terpolymers

The composition of the obtained terpolymers was established by ^{1}H NMR spectroscopy (Figure 15).

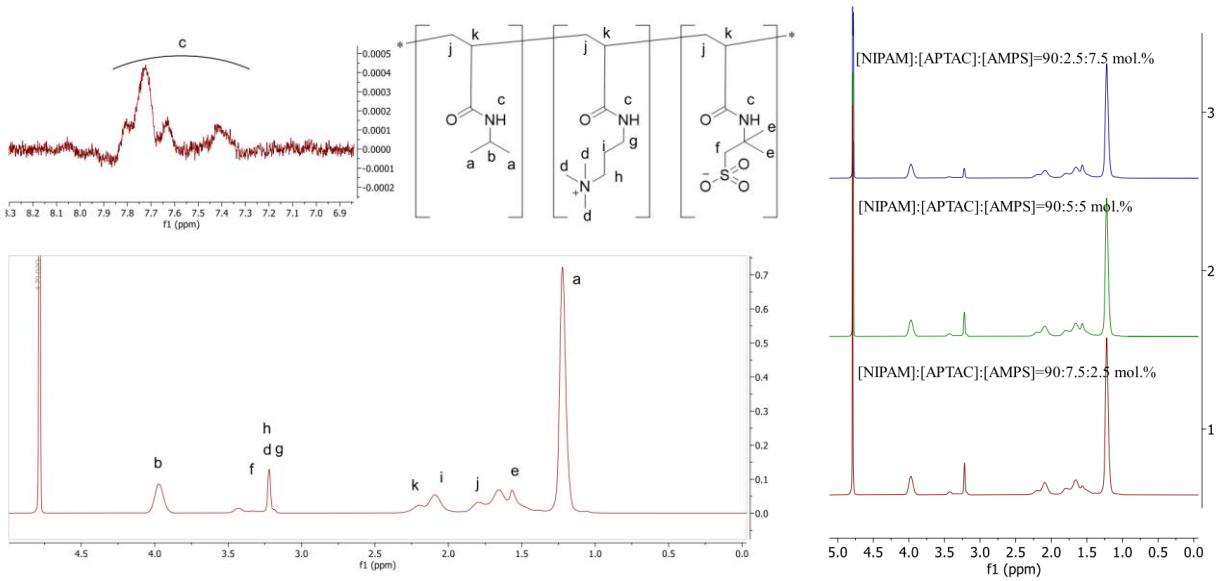

Figure 15 - ^{1}H NMR spectra of NIPAM-APTAC-AMPS terpolymers and identification of proton signals

The resonance bands observed at 1.8 and 2.2 ppm were attributed to the protons of methylene and methine groups of the main chain of the terpolymers respectively. Nevertheless, these peaks overlapped with the peaks of methyl and methylene protons of AMPS and APTAC. The resonance bands at 3.2-3.4 ppm were assigned to suspended protons of methyl and methylene groups in AMPS and APTAC. Since these signals were superimposed each other, the exact compositions of the NIPAM-APTAC-AMPS terpolymers could not be determined from the ^{1}H NMR spectra. Nevertheless, one can assume that the amount of APTAC and AMPS in terpolymers will coincide well with the initial monomer mixture because the reactivity of all monomers is similar and close to one [76]. Taking into account all reasons listed above, one can claim that the final composition of terpolymers possesses charge-balanced and charge-imbalanced structure. For instance, the amphoteric terpolymer [NIPAM]:[APTAC]:[AMPS]=90:5:5 mol.% composed of the equal number of positively (APTAC) and negatively (AMPS) charged monomers refers to a charge-balanced polyampholyte, while the terpolymers [NIPAM]:[APTAC]:[AMPS]=90:7.5:2.5 mol.% and [NIPAM]:[APTAC]:[AMPS]=90:2.5:7.5 mol.% containing an excess of positively (APTAC) or negatively (AMPS) charged monomers belong to charge-imbalanced polyampholytes.

Figure 16 shows the results of thermogravimetric (TGA) and differential thermal (DTA) analysis. The dry terpolymers show mass loss of ca. 5% between room temperature and 150°C. This additional weight loss is, however, hard to assign to loss of water alone because the TGA and DTA data do not show a clear step in this temperature range. The mass loss up to ca. 200-300°C may be a result of evaporation of residual water and beginning of the copolymers decomposition. Complete thermal decomposition of NIPAM-APTAC-AMPS terpolymers takes place at the interval of temperature between 410-420°C.

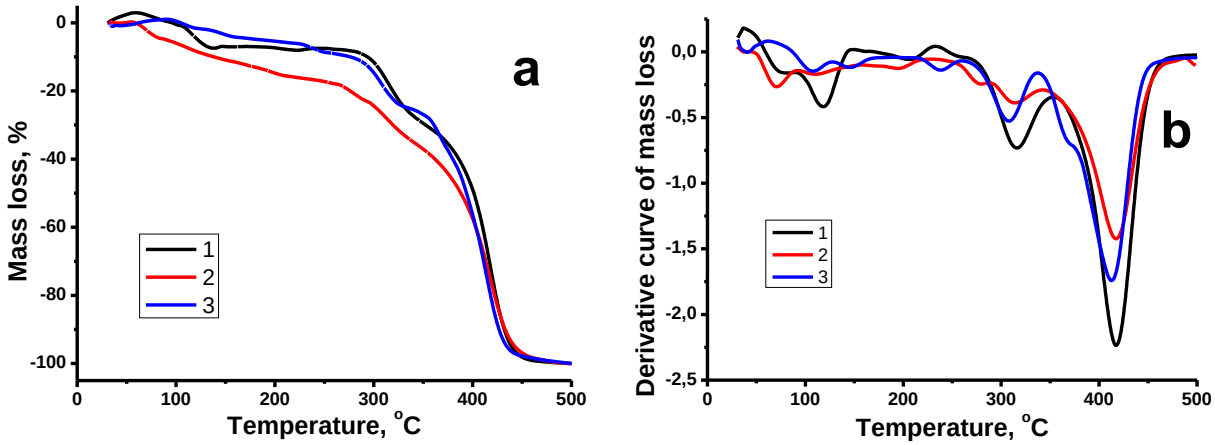

Figure 16 - TGA thermograms (a) and differential curves (b) of NIPAM-APTAC-AMPS terpolymers, where curve 1 – 90:5:5; curve 2 –90:7.5:2.5; curve 3 – 90:2.5:7.5 mol.%

Table 6 represents the values of M_w, M_n and PDI for NIPAM-APTAC-AMPS terpolymers measured by gel-permeable chromatography in aqueous solution.

Table 6 - The values of M_w, M_n and PDI for linear NIPAM-APTAC-AMPS terpolymers

Composition, mol. %			$M_w \times 10^{-5}$, Da	$M_n \times 10^{-4}$, Da	PDI = M_w/M_n
NIPAM	APTAC	AMPS			
90	5	5	1.4	4.6	≈3.0
90	7,5	2,5	0.5	3.1	≈1.6
90	2,5	7,5	2.5	6.4	≈4.0

The M_w of terpolymers is in the range of $(0.5\text{-}2.5)\cdot10^5$ Dalton, M_n is $(3.1\text{-}6.4)\cdot10^4$ Dalton. The PDI of terpolymers is between 1.6 and 4.0. The broad molecular weight distribution of terpolymers is probably due to application of free-radical polymerization method that does not allow controlling precisely the molecular weights of polymers.

Zeta potentials of charge-balanced and charge-imbalanced NIPAM-APTAC-AMPS terpolymers in aqueous solution were measured as a function of polymer concentration (Figure 17). The terpolymer [NIPAM]:[APTAC]:[AMPS]=90:7.5:2.5 mol.% with the excess of positively charged APTAC monomer independently on the polymer concentration (0.01-0.1 wt.%) has $\zeta = +7\pm1$ mV. In contrast, the amphoteric terpolymer [NIPAM]:[APTAC]:[AMPS]=90:2.5:7.5 mol.% with the excess of negatively charged AMPS monomer slightly depends on concentration (0.01-0.1 wt.%) and has $\zeta = -16\pm3$ mV. One can expect that in ideal case, when the amount of positive and negative charges in [NIPAM]:[APTAC]:[AMPS]=90:5:5 mol.% is equal and compensates each other, the overall charge of macromolecular chain is electroneutral, the value of ζ should be around of zero. However in our case

the ζ value of the charge-balanced amphoteric terpolymer [NIPAM]:[APTAC]:[AMPS] = 90:5:5 mol.% deviates from zero and is slightly positive independently on polymer concentration (0.01-0.1 wt.%). Its value equals -2±1 mV probably due to a tiny excess of the negatively charged AMPS monomer. Thus, the fact that the charge-balanced and charge-imbalanced amphoteric terpolymers have been synthesized is obvious [126].

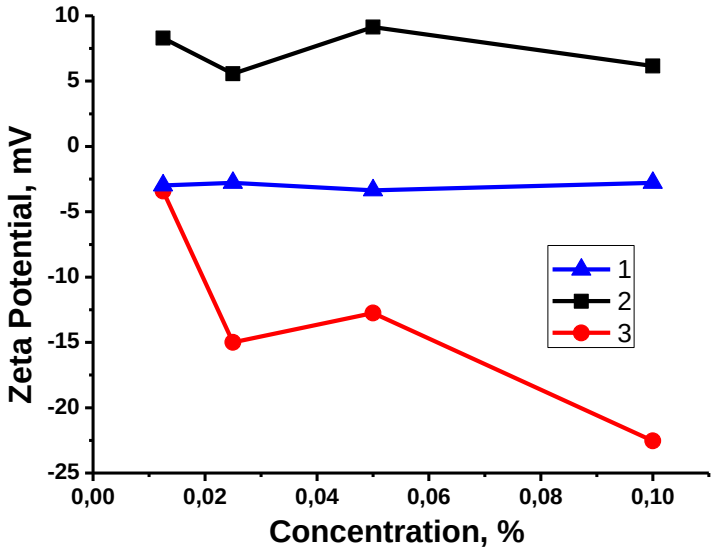

Figure 17 - Zeta potentials of NIPAM-APTAC-AMPS terpolymers, where curve 1 – 90:5:5; curve 2 – 90:7.5:2.5; curve 3 – 90:2.5:7.5 mol.%

3.2.1 Study of the thermo- and salt responsive properties of NIPAM-APTAC-AMPS terpolymers in aqueous and saline solutions

The average hydrodynamic size (R_h) and the VPTT of charge-balanced amphoteric terpolymer [NIPAM]:[APTAC]:[AMPS]=90:5:5 mol.% in deionized (DI) water and in NaCl solutions (μ = 0.001; 0.005; 0.01; 0.05; 0.1; 0.5; 1M NaCl) are presented in Figures 18 and 19.

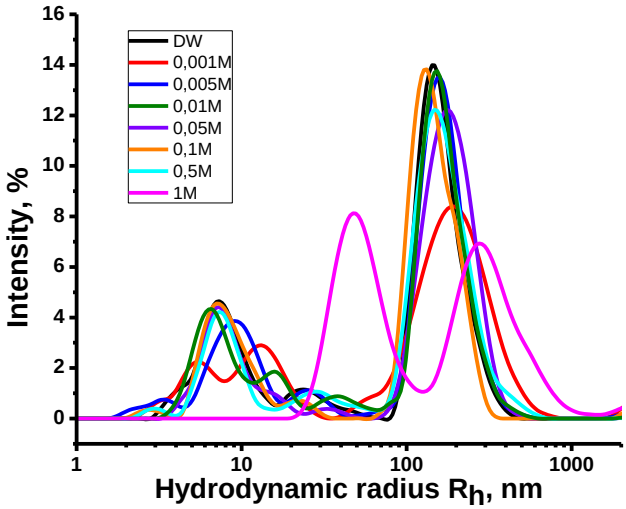

Figure 18 - The effect of the μ on the average hydrodynamic size of [NIPAM]:[APTAC]:[AMPS] = 90:5:5 mol.% at 25^{0}C

Figure 18 shows presence of two type of particles in solutions. Mean peak value of R_h of [NIPAM]:[APTAC]:[AMPS] = 90:5:5 mol.% equals to 7.4 and 150 nm in pure water. Evidently, that 7.4 nm represents individual macromolecules, whereas 150 nm corresponds to multimolecular aggregates. The relative contribution of the aggregates in the intensity distributions is big due to their high mass, though they are minor by their number. The individual chains of amphoteric terpolymer in deionized water may be imagined as well swollen coils since water is a good solvent for PNIPAM at room temperature. However, R_h=7.4 nm is not big enough for such a molecule. One should remember that the oppositely charged repeating units of the chain attract each other and may form ionic pairs similar to intrapolyelectrolyte complexes in pure water. Their low molar mass counterions become free, leave to the bulk water and this way increase the overall entropy of the system. Addition of low molar mass salt makes this entropic effect less pronounced: added salt breaks the intramolecular ionic pairs and chains become effectively more charged with increasing the ionic strength, though the number of charges along each chain remains constant. Coulomb interactions of ion pairs act on longer distances than H-bonds between PNIPAM and water and create polar regions of bound water within each coil, which enhance overall stability of the copolymer against phase separation upon heating.

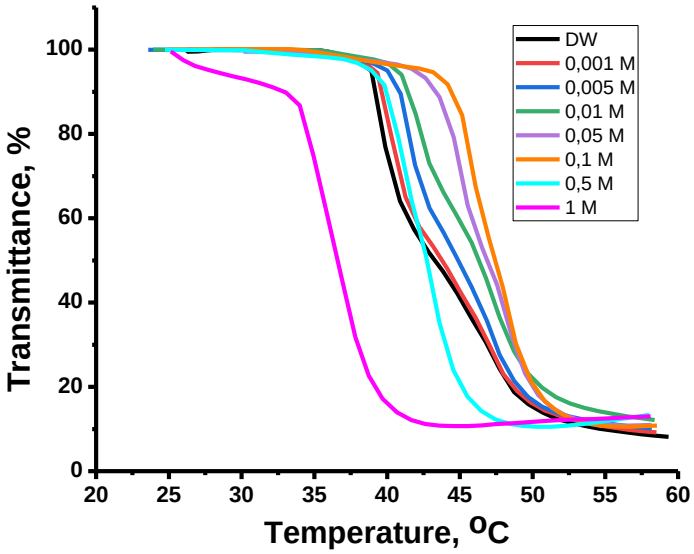

Figure 19 - Temperature dependent phase behavior of terpolymer [NIPAM]:[APTAC]:[AMPS] = 90:5:5 mol.% at various μ

The model presented above is fully supported by experiments. The volume phase transition temperature (VPTT) of [NIPAM]:[APTAC]:[AMPS] = 90:5:5 mol.% in DI water equals to 38.7°C (Table 7) and bigger than VPTT of PNIPAM itself (that is 32°C) [20]. When the ionic strength (μ) increases, the ion pairs between AMPS and APTAC break apart, copolymer becomes effectively more charged and VPTT shifts to the higher values. At μ above 0.1 M, all ionic pairs are not only broken but added salt screens all the charges of copolymer and original thermal behavior of pure PNIPAM is recovered.

Two phenomena must be discussed separately:

1) Aggregates formed by the copolymer above the VPTT are stable against further precipitation;

2) Transmittance vs. temperature curves show a shoulder above VPTT at μ below 0.1 M.

Formation of neutral colloidally stable multimolecular aggregates by poly(NIPAM) has been well documented and mechanisms responsible for their stability has been suggested [41, 132]. Existence of hydrated ion pairs from AMPS and APTAC within coils additionally contribute to the stability of particles above VPTT. Naturally, when aggregates are formed and dehydrate upon further heating, charged units cannot stay inside organic surrounding and they migrate to the surface of the aggregates, which is observed as a shoulder in the transmittance curves (Figure 20).

The conformational change of [NIPAM]:[APTAC]:[AMPS] = 90:5:5 mol.% in pure water upon heating is schematically shown in Figure 20. Dehydration of NIPAM fragments and enhancement of hydrophobic interactions with increasing of temperature result in formation of high-density hydrophobic NIPAM "core" surrounded by low-density hydrophilic "shell". The latter consists of AMPS and APTAC monomers that preserve the whole macromolecules in water and protect from precipitation.

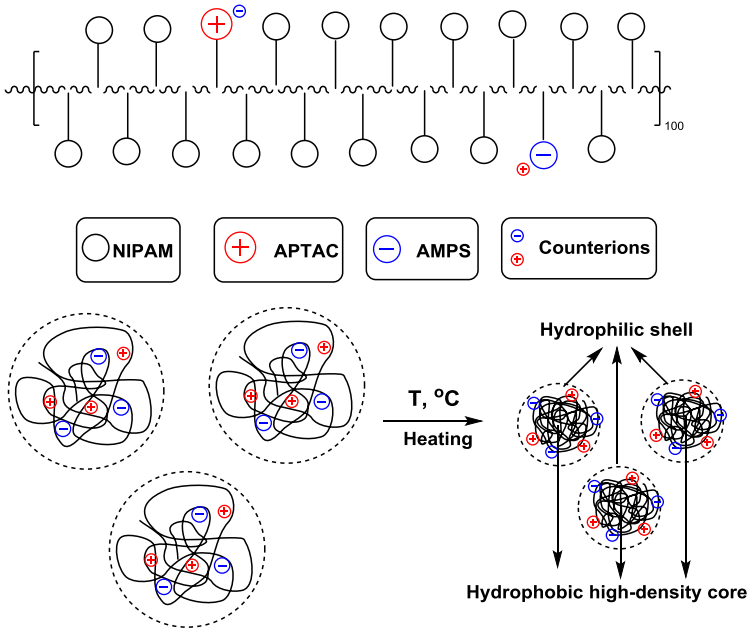

Figure 20 - Schematic representation of [NIPAM]:[APTAC]:[AMPS] = 90:5:5 mol.% terpolymer in DI water upon heating

At the interval of the μ = 0.001-0.1M NaCl the mean R_h values are equal to 7±1 nm and 175±25 nm. However, the value of VPTT gradually increases from 39.9°C in DI water to 46.1°C in 0.1M NaCl upon heating (Figure 21, Table 7).

Table 7 - Influence of temperature and ionic strength of the solution on the transmittance of terpolymers based on NIPAM-APTAC-AMPS

Terpolymer	Ionic strenght μ, mol·L^{-1} (NaCl)							
	0	0.001	0.005	0.01	0.05	0.1	0.5	1
	Volume phase transition temperature (VPTT), °C							
[NIPAM]:[APTAC]: [AMPS] = 90:5:5 mol.%	39.9	40.3	41.9	41.9	45.5	46.1	42.9	36.8
[NIPAM]:[APTAC]: [AMPS] = 90:2.5:7.5 mol.%	35.5	35.4	35.9	35.3	34.4	34.5	39.4	-
[NIPAM]:[APTAC]: [AMPS] = 90:7.5:2.5 mol.%	38.9	37.2	38.4	38.9	42.3	43.2	37.2	37.5

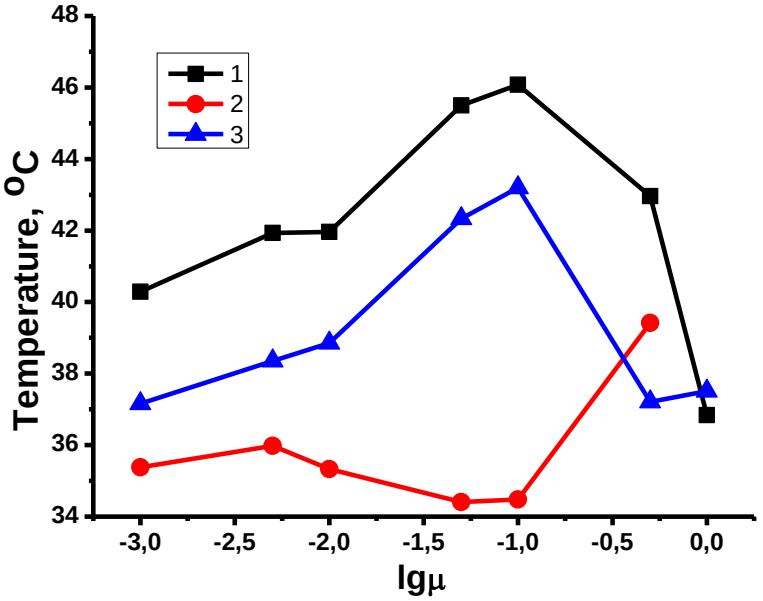

Figure 21 - Temperature dependent phase behavior of NIPAM-APTAC-AMPS terpolymers at various ionic strength (μ), where curve 1 - [NIPAM]:[APTAC]:[AMPS]=90:5:5 mol.%; curve 2 - [NIPAM]:[APTAC]:[AMPS]=90:2.5:7.5 mol.%; curve 3 - [NIPAM]:[APTAC]:[AMPS]=90:7.5:2.5 mol.%

These results can be explained as following. Upon heating the swollen in DI water macromolecular chains of amphoteric terpolymer due to strengthening of the hydrophobic interactions are supposed to transform to high-density hydrophobic "core" consisting of mostly NIPAM monomers. At the same time increasing of the ionic strength adjusted by NaCl strengthens the compactization of NIPAM chains but weakens the electrostatic attraction between positively and negatively charged monomers. As a result, the hydrophilic edge (or low-density hydrophilic "shell") consisting of AMPS and APTAC monomers is formed on the surface of compact macromolecules and preserves the polymer particles from precipitation (Figure 22).

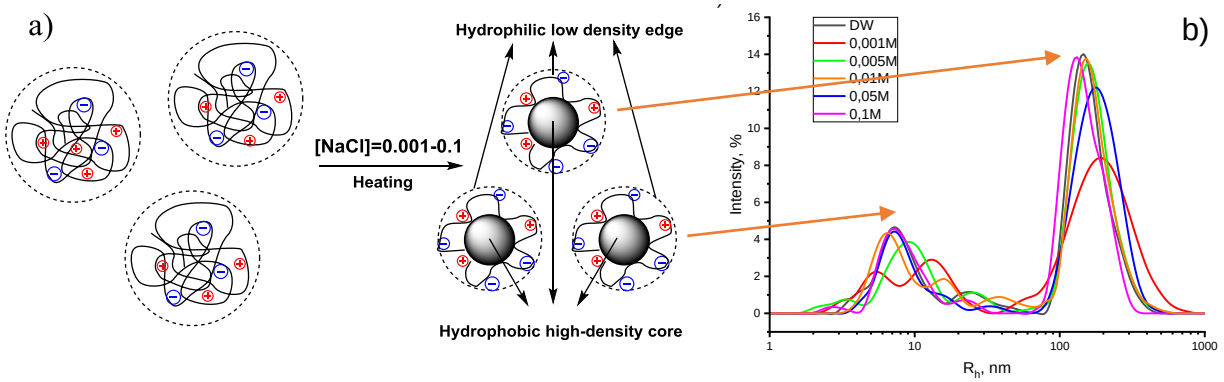

Figure 22 - Schematic representation of [NIPAM]:[APTAC]:[AMPS] = 90:5:5 mol.% macromolecules at the interval of μ = 0.001-0.1M NaCl upon heating (a) DLS data at μ = 0.001-0.1M NaCl (b)

However, in 1M NaCl solution the R_h maxima are shifted to 50 and 300 nm respectively. Probably at high μ the macromolecular coils aggregate. This statement is confirmed by the effect of temperature on the phase behavior of terpolymer [NIPAM]:[APTAC]:[AMPS]=90:5:5 mol.% in dependence of μ as shown in Figure 9. At the interval of μ between 0.5 and 1M NaCl the VPTT decreases from 39.5°C to 33.2°C (Table 7). The reversal or backward change of the VPTT in 0.5 and 1M NaCl solutions is probably due to aggregation of small particles to bigger one as demonstrated in Figure 23 and confirmed by DLS data. However, in 0.5 and 1M NaCl solutions the precipitation of aggregated macromolecular particles does not occur because the hydrophilic "shell" on the surface of such aggregates preserve them from precipitation.

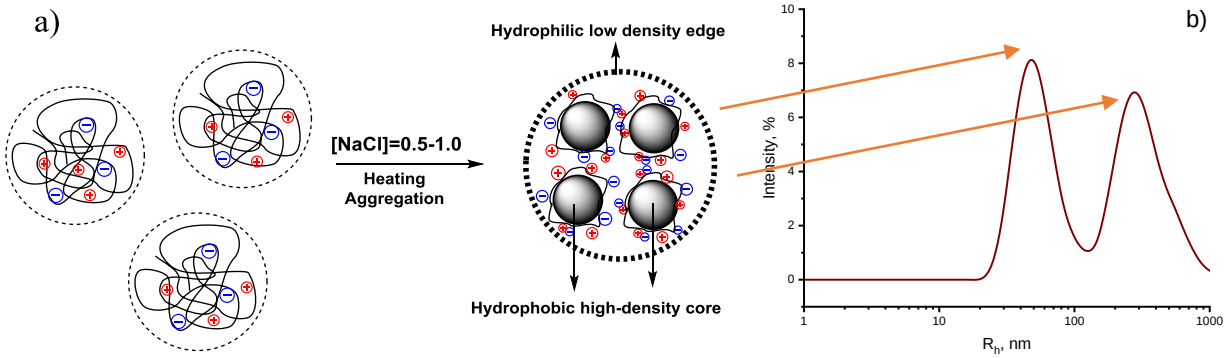

Figure 23 - Schematic representation of macromolecular size of [NIPAM]:[APTAC]:[AMPS] = 90:5:5 mol.% at the ionic strength 0.5 and 1M NaCl upon heating (a) and DLS data in 1M NaCl (b)

Thus as revealed from the obtained results, the macromolecular chains of [NIPAM]:[APTAC]:[AMPS] = 90:5:5 mol.% in DI water collapse upon heating due to dehydration of NIPAM chains and enhancement of hydrophobic interactions. At the interval of μ = 0.001-0.1 M NaCl macromolecular chains gradually shrink upon heating but preserve the solubility in spite of the turbidity. At high ionic strength μ = 0.5-1M NaCl the formation of bigger aggregates is observed.

Figure 24 represents the average hydrodynamic size of amphoteric terpolymer [NIPAM]:[APTAC]:[AMPS] =90:2.5:7.5 mol.% in DI water and in NaCl solutions

(μ = 0.001; 0.005; 0.01; 0.05; 0.1; and 0.5M). In 1M NaCl the terpolymer was insoluble. The average hydrodynamic radius of macromolecules R_h at μ = 0.001; 0.005; 0.01; 0.05; 0.1M NaCl is about 20-35 nm, but in 0.5M NaCl solution two obvious peaks with R_h equal to 20 and 200 nm are observed.

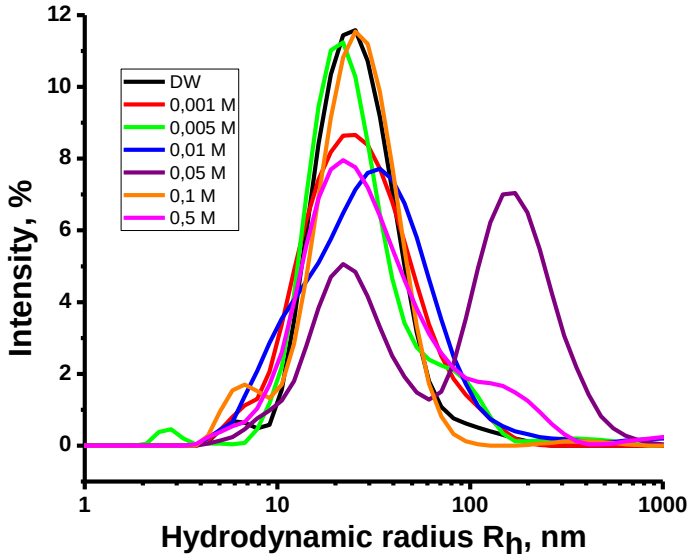

Figure 24 - Effect of the μ on the average hydrodynamic size of [NIPAM]:[APTAC]:[AMPS] = 90:2.5:7.5 mol.% at 25^{0}C

The effect of temperature on the phase behavior of terpolymer [NIPAM]:[APTAC]:[AMPS]=90:2.5:7.5 mol.% in DI water and at μ = 0.001-0.5M NaCl is shown in Table 7 and Figure 25.

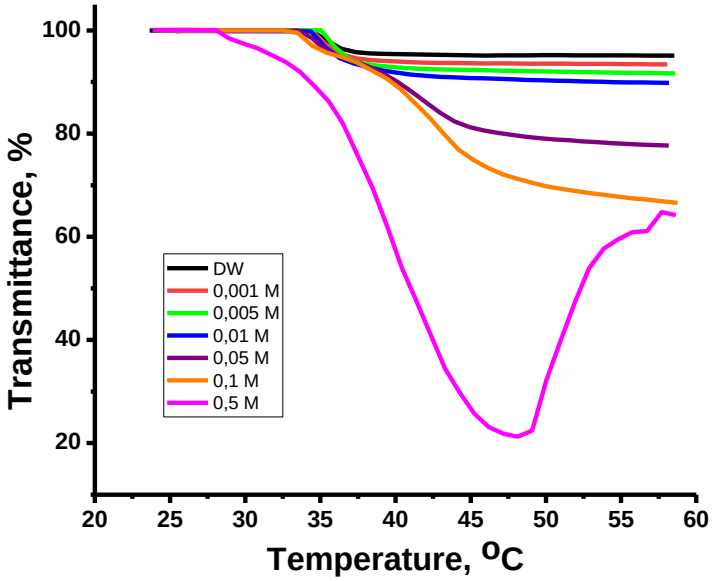

Figure 25 - Temperature dependent phase behavior of terpolymer [NIPAM]:[APTAC]:[AMPS] = 90:2.5:7.5 mol.% at various μ

At the interval of μ between 0.001 and 0.05M NaCl, the VPTT is slightly shifted to lower or higher temperatures. In this range a gradual increase of the

turbidity is observed. Increasing of the μ up to 0.5M NaCl leads to early phase separation of the polymer at 28 °C. At μ = 0.5 M NaCl there are fractures on the turbidity curves and the transparency decreases in the range of 40-47.5°C. Further heating of polymer solution at T > 47.5°C causes the precipitation of polymer chains because of salting-out effect leading to significant increase of the transparency.

In case of [NIPAM]:[APTAC]:[AMPS]=90:7.5:2.5 mol.% terpolymer, the average hydrodynamic size of macromolecules changes insignificantly as a function of the ionic strength (Figure 26). The average size of R_h lies in the regions of 6-8 nm and 150–300 nm.

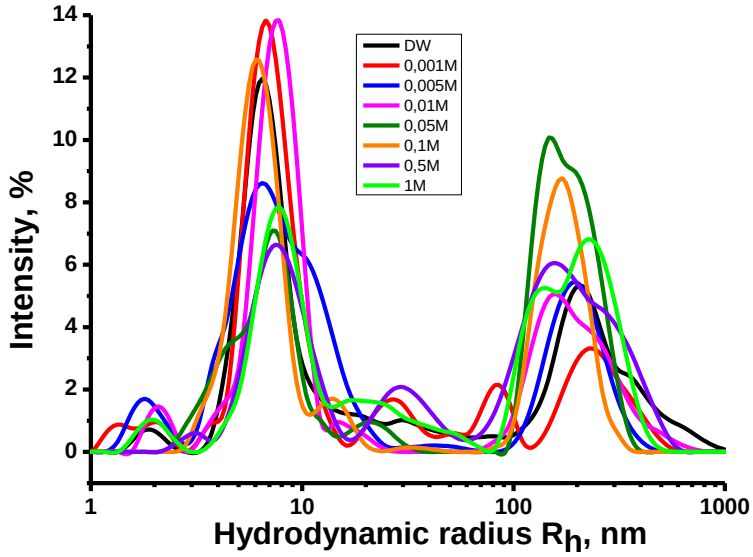

Figure 26 - Effect of the ionic strength of the solution on the average hydrodynamic size of [NIPAM]:[APTAC]:[AMPS] = 90:7.5:2.5 mol.% at 25^0C

The effect of temperature on the VPTT of the terpolymer [NIPAM]:[APTAC]:[AMPS]=90:7.5:2.5 mol.% at different ionic strength of the solution is shown in Table 7 and Figure 27.

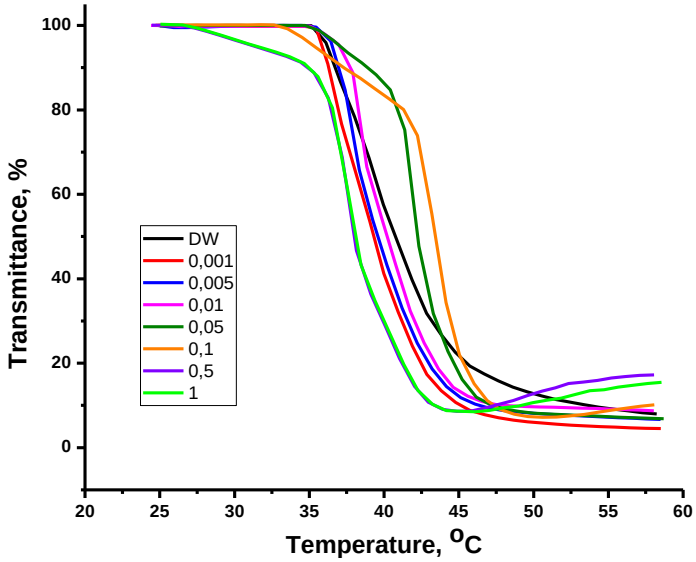

Figure 27 - Temperature dependent phase behavior of [NIPAM]:[APTAC]:[AMPS] = 90:7.5:2.5 mol.% at various μ

Increasing of the μ in the range of 0.001–0.1M gradually shifts the VPTT to higher temperatures. This is probably explained by screening of the positively charged APTAC fragments by counterions of the NaCl. However at higher ionic strength, μ = 0.5-1.0M NaCl the VPTT shifts backward, e.g. to lower temperatures. Apparently, at high concentration of NaCl the polyelectrolyte effect caused by the excess of positive charges is fully suppressed and the macromolecular chain becomes close to neutral chain and more hydrophobic. Increasing of the temperature enhances the hydrophobic interactions and aggregation of macromolecular chains. Thus, in aqueous-salt solutions the behavior of charge balanced amphoteric terpolymer ([NIPAM]:[APTAC]:[AMPS]=90:5:5 mol.%) differs from the properties of unbalanced polyampholytes ([NIPAM]:[APTAC]:[AMPS]=90:7.5:2.5 mol.% and [NIPAM]:[APTAC]:[AMPS]=90:2.5:7.5 mol.%). A small excess of positive or negative charges in terpolymers leads to domination of "polyelectrolyte effect". Expanded in pure water polyelectrolyte chains shrink in salt solution due to the screened electrostatic repulsion between uniformly charged monomers (polyelectrolyte effect). Compact structure of charge-balanced quenched polyampholyte unfolds in salt solution due to screening of the electrostatic attraction between oppositely charged monomers (the "antipolyelectrolyte effect") [126].

3.3 Synthesis and characterization of polyampholyte nanogels based on NIPAM-APTAC and NIPAM-AMPS

Polyampholyte nanogels of various compositions [NIPAM]-[APTAC] = 90:10 mol.% and [NIPAM]-[AMPS] = 90:10 mol.% (abbreviated as $NIPAM_{90}$-$APTAC_{10}$ and $NIPAM_{90}$-$AMPS_{10}$) were synthesized via conventional redox initiated free radical copolymerization (Figure 28).

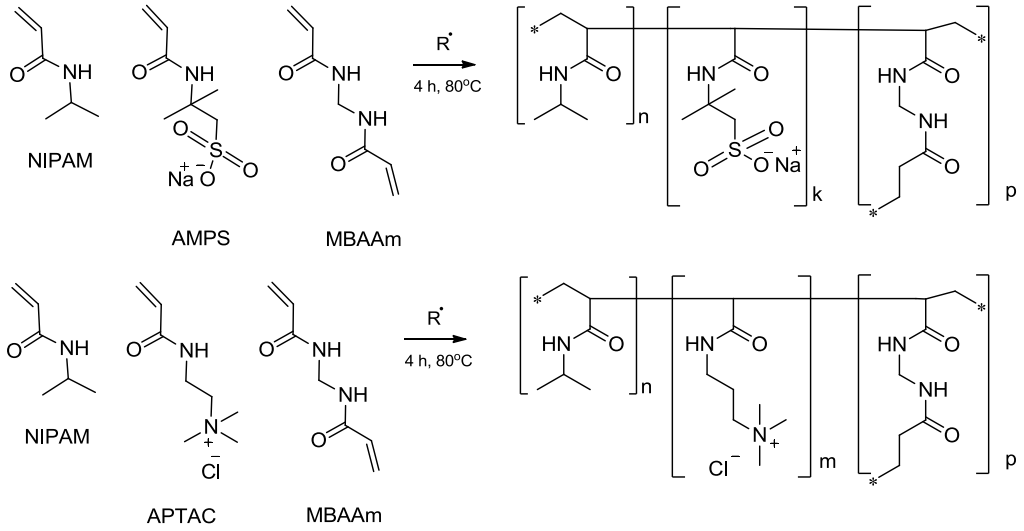

Figure 28 - Schematic representation of free radical copolymerization of NIPAM, APTAC and AMPS monomers for nanogels synthesis

The $NIPAM_{90}$-$APTAC_{10}$ and $NIPAM_{90}$- $AMPS_{10}$ nanogels contain either anionic or cationic monomers: $NIPAM_{90}$-$AMPS_{10}$ is negatively charged, $NIPAM_{90}$-$APTAC_{10}$ is positively charged.

The FTIR spectra of nanogels presented in Figure 29. The broad absorption band in the region of 3290–3500 cm^{-1} corresponds to the secondary and tertiary amine groups, and the absorption bands in the region of 2800–3000 cm^{-1} correspond to the asymmetric and symmetric vibrations of CH groups. Intensive peaks at ν =1640 and 1540 cm^{-1} belong to N-substituted groups (amide I and amide II). The S=O groups containing in AMPS fragments are detected at ν =1040 cm^{-1}.

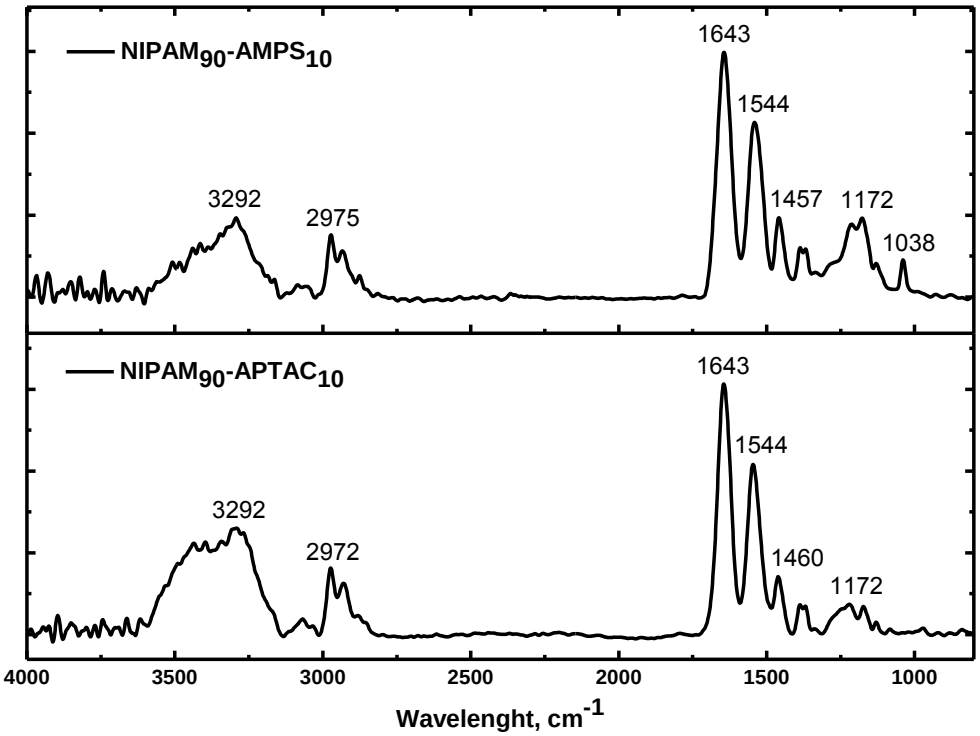

Figure 29 - FTIR spectra of NIPAM-APTAC and NIPAM-AMPS nanogels

Figure 30 shows the thermogravimetric and differential thermal analysis data for nanogels from which 3 regions can be defined.

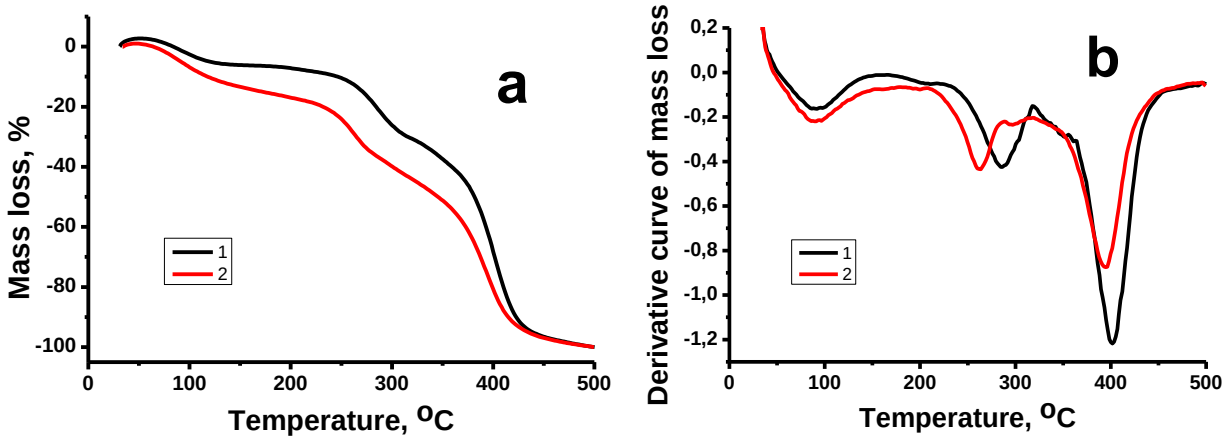

Figure 30 - TGA (a) and DTA (b) curves, where curve 1 - NIPAM$_{90}$-AMPS$_{10}$, curve 2 - NIPAM$_{90}$-APTAC$_{10}$

At >100°C, the sample mass is lost, probably due to the evaporation of physically adsorbed moisture. The weight loss between 250-300°C is probably due to the decomposition of NIPAM fragments. Complete thermal decomposition of nanogels occurs in the temperature range of 410-420°C [127].

3.3.1 Study of the thermo- and salt responsive properties of NIPAM-APTAC and NIPAM-AMPS nanogels in aqueous and saline solutions

Figures 31, 32 show the effect of temperature and salt additive on the phase behavior of the anionic NIPAM$_{90}$-AMPS$_{10}$ and cationic NIPAM$_{90}$-APTAC$_{10}$ nanogels. Since both NIPAM$_{90}$-AMPS$_{10}$ and NIPAM$_{90}$-APTAC$_{10}$ nanogels belong to anionic and cationic polyelectrolytes the salt additive leads to the screening of electrostatic repulsion between uniformly charged groups respectively. As a result, the macromolecular chains tend to shrink. However, at ionic strengths μ = 0.001 and 0.01 M, there are no changes in the phase behavior of the NIPAM$_{90}$-AMPS$_{10}$ nanogel and the transmittance remain constant. Only starting from μ = 0.1 M NaCl the polyelectrolyte effect is suppressed and the value of VPTT is equal to 42.1°C (Figure 31, Table 8). As the ionic strength increases further to μ = 0.5 and 1 M NaCl, the VPTT values of NIPAM$_{90}$-AMPS$_{10}$ decrease and are equal to 36.2 and 31.3°C, respectively. The VPTT value at μ = 1 M is less than the LCST of pure PNIPAM, which is ~33°C. Probably, at high concentrations of NaCl, screening of the electrostatic repulsion between the negatively charged AMPS groups is so effective that the phase behavior and solubility of NIPAM$_{90}$-AMPS$_{10}$ nanogel is determined by NIPAM$_{90}$ fragments.

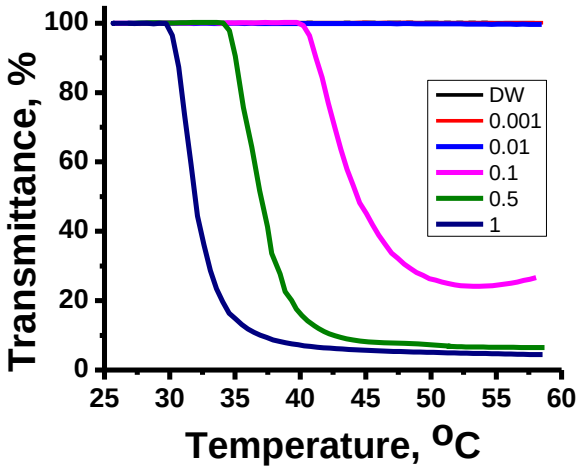

Figure 31 - Effect of temperature and ionic strength (μ) on transmittance of $NIPAM_{90}$-$AMPS_{10}$ nanogel

In case of $NIPAM_{90}$-$APTAC_{10}$ nanogel the ionic strength in the range μ = 0.001 - 0.1 M NaCl does not significantly change the phase behavior of the $NIPAM_{90}$-$APTAC_{10}$ nanogel and the values of VPTT are equal to 46.4, 47.7, and 45.2°C, respectively (Figure 32, Table 8). Even further increase of the ionic strength up to μ = 0.5 and 1 M slightly changes the solubility and phase behavior of the $NIPAM_{90}$-$APTAC_{10}$ nanogel. This is probably explained by stronger polyelectrolyte character of $NIPAM_{90}$-$APTAC_{10}$ nanogel compared to $NIPAM_{90}$-$AMPS_{10}$ and its less salt-sensitivity. An increase in temperature enhances inter- and intramolecular hydrophobic interactions between $NIPAM_{90}$ fragments, thereby causing a shift in the VPTT towards lower temperatures, that are equal to 41.8 and 35.9°C, respectively.

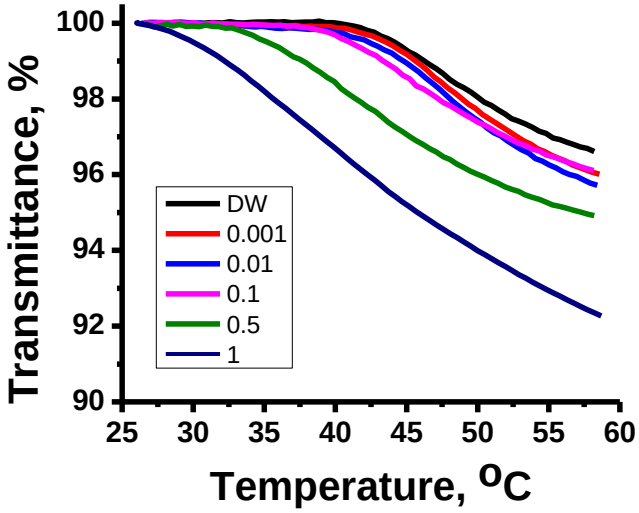

Figure 32 - Effect of temperature and ionic strength (μ) on transmittance of $NIPAM_{90}$-$APTAC_{10}$ nanogel

Table 8 - The effect of the ionic strength on the volume phase transition temperature of $NIPAM_{90}$-$AMPS_{10}$ and $NIPAM_{90}$-$APTAC_{10}$ nanogels

Nanogel	Ionic strength, μ, mol·L^{-1} (NaCl)					
	0	0.001	0.01	0.1	0.5	1.0
	Volume phase transition temperature, VPTT, °C					
$NIPAM_{90}$-$AMPS_{10}$	-	-	-	42.1	36.2	31.3
$NIPAM_{90}$-$APTAC_{10}$	48	46.4	47.7	45.2	41.8	35.9

Thus, $NIPAM_{90}$-$AMPS_{10}$ and $NIPAM_{90}$-$APTAC_{10}$ nanogels exhibit a strong polyelectrolyte effect and only at higher ionic strength μ > 0.1 M NaCl the polyelectrolyte effect is suppressed due to screening of the electrostatic repulsion between uniformly charged groups by low-molecular-weight electrolytes.

The mean hydrodynamic size was measured in a 0.1 wt.% solution of $NIPAM_{90}$-$AMPS_{10}$ and $NIPAM_{90}$-$APTAC_{10}$ nanogels in the temperature range from 25 to 50°C with an interval of 5°C in DI water and in NaCl solutions with μ = 0.001; 0.1 and 1 M.

The dependence of the average hydrodynamic particle size of the $NIPAM_{90}$-$AMPS_{10}$ nanogel on temperature and ionic strength is shown in Figure 29. It was previously described that the ionic strength equal to μ = 0.001 M does not affect the phase behavior of the nanogel, the transmittance remains constant (Figure 31). Therefore, an increase of temperature does not affect the nanogel particle size, in the temperature range of 25-50°C in 0.001 M NaCl solution R_h is ~ 10-20 nm (Figure 33a). At μ = 0.1 M and temperatures of 25–35°C, there are particles with sizes of ~12, 60 and 100 nm (Figure 33b). The VPTT of the nanogel in a 0.1 M NaCl solution is 42.1°C (Table 8); upon reaching 40°C, in addition to particles with a size of ~12 nm, the aggregation of nanogel particles is observed and R_h increases up to 300 nm. At 45 and 50°C, the R_h particle size is ~250 and 300 nm, respectively.

At 25°C and ionic strength μ = 1 M, the particle size is ~15 nm (Figure 33c). Increasing the temperature to 30°C leads to aggregation of nanoparticles and their size R_h is 240 nm. The VPTT of the $NIPAM_{90}$-$AMPS_{10}$ nanogel in 1 M NaCl is 31.3°C (Table 8), therefore, an increase in size up to ~550 nm at 35-40°C is observed. A further increase in temperature to 45-50°C leads to a decrease in the particle size to 310–420 nm; probably, the formed nanogel aggregates begin to shrink.

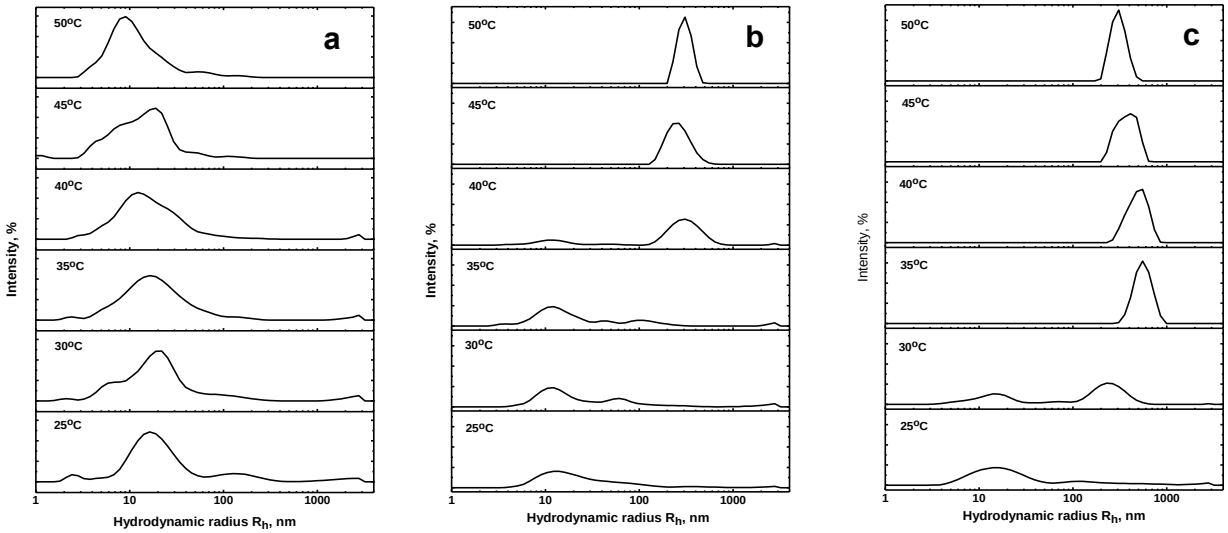

Figure 33 - Effect of temperature and ionic strength (μ) on the mean hydrodynamic radius (R_h) of $NIPAM_{90}$-$AMPS_{10}$ at μ = (a) 0.001, (b) 0.1 and (c) 1.0

The effect of temperature and salt additive on the average hydrodynamic particle size of the $NIPAM_{90}$-$APTAC_{10}$ nanogel is shown in Figure 34. At ionic strength μ = 0.001 and 0.1 M and in the temperature range of 25-35°C, the particle size R_h is ~ 15, 115 nm (Figure 34a, 34b). An increase of temperature to 40°C leads to a decrease in the size of R_h particles to ~10 and 60 nm. At 45 and 50°C, temperatures close to VPTT (Table 8), the particle size distribution becomes monomodal and have values ~ 95 nm in 0.001 M NaCl solution and ~ 60 nm in 0.01 M. In solutions with ionic strength μ = 1 M at room temperature, the R_h is ~10 and 90 nm (Figure 34c). With a further increase in temperature from 30 to 50°C, the average R_h values are in the range of 60-70 nm; therefore, at temperatures close to the VPTT, no significant changes in size occur [127].

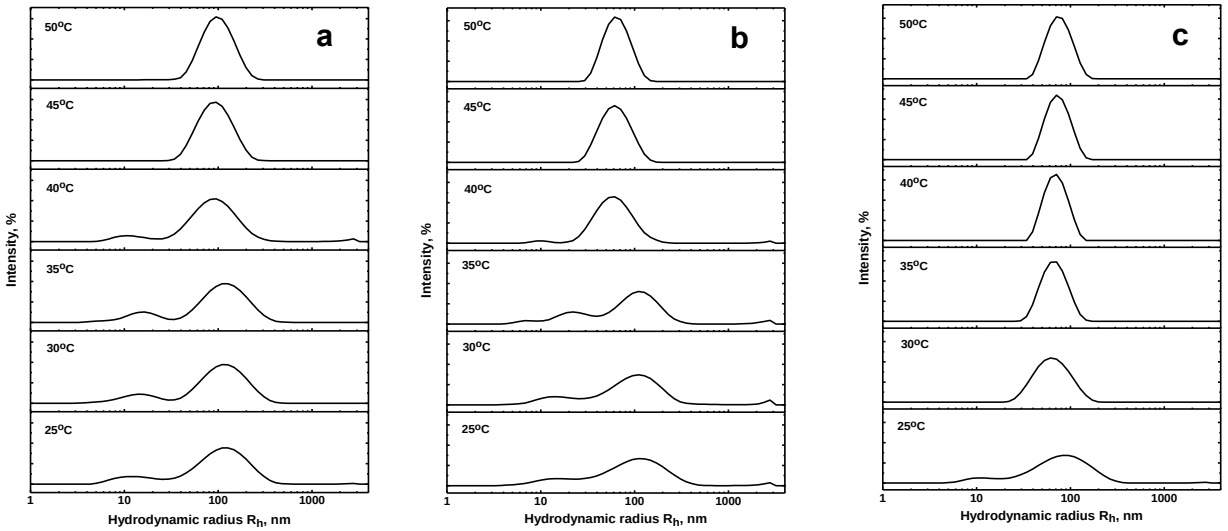

Figure 34 - Effect of temperature and ionic strength (μ) on the mean hydrodynamic radius (R_h) of $NIPAM_{90}$-$APTAC_{10}$ at μ = (a) 0.001, (b) 0.1 and (c) 1.0

3.4 Synthesis and characterization of polyampholyte nanogels based on NIPAM-APTAC-AMPS

Polyampholyte nanogels of various compositions [NIPAM]-[APTAC]-[AMPS] = 90:5:5; 90:2.5:7.5 and 90:7.5:2.5 mol.% (abbreviated as $NIPAM_{90}$-$APTAC_5$-$AMPS_5$, $NIPAM_{90}$-$APTAC_{2.5}$-$AMPS_{7.5}$, $NIPAM_{90}$-$APTAC_{7.5}$-$AMPS_{2.5}$) were synthesized via conventional redox initiated free radical copolymerization (Figure 35) [133].

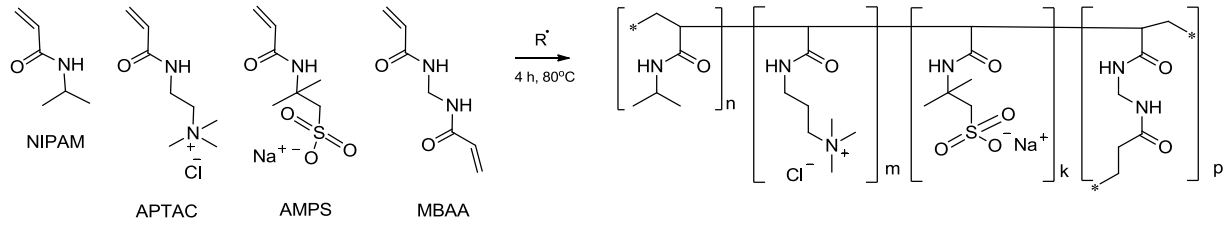

Figure 35 - Schematic representation of free radical copolymerization of NIPAM, APTAC and AMPS monomers for nanogels synthesis

Based on research by Braun et al. [76], it is expected that the composition of final products will closely match the composition of initial mixture of monomers with drifting ± 0.5 mol.%. A good agreement between the calculated and found sulfur content confirms the same composition of initial monomer mixture and the obtained nanogels (Table 9).

Table 9 - The results of elemental analysis of NIPAM-APTAC-AMPS nanogels

Initial monomer mixture, mol.%			Calculated/Found	Percentage of elements, wt.%			
				H	C	N	S
NIPAM	APTAC	AMPS					
90	5	5	Calculated	9.26	59.69	11.89	1.29
			Found	7.08	44.85	8.96	1.26
90	7.5	2.5	Calculated	9.4	60.21	12.23	0.65
			Found	8.52	54.04	10.79	1.35
90	2.5	7.5	Calculated	9.12	59.18	11.55	1.93
			Found	8.47	52.63	10.91	1.58

Figure 36 shows the FTIR spectra of NIPAM-APTAC-AMPS nanogels. The broad absorption band in the region of 3290–3500 cm^{-1} corresponds to the secondary and tertiary amine groups, and the absorption bands in the region of 2800–3000 cm^{-1} correspond to the asymmetric and symmetric vibrations of CH groups. The absorption bands at 1640 and 1540 cm^{-1} belong to the vibrations of the N-substituted groups, which are the amide I and amide II groups, respectively. The absorption band at 1460 cm^{-1} is characteristic of the bending vibrations of the CH groups. Finally, the absorption band in the region of 1040 cm^{-1} corresponds to the fluctuations of the S=O groups of the AMPS units.

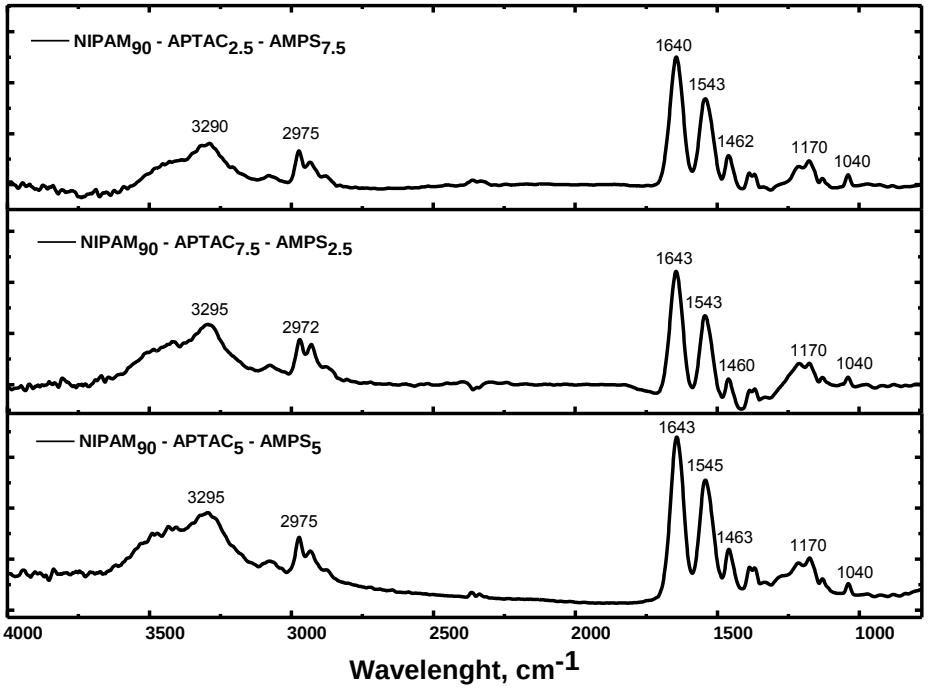

Figure 36 - FTIR spectra of NIPAM-APTAC-AMPS nanogels

The composition of the resultant polyampholyte nanogels was determined by ^{1}H NMR spectroscopy (Figure 37).

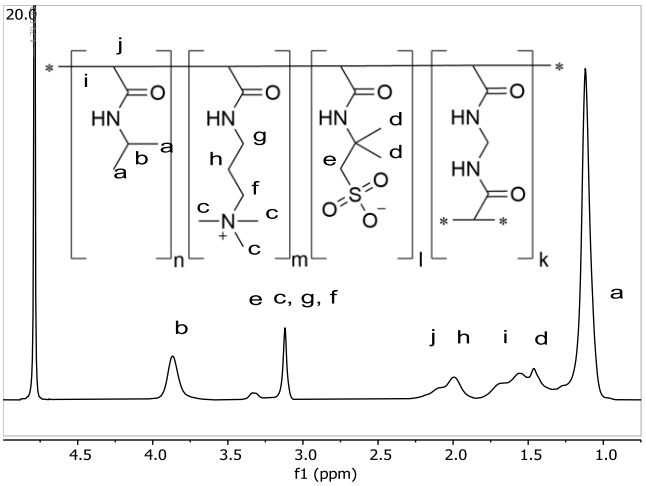

Figure 37 - ^{1}H NMR spectra of NIPAM-APTAC-AMPS nanogels and identification of proton signals

The resonance bands observed at 1.8 and 2.2 ppm were attributed to the protons of the methylene and methine groups of the main chain of the nanogels, respectively. However, these peaks overlapped with the methyl and methylene protons of AMPS and APTAC. The resonance bands at 3.2-3.4 ppm were assigned to the suspended protons of the methyl and methylene groups in AMPS and APTAC. It can be assumed that the amount of APTAC and AMPS in nanogels will be in good agreement with the initial mixture of monomers, since the reactivity of all monomers

is similar and close to one [76]. Taking into account all above reasons, it can be argued that the final composition of nanogels has a balanced and charge-imbalanced structure. For example, the $NIPAM_{90}$-$APTAC_5$-$AMPS_5$ amphoteric nanogel, consisting of an equal amount of positively (APTAC) and negatively (AMPS) charged monomers, refers to a charge-balanced polyampholyte, while the $NIPAM_{90}$-$APTAC_{2.5}$-$AMPS_{7.5}$ and $NIPAM_{90}$- $APTAC_{7.5}$-$AMPS_{2.5}$ containing an excess of positively (APTAC) or negatively (AMPS) charged monomers are charge-imbalanced polyampholyte nanogels.

To quantitatively describe the degree of the volume phase transition of NIPAM-APTAC-AMPS nanogels, ^{1}H NMR measurements were performed as a function of temperature (Figures 37 and 38). Almost all the protons of the PNIPAM units can be observed in the ^{1}H NMR spectra and assigned. However, the exact number of APTAC and AMPS units cannot be precisely determined, due to overlapping of certain peaks (Figure 37).

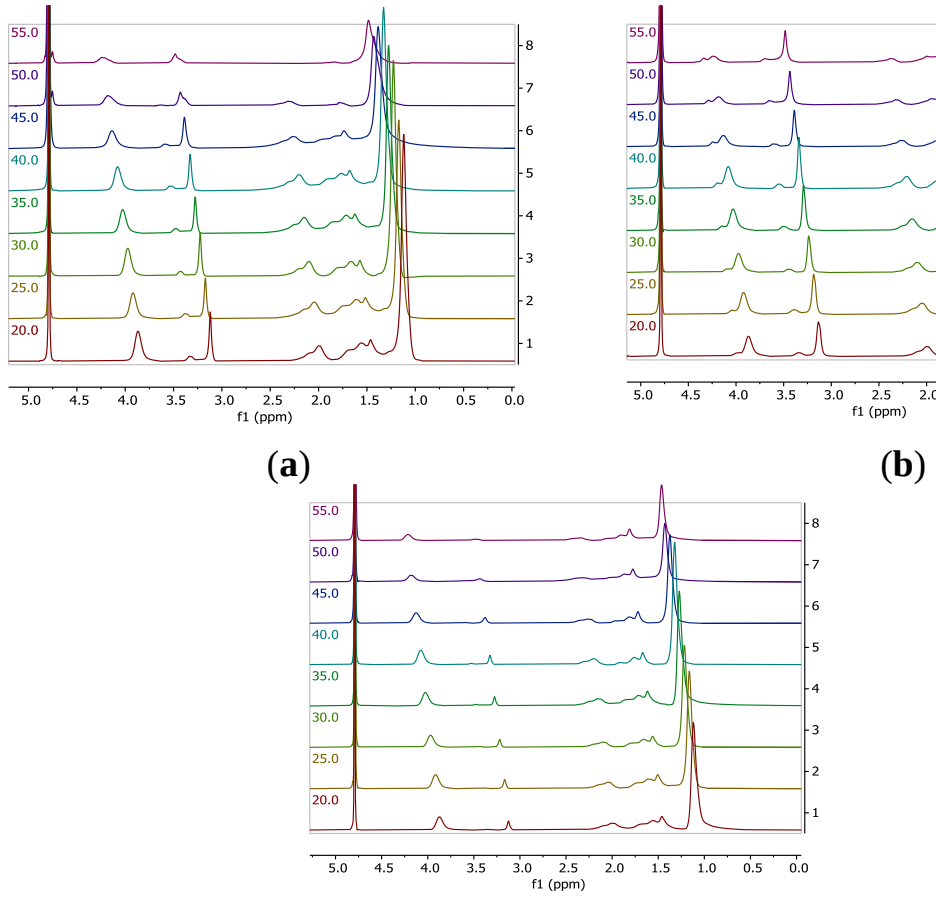

Figure 38 - Temperature-variable ^{1}H NMR of NIPAM-APTAC-AMPS nanogels: (a) $NIPAM_{90}$- $APTAC_5$-$AMPS_5$; (b) $NIPAM_{90}$-$APTAC_{7.5}$-$AMPS_{2.5}$; (c) $NIPAM_{90}$-$APTAC_{2.5}$-$AMPS_{7.5}$

The resonance peaks *a* and *b* are attributed to PNIPAM segments, with peak *b* chosen as the reference to calculate the degree of volume phase transition of the NIPAM-APTAC-AMPS nanogels. The D_2O peak does not shift over the whole temperature range of 25 to 55°C. Though, as expected, all other peaks shifted toward

the lower field, and a notable decrease in intensity was observed as the temperature was raised [134, 135]. The proton signals of PNIPAM moieties after volume phase transition were barely detectable, and only the protons from the surface of the nanogel particles, still soluble in D_2O, could be detected.

By using Equation 1, characterization of the degree of volume phase transition is possible:

$$p = 1 - \left(\frac{I}{I_0}\right), \tag{1}$$

where p is volume phase-separated fraction; and, I and I_0 are the integrated intensities of peak b at the specified temperature and at 20°C, respectively.

Figure 39 shows how changing temperature influences the volume phase-separated fraction, p, for different compositions of NIPAM-APTAC-AMPS nanogels, which exhibit a much weaker volume phase transition than free linear PNIPAM, due to the strongly charged APTAC and AMPS groups along the macromolecular chain. At higher temperatures, the hydrophobization of NIPAM groups can create a hydrophobic core, while the ionic APTAC and AMPS groups can stabilize the nanogel particles in an aqueous medium. Therefore, permeability, stability and dispersion of drug-loaded amphoteric nanogels can potentially be used in drug delivery systems [135].

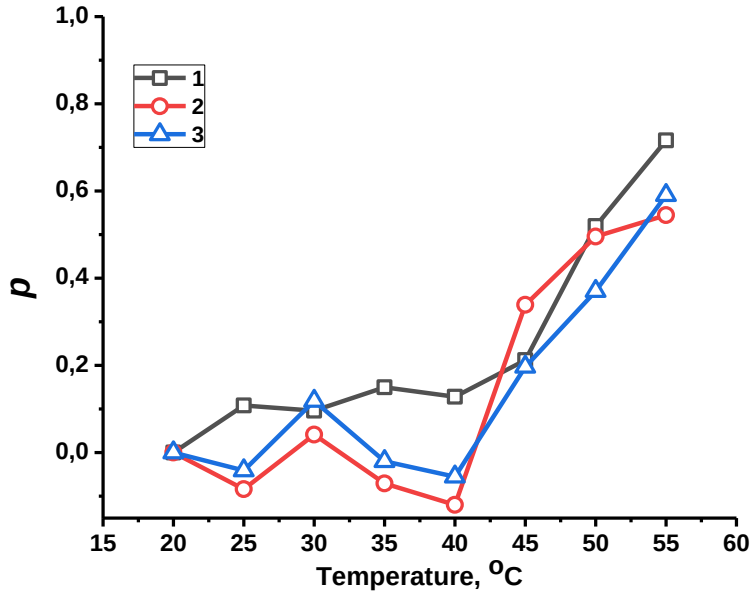

Figure 39 - Temperature dependent volume phase-separated fraction (p) for NIPAM-APTAC-AMPS nanogels in D_2O, with curves (1) $NIPAM_{90}$-$APTAC_5$-$AMPS_5$; (2) $NIPAM_{90}$-$APTAC_{7.5}$-$AMPS_{2.5}$; (3) $NIPAM_{90}$-$APTAC_{2.5}$-$AMPS_{7.5}$

Following volume phase transition, NIPAM-APTAC-AMPS nanogels demonstrate a higher volume phase-separated fraction, from 0,54 to 0,72, which is much lower than that of linear pure PNIPAM, p = 0.95. Introduction of APTAC and

AMPS groups can be concluded to be responsible for decreases in volume phase transition temperature. For precise determination of volume phase transition temperatures, Boltzmann fitting was calculated using Equation 2 for all points in Figure 39.

$$y = \frac{A_1 - A_2}{1 + e^{\frac{(x - x_0)}{dx}}} + A_2, \quad (2)$$

where A_1 is the minimum value of the function; A_2 is the maximum value of the function; x_0 is the value on the *x* axis corresponding to the inflection of the curve, which corresponds to the volume phase transition temperature, VPTT; and, *dx* is the domain where x_0 lies [136].

Charge-balanced $NIPAM_{90}$-$APTAC_5$-$AMPS_5$ has a transition temperature of around 48.7°C, but for the charge-imbalanced, positively and negatively, nanogels the transition temperatures are 44.8 and 48.7°C, respectively. The volume phase transition temperature of the nanogels, as determined by UV-Vis in deionized water, is equal to 40.4°C for the charge-balanced gel, 41.5°C for the negatively charged variant, and 44.1°C for the positively charged one. These values are lower than calculated using Equation 1, because in the volume phase separation fraction, the presence of ionic APTAC and AMPS are thought to weaken the volume phase transition behavior of the nanogels.

The results of thermogravimetric and differential thermal analysis for NIPAM-APTAC-AMPS nanogels are shown in Figure 40 (a, b).

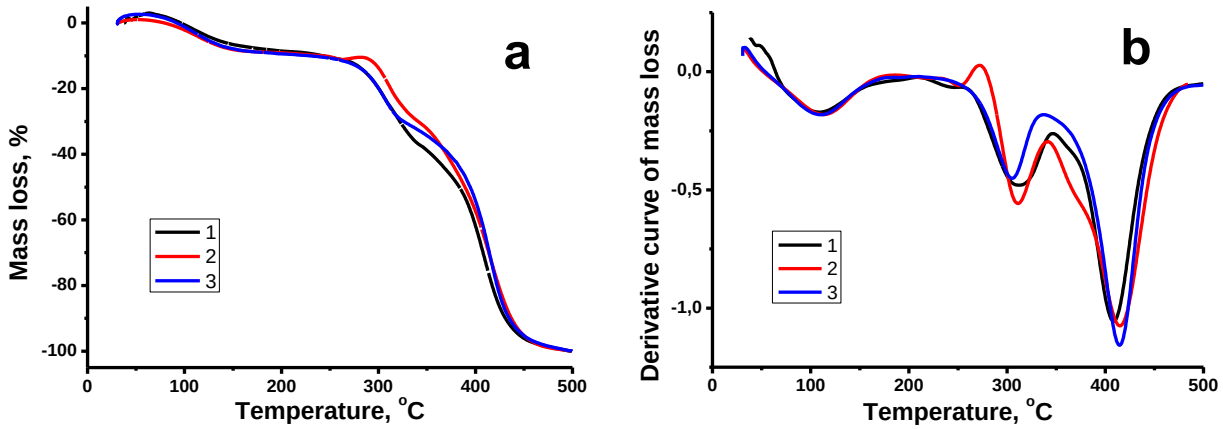

Figure 40 - TGA thermograms (a) and differential curves (b) of nanogels, where curve 1 - $NIPAM_{90}$-$APTAC_5$-$AMPS_5$; curve 2 - $NIPAM_{90}$-$APTAC_{7.5}$-$AMPS_{2.5}$; curve 3 - $NIPAM_{90}$-$APTAC_{2.5}$-$AMPS_{7.5}$

The TGA curves demonstrate that three losses in weight occur. The first, at >100°C, is probably due to evaporation of physically adsorbed moisture. The second, at >300°C, is due to decomposition of NIPAM fragments. Complete thermal decomposition of the nanogels occurs in the temperature range of 410-420°C.

The zeta potentials of charge-balanced and charge-imbalanced solutions of 0.1 wt.% NIPAM-APTAC-AMPS nanogels were measured at 25°C. In aqueous

solution, $NIPAM_{90}$-$APTAC_{7.5}$-$AMPS_{2.5}$, with an excess of positively charged APTAC monomer, has $\zeta = +4\pm1$ mV. $NIPAM_{90}$-$APTAC_{2.5}$-$AMPS_{7.5}$, with an excess of negatively charged AMPS monomer, has $\zeta = -7\pm1$ mV. In the case of the charge-balanced $NIPAM_{90}$-$APTAC_5$-$AMPS_5$, the zeta potential is slightly positive, $\zeta = +1.5\pm1$ mV. Likely, this is due to a small excess of positively charged APTAC monomer.

The temperature dependence of the zeta potentials of the NIPAM-APTAC-AMPS nanogels in 0.001 M NaCl solution is shown in Figure 41. In a temperature range of 25°C to 60°C, the charge-balanced nanogels have a zeta potential value of +4±2 mV. However, in the case of charge-imbalanced nanogels, the zeta potential rose after the temperature of the solution had been increased. Thus, the positively charged nanogel, $NIPAM_{90}$-$APTAC_{7.5}$-$AMPS_{2.5}$, has a zeta potential of around +5 mV at a temperature of 25°C, but as the temperature rises to 40°C, the zeta potential increases up to +25 mV. On the other hand, in the same temperature range, the negatively charged nanogel, $NIPAM_{90}$-$APTAC_{2.5}$-$AMPS_{7.5}$, displayed a monotonic change in the zeta potential from -5 mV up to -30 mV. At 25°C, the nanogels are thought to be predominantly in the swollen coiled state. With an increase in temperature, hydrophobic interactions between isopropyl radicals are enhanced, causing compactization of coils and the progressive release of charged groups to the outer layers of these compressed coils. This leads to the accumulation of positive or negative charges on the outside of charge-imbalanced nanogel particles, and an increase in the zeta-potential of the macromolecules. For charge-balanced nanogels, this effect also takes place, but due to mutual compensation of positively and negatively charged APTAC and AMPS groups, the zeta value changes insignificantly [128].

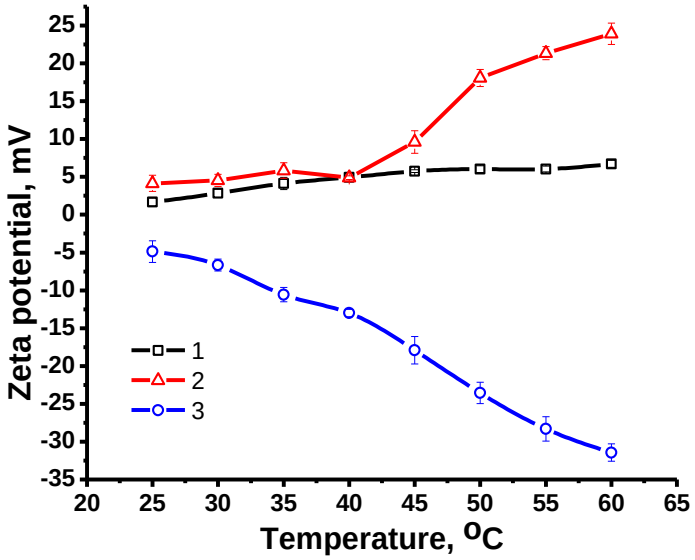

Figure 41 - Zeta potentials of nanogels in 0.001 M NaCl solution, where curve 1 - $NIPAM_{90}$-$APTAC_5$-$AMPS_5$; curve 2 - $NIPAM_{90}$-$APTAC_{7.5}$-$AMPS_{2.5}$; curve 3 - $NIPAM_{90}$-$APTAC_{2.5}$-$AMPS_{7.5}$

SEM data show that nanogel particles have glued or stuck aggregates connected by narrow necks and voids of nanometer and micron size (Figure 42). Due to multiple contacts between spherical or wormlike nanogels, macroscopic gelation occurs, leading to formation of three-dimensional networks of nanogels [137].

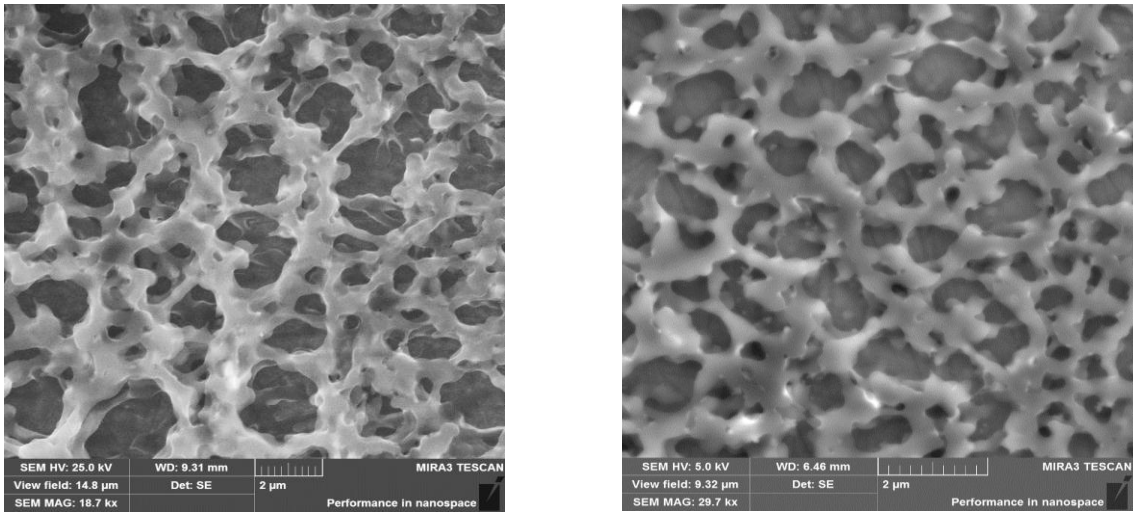

Figure 42 - SEM photographs of nanogels based on NIPAM-APTAC-AMPS

3.4.1 Study of the thermo- and salt responsive properties of polyampholyte nanogels based on NIPAM-APTAC-AMPS

In the charge-balanced nanogel, $NIPAM_{90}$-$APTAC_5$-$AMPS_5$, the oppositely charged monomers mutually compensate each other in pure water. However, the VPTT of $NIPAM_{90}$-$APTAC_5$-$AMPS_5$ increases upon the addition of salt, which can be explained by the antipolyelectrolyte effect (Figure 43). At the lower and moderate ionic strength, μ = 0.001-0.1 M NaCl, the electrostatic attraction between positively and negatively charged monomers gradually decreases, which leads to unfolding of polymer chains, additional hydrophilization, and an increase of the VPTT. At the high ionic strengths, μ = 0.5 and 1 M NaCl, the macromolecular system becomes similar to neutral polymer, because the salt ions completely screen the positive and negative charges of the macromolecules. Under such conditions, the solubility and volume phase behavior of $NIPAM_{90}$-$APTAC_5$-$AMPS_5$ is likely determined by the NIPAM fragments. Moreover, the higher the ionic strength, the more often the salting out effect occurs, leading to overall hydrophobization of the macromolecular chains and, consequently, to a decrease in the VPTT (Figure 44, Table 10).

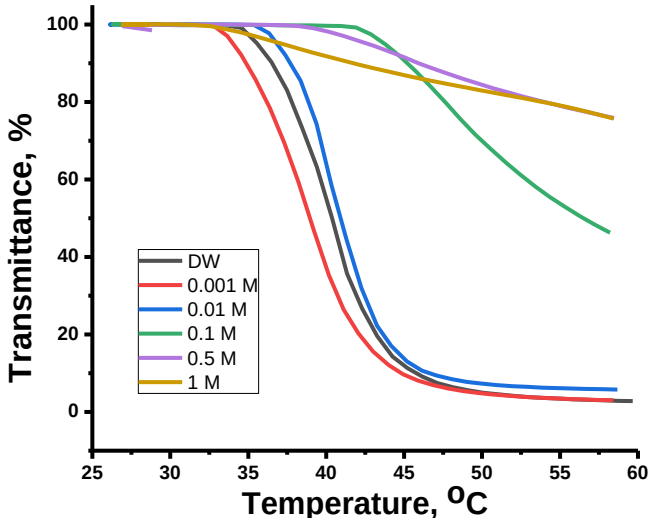

Figure 43 - Effect of temperature and ionic strength of the solution on the transmittance of the NIPAM$_{90}$-APTAC$_5$-AMPS$_5$ nanogel

Table 10 - Influence of temperature and ionic strength of the solution on the transmittance of nanogels based on NIPAM-APTAC-AMPS

Nanogel	Ionic strenght μ, mol·L^{-1} (NaCl)					
	0	0.001	0.01	0.1	0.5	1.0
	Volume phase transition temperature (VPTT), °C					
NIPAM$_{90}$-APTAC$_5$-AMPS$_5$	40.4	39.2	40.4	47.8	45.1	38.3
NIPAM$_{90}$-APTAC$_{7.5}$-AMPS$_{2.5}$	44	45.0	44.4	44.3	39.5	33.5
NIPAM$_{90}$-APTAC$_{2.5}$-AMPS$_{7.5}$	41.5 -	40.7 -	41.7 -	42.0 -	39.6 51.1	33.0 47.1

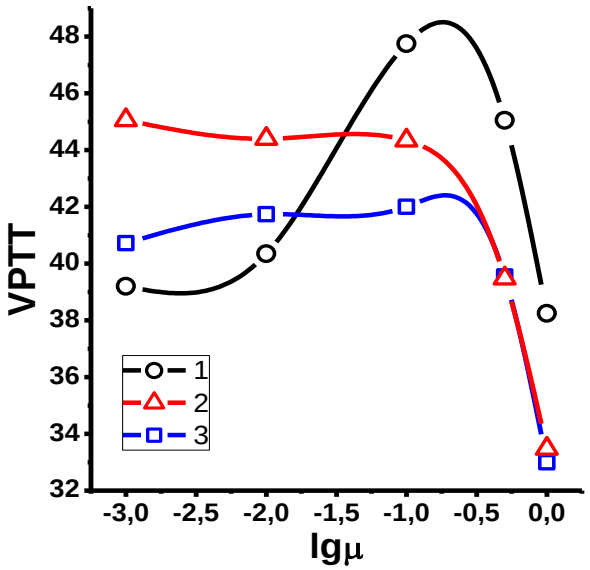

Figure 44 - Temperature dependent phase behavior of nanogels based on NIPAM-APTAC-AMPS at various ionic strength (μ), with curves 1 - NIPAM$_{90}$-APTAC$_5$-AMPS$_5$; 2 - NIPAM$_{90}$-APTAC$_{7.5}$-AMPS$_{2.5}$; 3 - NIPAM$_{90}$-APTAC$_{2.5}$-AMPS$_{7.5}$

Distributions of the mean hydrodynamic radius (R_h) were studied for the $NIPAM_{90}$-$APTAC_5$-$AMPS_5$ nanogel within a temperature range of 25-50°C and at μ = 0.001, 0.1 and 1 M NaCl (Figure 45). At 25°C and μ = 0.001 M, $NIPAM_{90}$-$APTAC_5$-$AMPS_5$ has a particle size of R_h = 18-20 nm (Figure 45a). Several peaks corresponding to ~10, 40 and 90 nm are observed in solutions at higher ionic strengths (μ = 0.1 and 1.0). The appearance of such large particles is probably connected with the unfolding of macromolecular chains, due to the antipolyelectrolyte effect, and the formation of clumps of nanogel particles. However, such clumps are not numerous.

Unfolding of nanogel particles is promoted when temperature is increased. In the transition region, T = 35-40°C, the R_h of the clumps reached 500-600 nm at μ = 0.001 M NaCl. Under these conditions, the antipolyelectrolyte effect is negligible, and the hydrophobicity of the NIPAM units dominates. Volume phase transition occurs at 47.8°C and μ = 0.1 M. Unfolding of the nanogel particles increases as the temperature is raised, up to a maximum at 45.1°C, but then the structure of the particles remains constant (Figure 45b). Further increases in ionic strength result in electrostatic screening of the APTAC and AMPS units. The antipolyelectrolyte effect is suppressed at μ = 1 M, at which point volume phase transition is solely determined by the NIPAM units (Figure 45c). In all the solutions studied, clumping in the nanogels remained colloidally stable above the VPTT, and no macroscopic phase separation was observed.

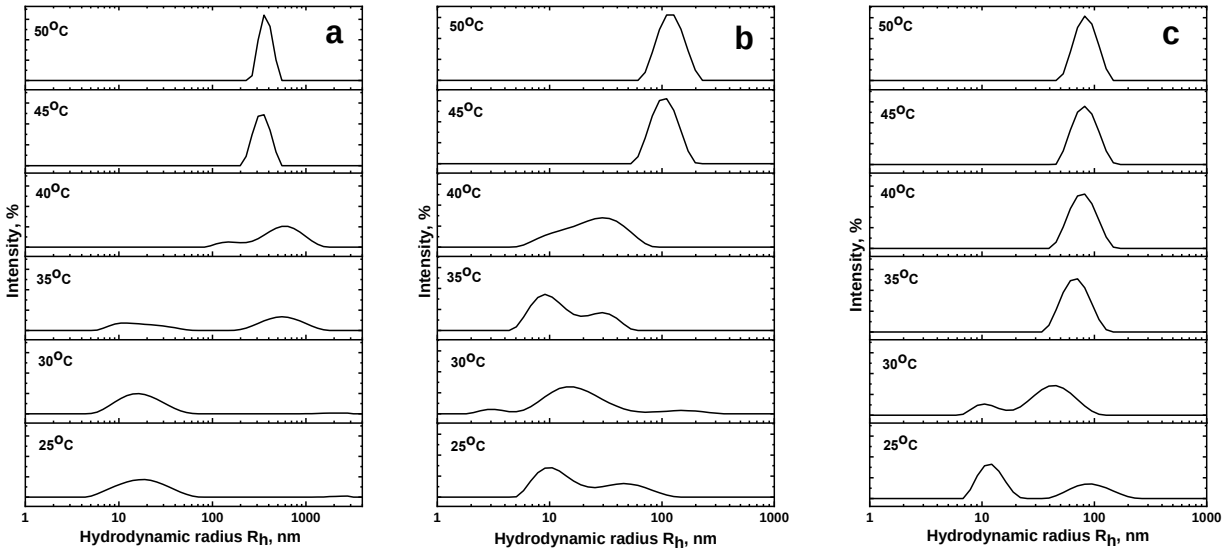

Figure 45 - Influence of temperature and ionic strength of the solution (μ) on the average hydrodynamic radius (R_h) of $NIPAM_{90}$-$APTAC_5$-$AMPS_5$: μ = (a) 0.001; (b) 0.1 and (c) 1

The positively-charged nanogel, $NIPAM_{90}$-$APTAC_{7.5}$-$AMPS_{2.5}$, was shown to be in an expanded state in pure water (Figure 46). However, the nanogel particles shrink as the salt concentration increases, μ = 0.5-1.0 M NaCl, due to the screened electrostatic repulsion between uniformly charged macroions, demonstrating the polyelectrolyte effect, leading to sharp decreases in the VPTT, which was shown to

be less responsive to temperature in the range of μ= 0.001-0.1 M NaCl, but sharply decreased at the higher salt concentrations. An attempt has been made to interpret this phenomenon in terms of core-shell competition, in which a positively charged core acts like a polyampholyte and a negatively-charged shell functions like a polyelectrolyte, as salinity is increased (Table 10).

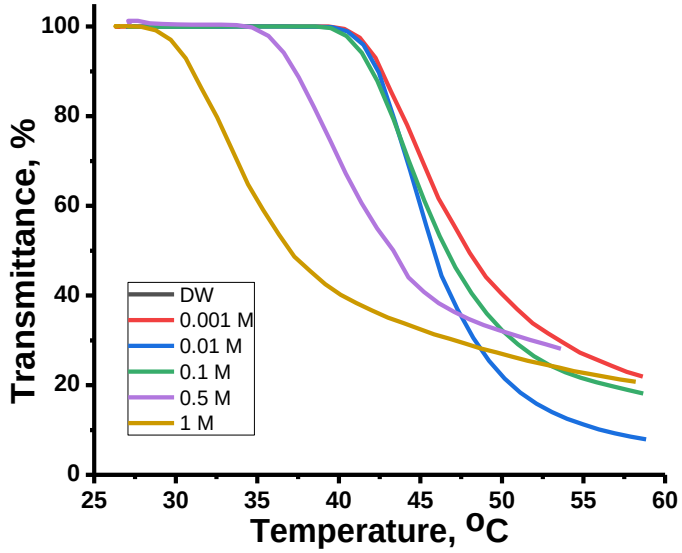

Figure 46 - Effect of temperature and ionic strength on the transmittance of the $NIPAM_{90}$-$APTAC_{7.5}$-$AMPS_{2.5}$ nanogel

$NIPAM_{90}$-$APTAC_{2.5}$-$AMPS_{7.5}$ contains an excess of negatively charged AMPS, so its behavior is similar to $NIPAM_{90}$-$APTAC_{7.5}$-$AMPS_{2.5}$ (Figure 47). However, the interpretation of the volume phase behavior of $NIPAM_{90}$-$APTAC_{2.5}$-$AMPS_{7.5}$, with respect to the combined action of temperature and salinity, is complicated and requires further detailed research. The transmittance curves for $NIPAM_{90}$-$APTAC_{2.5}$-$AMPS_{7.5}$ are quite different from $NIPAM_{90}$-$APTAC_{7.5}$-$AMPS_{2.5}$, and at high ionic strengths, μ = 0.5 and 1 M, contain two volume phase transition temperatures, VPTT = 51.1 and 47.1°C respectively (Table 10).

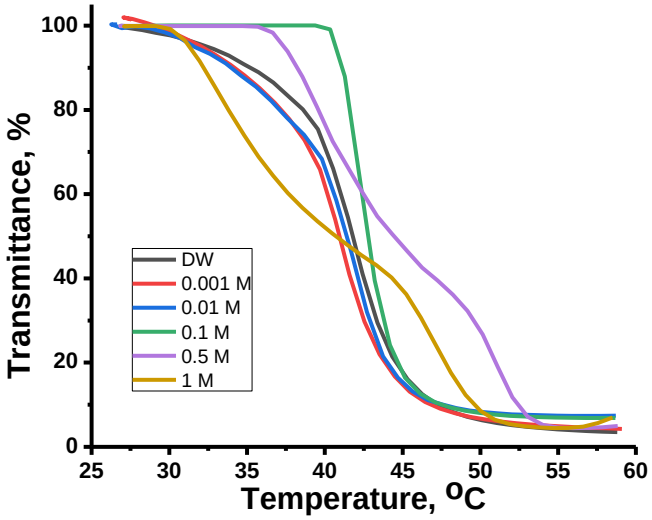

Figure 47 - Effect of temperature and ionic strength on the transmittance of the NIPAM$_{90}$-APTAC$_{2.5}$-AMPS$_{7.5}$ nanogel

Figure 48 presents the effect of temperature, ranging from 25 to 50°C, and ionic strength on the hydrodynamic nanogel particle size of NIPAM$_{90}$-APTAC$_{7.5}$-AMPS$_{2.5}$. The mean average, R_h, is ~10 nm for the NIPAM$_{90}$-APTAC$_{7.5}$-AMPS$_{2.5}$ nanogel in solutions where μ < 0.1 M NaCl at room temperature. R_h increases to 100-110 nm when the temperature is raised to 40°C. However, in solutions with an ionic strength of 1 M, even at room temperature, 25°C, a larger average hydrodynamic size was observed, compared to those with a lower μ, though an increase in temperature did not cause a major change in size.

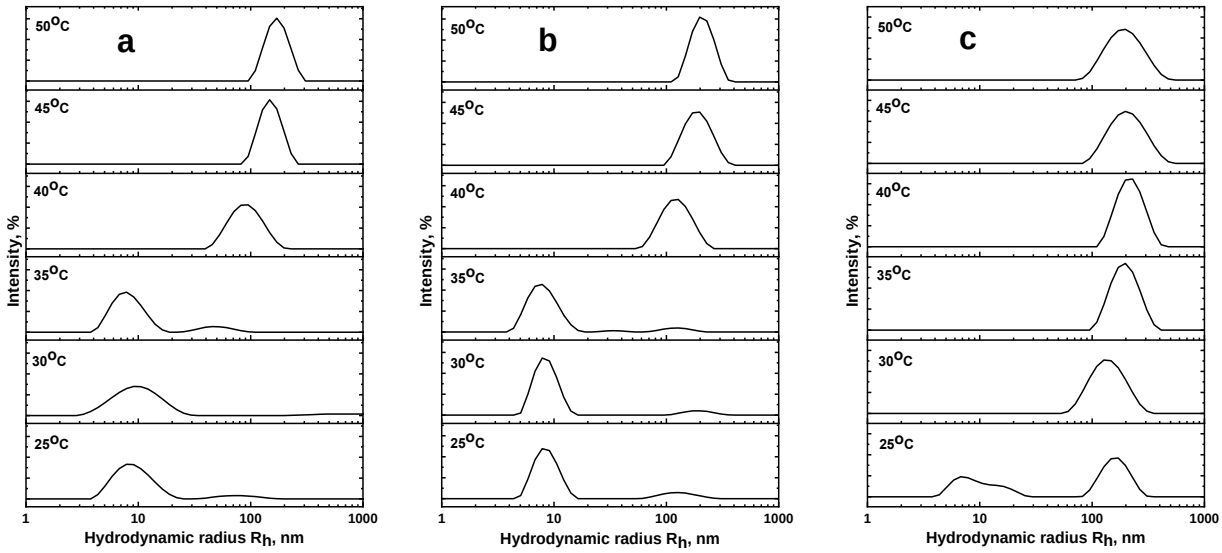

Figure 48 - Effect of temperature and ionic strength (μ) on the mean hydrodynamic radius (R_h) of NIPAM$_{90}$-APTAC$_{7.5}$-AMPS$_{2.5}$: μ = (a) 0.001; (b) 0.1 and (c) 1

Figure 49 represents the effect of temperature, from 25 to 50°C, and ionic strength on the hydrodynamic size of $NIPAM_{90}$-$APTAC_{2.5}$-$AMPS_{7.5}$. $NIPAM_{90}$-$APTAC_{2.5}$-$AMPS_{7.5}$ did not demonstrate strict regularity in terms of average hydrodynamic radius at room temperature, 25°C, and clumping of nanogel particles could already be observed. At higher temperatures, sizes gradually increased. The R_h dramatically rose above VPTT, due to formation of multi-particle clumps. Small ones, of 10-20 nm, were detected below the VPTT [128].

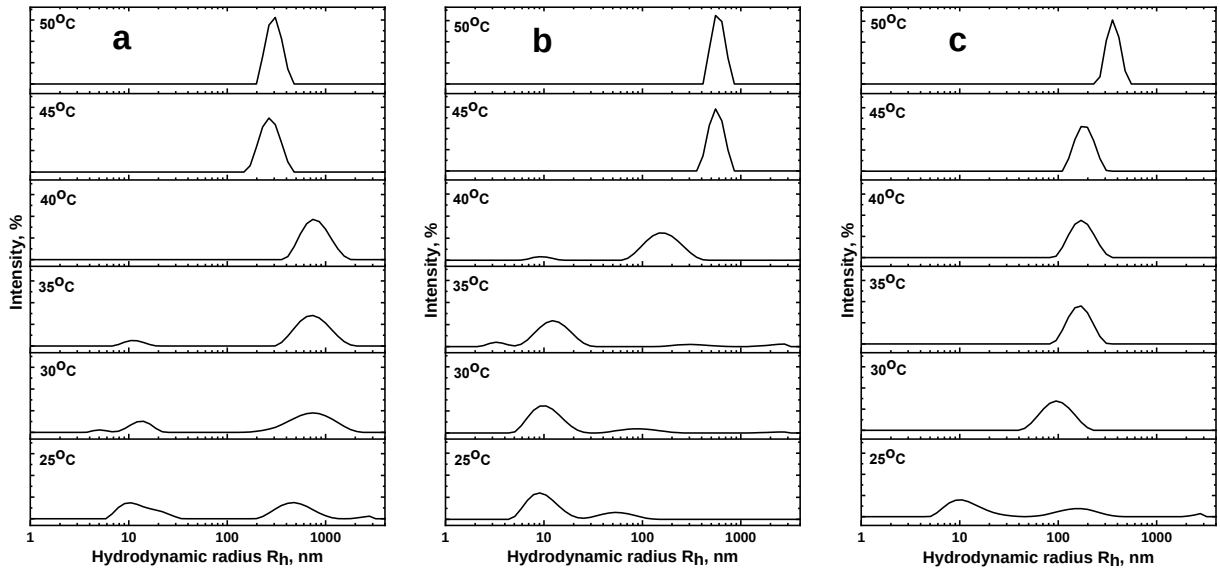

Figure 49 - Effect of temperature and ionic strength (μ) on the mean hydrodynamic radius (R_h) of $NIPAM_{90}$-$APTAC_{2.5}$-$AMPS_{7.5}$: μ = (a) 0.001; (b) 0.1 and (c) 1

3.4.2 Immobilization of model drugs – anionic dye methyl orange and cationic dye methylene blue within the matrix of charge-imbalanced amphoteric nanogels $NIPAM_{90}$-$APTAC_{7.5}$-$AMPS_{2.5}$ and $NIPAM_{90}$-$APTAC_{2.5}$-$AMPS_{7.5}$ followed by study of dye release kinetics as a function of temperature and ionic strength

To study the kinetics of the release of model drugs depending on temperature and salt additive, we immobilized an anionic dye - methyl orange (MO) and a cationic dye - methylene blue (MB) into a matrix of linear polyampholytes and nanogels based on NIPAM-APTAC-AMPS. This is due to the fact that the release of dyes into the environment can be easily detected using visible spectroscopy, because the MO absorption band maximum is 464 nm, while for MB it corresponds to 611 and 662 nm.

The $NIPAM_{90}$-$APTAC_{7.5}$-$AMPS_{2.5}$ nanogel with an excess of the positively charged APTAC monomer was chosen for the immobilization of the MO anionic dye. Whereas the $NIPAM_{90}$-$APTAC_{2.5}$-$AMPS_{7.5}$ nanogel with an excess of the negatively charged AMPS monomer was chosen for immobilization of the cationic dye MB. Since the determination of the composition of the nanogel-dye complexes

presents a certain experimental difficulty, we first carried out the conductometric titration of an aqueous solution of the linear terpolymer $NIPAM_{90}$-$APTAC_{7.5}$-$AMPS_{2.5}$ with the anionic dye MO and the linear terpolymer $NIPAM_{90}$-$APTAC_{2.5}$-$AMPS_{7.5}$ with the cationic dye MB at polymer concentrations $1 \cdot 10^{-1}$ mM and dye concentrations 1 mM (Figure 50).

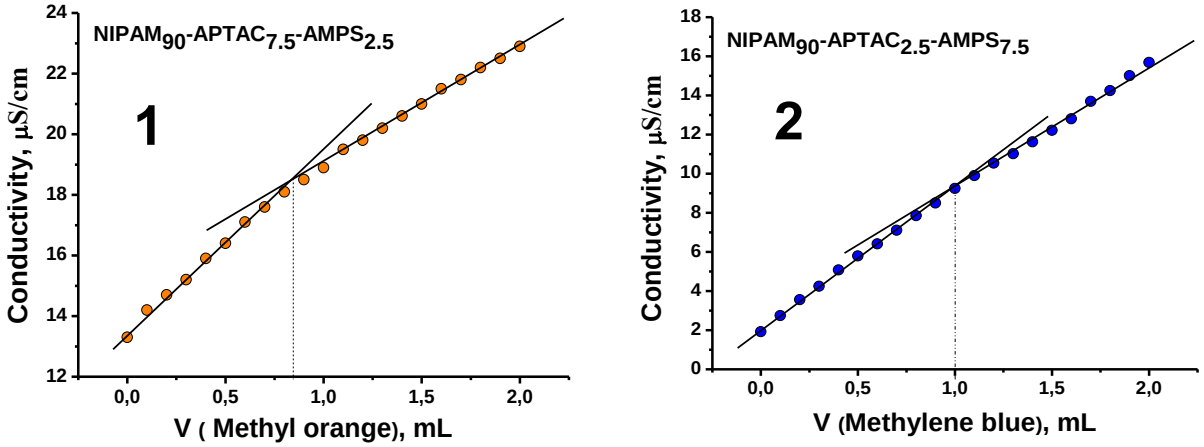

Figure 50 - Conductometric titration of linear terpolymer $NIPAM_{90}$-$APTAC_{7.5}$-$AMPS_{2.5}$ with anionic dye MO (1) and linear terpolymer $NIPAM_{90}$-$APTAC_{2.5}$-$AMPS_{7.5}$ with cationic dye MB (2) at a polymer concentration of $1 \cdot 10^{-1}$ mM and concentration dyes 1 mM

In case of the $NIPAM_{90}$-$APTAC_{7.5}$-$AMPS_{2.5}$ linear terpolymer, the inflection point corresponds to the composition of the complex [$NIPAM_{90}$-$APTAC_{7.5}$-$AMPS_{2.5}$]/[MO] = 1:0.8 mol/mol, which is close to the equimolar ≈ 1:1. In case of the $NIPAM_{90}$-$APTAC_{2.5}$-$AMPS_{7.5}$ system, the inflection point corresponds to the composition of the complex [$NIPAM_{90}$-$APTAC_{2.5}$-$AMPS_{7.5}$]/[MB] = 1:1 mol/mol. Thus, linear NIPAM-APTAC-AMPS polyampholytes with an excess of positive (APTAC) or negative (AMPS) monomers form 1:1 equimolar complex with ionic dyes (MO and MB). For this reason, further study of the dyes release from the volume of the NIPAM-APTAC-AMPS nanogels was carried out for equimolar nanogel-dye compositions found for linear polyampholytes.

The electrostatic binding of anionic and cationic dyes by charged groups of amphoteric nanogels NIPAM-APTAC-AMPS with release of NaCl is represented in Figure 51:

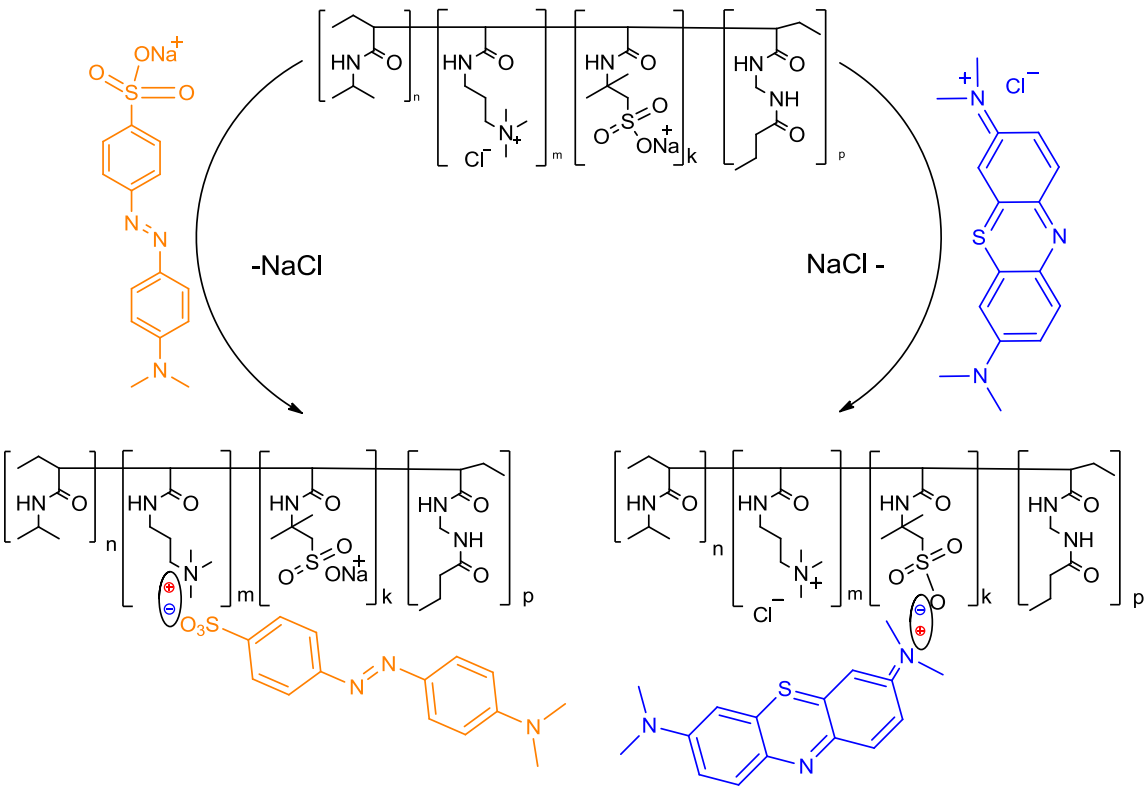

Figure 51 - Formation of equimolar complexes between polyampholyte nanogels and ionic dyes

The release (or diffusion to the outer solution) of dyes was carried out using a simple “glass in a glass” device with constant stirring, shown in Figure 52. For this, the inner glass, the bottom of which was covered with a dialysis membrane (molecular weight cut off is 12-14 kDa), was filled with a mixture of 10 mL of dye (MO or MB) with $5 \cdot 10^{-2}$ mM concentration and 0.1 wt.% of nanogel ($NIPAM_{90}$-$APTAC_{2.5}$-$AMPS_{7.5}$ or $NIPAM_{90}$-$APTAC_{7.5}$-$AMPS_{2.5}$). It was dipped to the outer vessel containing 20 mL of distilled water or aqueous NaCl solution (μ = 1, $1 \cdot 10^{1}$ and $1 \cdot 10^{2}$ mM). All measurements were carried out under stirring at 25°C and at $T_{p.t.t.}$ of nanogels determined as described above. Covering the bottom part of the inner glass with a dialysis membrane retains the nanogel in the inner vessel and keeps the concentration of nanogel constant. At the same time, pores of the dialysis membrane did not prevent diffusion of the released dye molecules (MB or MO) into the outer beaker. At certain time intervals, 2 mL of sample was taken from the outer beaker for the UV-Vis analysis. The experiments were performed under the sink conditions: to keep the volume of the solution constant, the 2 mL solution taken for analysis was compensated by adding 2 mL of distilled water or aqueous-salt solution.

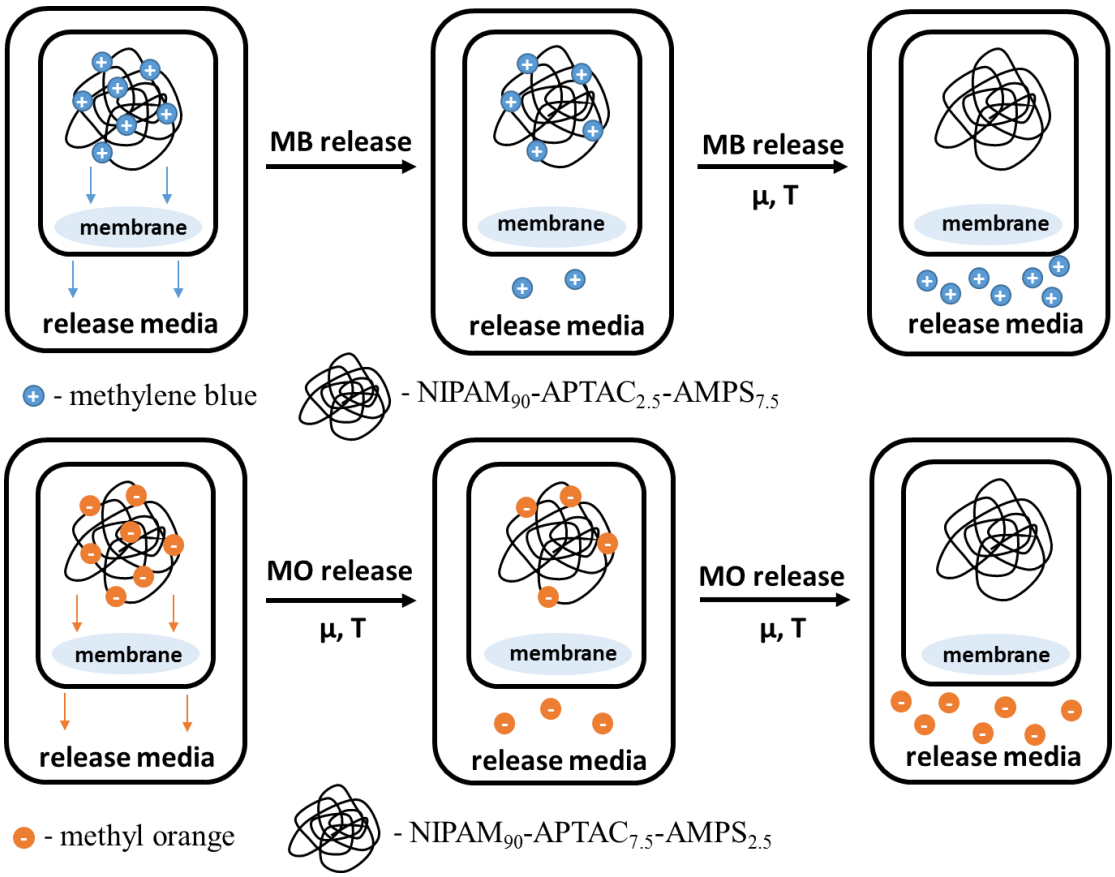

Figure 52 - "Glass-in-glass" device for dye release from the nanogel matrix

The concentration of dyes released into distilled water or saline solutions was determined using a UV-visible spectrophotometer at 464 nm for MO and 662 nm for MB and expressed by Equation 3:

$$\text{Dye release (\%)} = \frac{[released\ \text{dye}]}{[total\ dye]} \cdot 100 \quad (3)$$

The kinetics and mechanism of dye release from the nanogel matrix was determined using the Ritger-Peppas model, which is expressed by Equation 4 [138]:

$$M_t/M_\infty = kt^n \quad (4)$$

where M_t is the concentration of dye released at time t, M_∞ is the concentration of dye at infinite time t_∞, k is kinetic constant, n is exponent of diffusion indicating the mechanism of dye transport from the nanogel matrix).

According to literature survey the values of n can be the following: when n = 0.5, diffusion is the main driving force (Fickian diffusion); when n = 1, the dye release is largely controlled by degradation (Case II transport); when $0.5 < n < 1.0$, the dye release is followed by both diffusion and erosion controlled mechanisms (non-Fickian diffusion or anomalous mechanism of the drug release.

The cumulative release was calculated by Equation 5 [139]:

$$\text{Cumulative percentage release, \%} = \frac{\text{Volume of sample withdrawn, mL}}{\text{Bath volume, mL}} \cdot P_{(t-1)} + P_t, \quad (5)$$

where P_t is percentage release at time t; $P_{(t-1)}$ is percentage release previous to t.

Figure 53 shows the cumulative release of MO from nanogel $NIPAM_{90}$-$APTAC_{7.5}$-$AMPS_{2.5}$ into deionized water and aqueous-salt solution containing 1, $1 \cdot 10^1$ and $1 \cdot 10^2$ mM NaCl. The released amount of MO from the nanogel matrix is summarized in Table 11.

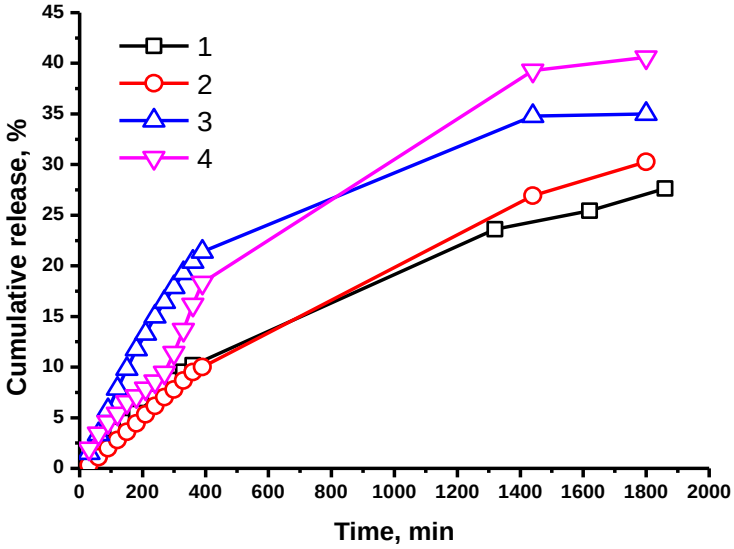

Figure 53 - Cumulative release of MO from $NIPAM_{90}$-$APTAC_{7.5}$-$AMPS_{2.5}$ nanogel at 25°C in different media: (1) DI water; (2) 1 mM NaCl, (3) $1 \cdot 10^1$ mM NaCl and (4) $1 \cdot 10^2$ mM NaCl. [MO] = $5 \cdot 10^{-2}$ mM

Table 11 - The equilibrium release data of MO for nanogel $NIPAM_{90}$-$APTAC_{7.5}$-$AMPS_{2.5}$ at 25°C

μ, mol·L^{-1} (NaCl)	Released amount of MO during 30 h, (%)
0	27.0±0.5
1	30.0±0.5
$1 \cdot 10^1$	35.0±0.5
$1 \cdot 10^2$	41.0±0.5

Gradually increasing MO release into the external solution is associated with destruction of the electrostatic interactions between the cationic groups of nanogel and the anionic dye upon increasing μ.

The release kinetics of MO from nanogel $NIPAM_{90}$-$APTAC_{7.5}$-$AMPS_{2.5}$ were fit using the Ritger–Peppas equation. The values of n and k are presented in Table

12. The values of *n* in DI water, 1 and $1 \cdot 10^1$ mM NaCl are around 1 and indicating Case II transport release mechanism. When MO is released into $1 \cdot 10^2$ mM NaCl the *n* value equals 0.69, which indicates non-Fickian (anomalous) diffusion.

Table 12 - The values of *n* and *k* of MO for nanogel $NIPAM_{90}$-$APTAC_{7.5}$-$AMPS_{2.5}$ at 25 °C

Release medium	*n*	$k \cdot 10^2$	Release mechanism
MO+$NIPAM_{90}$-$APTAC_{7.5}$-$AMPS_{2.5}$ into DI water	1.04±0.02	0.09	Case II transport
MO+$NIPAM_{90}$-$APTAC_{7.5}$-$AMPS_{2.5}$ into 1 mM NaCl	1.12±0.02	0.05	Case II transport
MO+$NIPAM_{90}$-$APTAC_{7.5}$-$AMPS_{2.5}$ into $1 \cdot 10^1$ mM NaCl	1.03±0.02	0.16	Case II transport
MO+$NIPAM_{90}$-$APTAC_{7.5}$-$AMPS_{2.5}$ into $1 \cdot 10^2$ mM NaCl	0.7±0.02	0.50	non-Fickian diffusion

The release kinetics of MB from $NIPAM_{90}$-$APTAC_{2.5}$-$AMPS_{7.5}$ nanogel was studied in aqueous-salt solutions at μ = 1, $1 \cdot 10^1$ and $1 \cdot 10^2$ mM NaCl (Figure 54). When μ = 1 and $1 \cdot 10^1$ mM NaCl (up to 400 min), the intensive diffusion of MB from the nanogel matrix is observed. This owes to the step-by-step destruction of the nanogel-dye complex due to screening of the negative charges of the nanogel by NaCl ions. At time interval from 400 to 1600 min, the MB diffusion rate reaches a plateau. This indicates the stationary nature of the release of the dye molecules from the bulk of the nanogel. At μ = $1 \cdot 10^2$ mM NaCl the rate of the dye diffusion from the nanogel matrix increases linearly, but after 1400 and 1600 min it reaches a plateau.

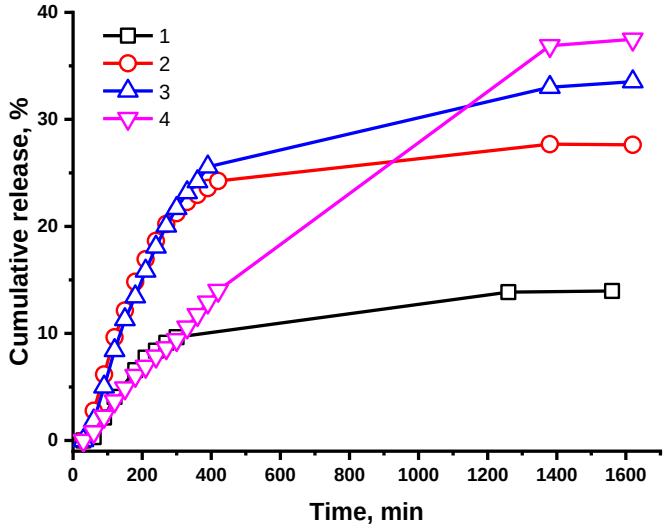

Figure 54 - Cumulative release of MB from $NIPAM_{90}$-$APTAC_{2.5}$-$AMPS_{7.5}$ nanogel in different media at 25°C: (1) DI water, (2) 1 mM NaCl, (3) $1 \cdot 10^1$ mM NaCl and (4) $1 \cdot 10^2$ mM NaCl

The released amount of MB from the nanogel matrix is summarized in Table 13.

Table 13 - The equilibrium release data of MB for nanogel $NIPAM_{90}$-$APTAC_{2.5}$-$AMPS_{7.5}$ at 25 °C

μ, mol·L^{-1} (NaCl)	Released amount of MB during 27 h, (%)
0	14.0±0.5
1	28.0±0.5
$1 \cdot 10^1$	34.0±0.5
$1 \cdot 10^2$	37.0±0.5

The values of *n* equal one upon release of MB from the $NIPAM_{90}$-$APTAC_{2.5}$-$AMPS_{7.5}$ nanogel into deionized water and $1 \cdot 10^2$ mM NaCl solution indicating that the release mechanism is controlled by degradation, whereas the release into 1 and $1 \cdot 10^1$ mM NaCl corresponds to the diffusion and erosion-controlled mechanism (Table 14).

Table 14 - The values of *n* and *k* for release of MB for nanogel $NIPAM_{90}$-$APTAC_{2.5}$-$AMPS_{7.5}$ at 25°C

Release medium	*n*	$k \cdot 10^2$	Release mechanism
MB+$NIPAM_{90}$-$APTAC_{2.5}$-$AMPS_{7.5}$ into DI water	1.2±0.02	0.76	Case II transport
MB+$NIPAM_{90}$-$APTAC_{2.5}$-$AMPS_{7.5}$ into 1 mM NaCl	0.7±0.02	1.25	non-Fickian diffusion
MB+$NIPAM_{90}$-$APTAC_{2.5}$-$AMPS_{7.5}$ into $1 \cdot 10^1$ mM NaCl	0.9±0.02	0.32	non-Fickian diffusion
MB+$NIPAM_{90}$-$APTAC_{2.5}$-$AMPS_{7.5}$ into $1 \cdot 10^2$ mM NaCl	1.3±0.02	0.02	Case II transport

Figure 55 shows the cumulative release of MO from the $NIPAM_{90}$-$APTAC_{7.5}$-$AMPS_{2.5}$ nanogel into NaCl solutions at the volume phase transition temperatures measured during 5 hours.

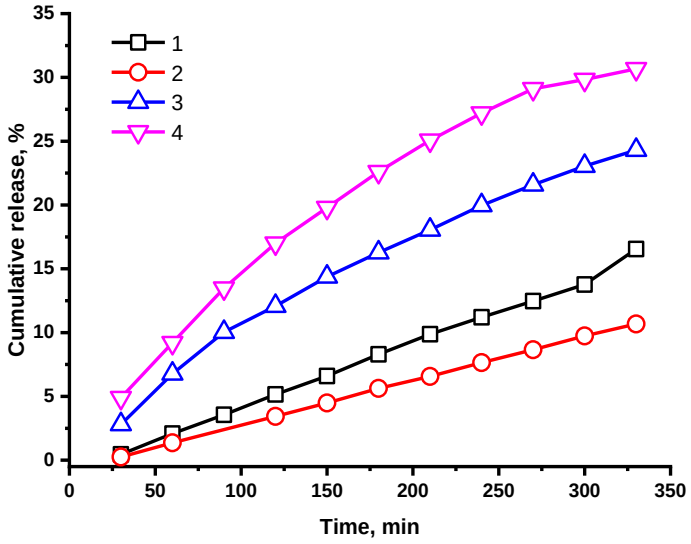

Figure 55 - Cumulative release of MO from NIPAM$_{90}$-APTAC$_{7.5}$-AMPS$_{2.5}$ nanogel in different media at VPTT : 1 – DI water; 2 – 1 mM NaCl; 3 – $1 \cdot 10^1$ mM NaCl; 4 – $1 \cdot 10^2$ mM NaCl

The effect of μ on the volume phase transition temperatures VPTT and released amount of MO from NIPAM$_{90}$-APTAC$_{7.5}$-AMPS$_{2.5}$ nanogel is summarized in Table 15.

Table 15 - Influence of the ionic strength (μ) on the volume phase transition temperatures (VPTT) and released amount of MO from NIPAM$_{90}$-APTAC$_{7.5}$-AMPS$_{2.5}$ nanogel

μ, mol·L^{-1} (NaCl)	Volume hase transition temperature, VPTT (°C)	Released amount of MO during 5 h, (%)
0	44.0±0.1	17.0±0.5
1	45.1±0.1	11.0±0.5
$1 \cdot 10^1$	44.4±0.1	24.0±0.5
$1 \cdot 10^2$	44.3±0.1	31.0±0.5

The amount of released MO into deionized water at 44°C equals 17%. However, in a 1 mM solution at VPTT = 45.1°C it decreases down to 11%. The released amount of MO into $1 \cdot 10^1$ mM and $1 \cdot 10^2$ mM solutions at VPTT equals 24 and 31% respectively. Therefore, an increase in temperature increases the MO release from the nanogel into deionized water, $1 \cdot 10^1$ and $1 \cdot 10^2$ mM NaCl solutions (Table 15).

The release of MO from nanogel matrix into $1 \cdot 10^1$ mM salt solution at the phase transition temperature leads to a decrease in *n* down to 0.85 and the diffusion mechanism changes to non-Fickian (Table 16) .

Table 16 - The values of *n* and *k* for release of MO for nanogel $NIPAM_{90}$-$APTAC_{7.5}$-$AMPS_{2.5}$ at VPTT

Release medium	*n*	$k \cdot 10^2$	Release mechanism
MO+$NIPAM_{90}$-$APTAC_{7.5}$-$AMPS_{2.5}$ into DI water	1.4±0.02	0.04	Case II transport
MO+$NIPAM_{90}$-$APTAC_{7.5}$-$AMPS_{2.5}$ into 1 mM NaCl	1.1±0.02	0.09	Case II transport
MO+$NIPAM_{90}$-$APTAC_{7.5}$-$AMPS_{2.5}$ into $1 \cdot 10^1$ mM NaCl	0.9±0.02	0.08	non-Fickian diffusion
MO+$NIPAM_{90}$-$APTAC_{7.5}$-$AMPS_{2.5}$ into $1 \cdot 10^2$ mM NaCl	0.8±0.02	1.3	non-Fickian diffusion

The effect of the volume phase transition temperature on the MB release from the $NIPAM_{90}$-$APTAC_{2.5}$-$AMPS_{7.5}$ nanogel is shown in Figure 56. The dye release in deionized water did not change during 5 hours as the temperature increased from 25 to 41.6°C. The diffusion of MB from the nanogel into NaCl solutions with different $\mu = 1$, $1 \cdot 10^1$ and $1 \cdot 10^2$ mM at the phase transition temperature increases by 7-15% (Table 17).

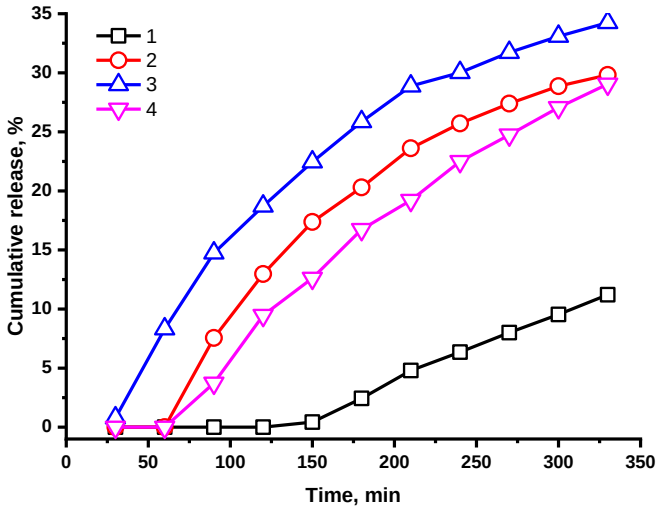

Figure 56 - Cumulative release of MB from $NIPAM_{90}$-$APTAC_{2.5}$-$AMPS_{7.5}$ nanogel in different media at VPTT: (1) DI water, (2) 1 mM NaCl, (3) $1 \cdot 10^1$ mM NaCl and (4) $1 \cdot 10^2$ mM NaCl

Table 17 - The equilibrium release data of MB for nanogel $NIPAM_{90}$-$APTAC_{2.5}$-$AMPS_{7.5}$ at VPTT

μ, mol·L^{-1} (NaCl)	Volume phase transition temperature, VPTT (°C)	Release amount of MB during 5 hrs, (%)
0	41.6±0.1	11±0.5
1	40.8±0.1	30±0.5
$1 \cdot 10^1$	41.8±0.1	34±0.5
$1 \cdot 10^2$	41.4±0.1	29±0.5

The influence of VPTT on the change in the diffusion mechanism occurred when the MB was released into a 1 M NaCl. The *n* value changed to 1 and the mechanism became - Case II transport (Table 18) [130].

Table 18 - The values of *n* and *k* for release of MB for nanogel $NIPAM_{90}$-$APTAC_{2.5}$-$AMPS_{7.5}$ at VPTT

Release medium	*n*	$k \cdot 10^2$	Release mechanism
MB+$NIPAM_{90}$-$APTAC_{2.5}$-$AMPS_{7.5}$ into 1 mM NaCl	1±0.04	0.33	Case II transport
MB+ $NIPAM_{90}$-$APTAC_{2.5}$-$AMPS_{7.5}$ into $1 \cdot 10^1$ mM NaCl	0.8±0.02	1.3	non-Fickian diffusion
MB+$NIPAM_{90}$-$APTAC_{2.5}$-$AMPS_{7.5}$ into $1 \cdot 10^2$ mM NaCl	1.2±0.02	0.06	Case II transport

3.5 Synthesis and characterization of polyampholyte microgels based on AAm-APTAC-AMPS

Polyampholyte microgels [AAm]-[APTAC]-[AMPS] = 90-5-5; 80-10-10; 70-15-15 mol.% (abbreviated as AAm_{90}-$APTAC_5$-$AMPS_5$, AAm_{80}-$APTAC_{10}$-$AMPS_{10}$, AAm_{70}-$APTAC_{15}$-$AMPS_{15}$) were synthesized via inverse emulsion polymerization (Figure 57) [140].

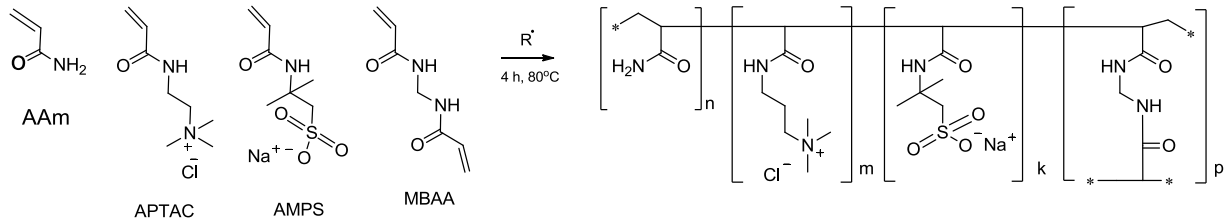

Figure 57 - Schematic representation of copolymerization of AAm, APTAC and AMPS monomers to obtain polyampholyte microgels

The results of elemental analysis of AAm-APTAC-AMPS microgels are given in the Table 19. It is expected that the composition of the resulting microgels will closely match with the composition of initial mixture of monomers with drifting ± 2 mol.% [76]. Good agreement between the calculated and found sulfur content confirms the same composition of initial monomer mixture and the obtained products.

Table 19 - The results of elemental analysis of AAm-APTAC-AMPS microgels

Initial monomer mixture, mol.%			Calculated/Found	Percentage of elements, wt.%			
				H	C	N	S
AAm	APTAC	AMPS					
90	5	5	Calculated	8.05	48.3	17.15	1.86
			Found	6.86	44.59	14.96	1.68
80	10	10	Calculated	7.14	46.59	15.32	3.18
			Found	7.09	44.2	13.48	3.12
70	15	15	Calculated	6.25	45.33	13.98	4.16
			Found	7.39	44.33	12.79	3.87

Figure 58 shows the FTIR spectra of AAm-APTAC-AMPS polyampholyte microgels. The broad absorption band in the region of 3200–3500 cm^{-1} corresponds to the secondary and tertiary amine groups, and the absorption bands in the region of 2800–3000 cm^{-1} correspond to the asymmetric and symmetric vibrations of CH groups. The absorption bands at 1630 and 1590 cm^{-1} belong to the vibrations of the N-substituted groups, which are the amide I and amide II groups, respectively. The absorption band at 1450 cm^{-1} is characteristic of the bending vibrations of the CH groups. The absorption band at 1430 cm^{-1} corresponds to the vibrations of the C-N groups. Finally, the absorption band in the region of 1040 cm^{-1} corresponds to the fluctuations of the S=O groups of the AMPS units.

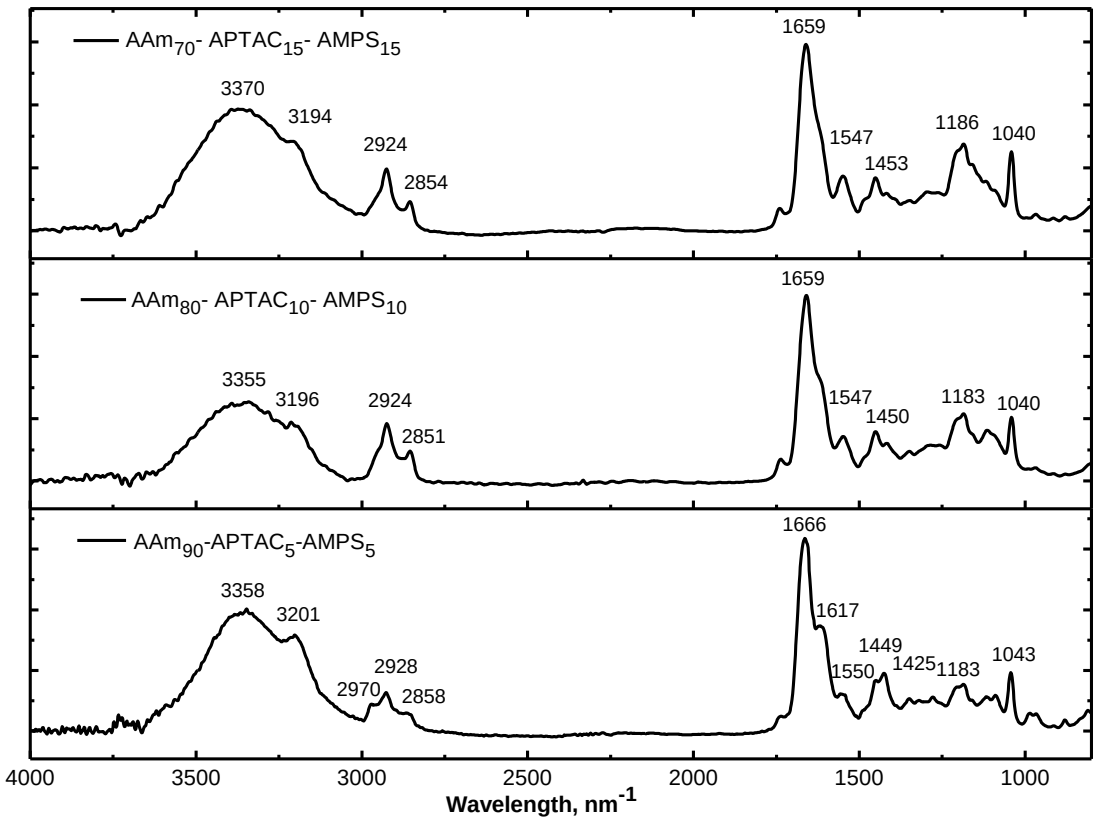

Figure 58 - FTIR spectra of AAm-APTAC-AMPS microgels

The most attention was paid to the AAm_{80}-$APTAC_{10}$-$AMPS_{10}$ microgel because its linear analog showed the best swelling capacity and the viscosifying effect for potential application in oil recovery.

From TEM images it can be observed that AAm_{80}-$APTAC_{10}$-$AMPS_{10}$ microgel have spherical shape and contain both nanogels and microgels (Figure 59). It is seen that different sized nano- and microgel particles are aggregated into bigger micron-sized species to minimize the surface energy of the particles [103].

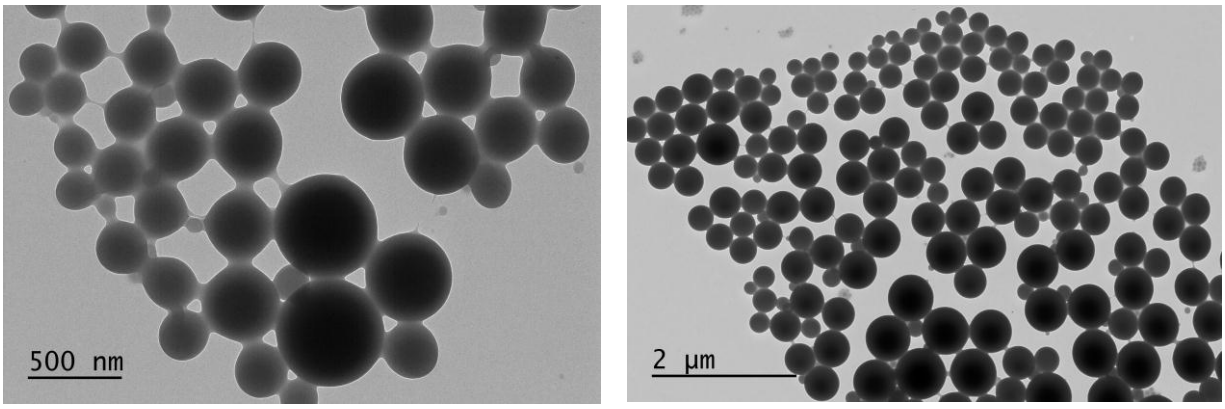

Figure 59 - TEM images of nano- and microgels of AAm_{80}-$APTAC_{10}$-$AMPS_{10}$

The influence of the monomer concentration, the surfactant concentration, the HLB values, the ratio of the water/organic phase on the mean hydrodynamic radius

(R_h) of AAm_{80}-$APTAC_{10}$-$AMPS_{10}$ microgel particles was studied (Figure 60). As shown in Figure 50a, the R_h of microgels decreases from 310 to 130 nm when the concentration of monomers increases from 1.0 to 4.5 mol·L^{-1} (60:40 vol.% of water-organic mixture, 6 wt.% of surfactants, HLB=6). Transparent emulsions were obtained when monomers concentration was equal to 3 mol·L^{-1}. (Table 20, Figure 61a). Probably it is connected with the presence of preferentially nanosized particles. The other emulsions were either opaque or milky. At higher monomer concentration 4.5 mol·L^{-1} the particles size increased up to ~240 nm.

Table 20 – Parameters of AAm_{80}-$APTAC_{10}$-$AMPS_{10}$ microgels synthesis at various concentrations of monomers

Concentration of monomers, mol·L^{-1}	HLB	Water phase		Organic phase			Initiator, wt.%
		60 vol.%		40 vol.%			
		Monomers, wt.%	Water, wt.%	Isooctane, wt.%	Surfactants, wt.%		
					SPAN80	TWEEN80	
1	5,5	15	45	34	6		0,1
2							
3							
4							
4,5							

To evaluate the influence of surfactants HLB on the particle size of AAm_{80}-$APTAC_{10}$-$AMPS_{10}$ microgels, the mixture of nonionic surfactants (SPAN80 and TWEEN80) was chosen as an emulsifier [141]. The SPAN80 with an HLB value of 4.3 was used as the main component and TWEEN80 with an HLB value of 15 as a co-surfactant. Since both SPAN80 and TWEEN80 belong to monooleates the compatibility and synergistic effect of their mixture is highest compared to other surfactants [142].

The HLB value of the surfactant mixture was calculated by the Equation 6:

$$HLB = \frac{w_A\, HLB_A + \omega_B HLB_B}{w_A + \omega_B} \quad (6)$$

where - ω_A is the amount of emulsifier A with known HLB_A; ω_B is the amount of emulsifier B with unknown HLB_B.

With increasing the surfactant concentration from 3 to 9 wt.% (60:40 vol.% of water-organic mixture, 2 mol·L^{-1} of monomers concentration, HLB=6) the particles radius decreased from 325 to 160 nm in a complex manner (Table 21, Figure 61b). Probably the deviations (210 ± 10 nm) are related to errors of DLS measurement. Increasing the concentration of surfactants from 3 to 4 wt.% leads to a sharp decrease in the size from 325 to 210 nm. A further increase in the surfactants content leads to more stable microgel dispersions with particle sizes of about 160 nm. Due to instability of colloidal system, the DLS measurements were not carried out for the microgels with surfactant content less than 3 wt.%. Our result is consistent

with dependence of Z-average diameter of inverse emulsion particles as a function of surfactant content [141].

Table 21 - Parameters of AAm_{80}-$APTAC_{10}$-$AMPS_{10}$ microgels synthesis at various surfactant concentration

Surfactant concentration, wt.%	HLB	Concentration of monomers, mol·L^{-1}	Water phase 60 vol.%		Organic phase 40 vol.%			Initiator, wt.%
			Monomers, wt.%	Water, wt.%	Isooctane, wt.%	Surfactants, wt.%		
						SPAN80	TWEEN80	
3	5,5	2	15	45	34	6		0,1
4								
5								
6								
7								
8								
9								

For determination of the optimal surfactant concentration, interfacial tension (IFT) was measured using a KRUSS tensiometer SDT (Figure 60).

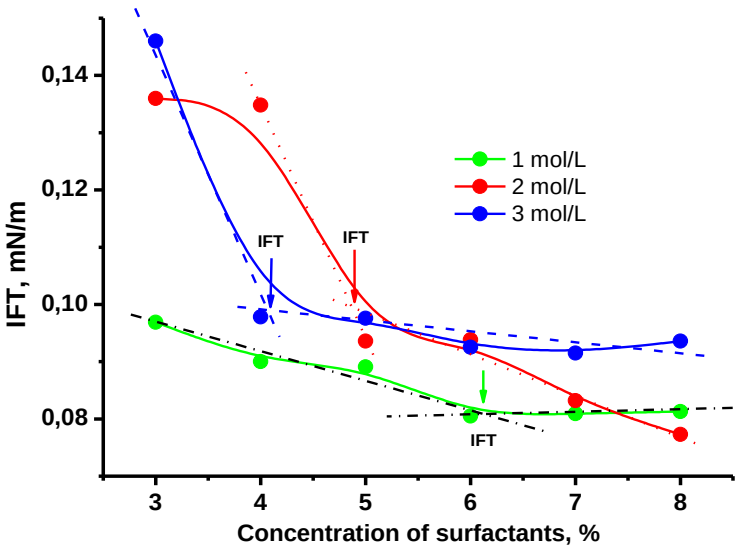

Figure 60 - Changing of IFT for 1, 2 and 3 mol·L^{-1} monomer concentrations in the presence of various concentration of surfactants. The arrows show the values of IFT

The IFT coefficients without surfactants are equal to 2.49±0.01, 2.36±0.01 and 1.31±0.01 mN/m at monomer concentrations 1, 2 and 3 mol·L^{-1} respectively. In the presence of surfactants, the IFT parameters decreases up to 0.10-0.08 mN·m^{-1}, e.g. 13-31 times in comparison with absence of surfactants. It means that the higher surfactant concentration corresponds to lower value of IFT. The minimal IFT values correspond to surfactant concentration of 6.13±0.01, 4.88±0.01 and 4.01±0.01 wt.% at monomer concentration 1, 2 and 3 mol·L^{-1} respectively. Thus, increasing the

monomer concentration decreases the surfactant concentration due to the fact that the AMPS and APTAC also play the role of additional hydrophilic surfactants and, therefore, can affect the stability of the microgels.

Furthermore, the size and colloidal stability of the nanogels and microgels also prone to depend on the HLB values of surfactants (60:40 vol.% of water-organic mixture, 2 mol·L^{-1} of monomers concentration, 6 wt.% of surfactants). At the value of HLB=5, the particles with R_h~480 nm were obtained (Table 22, Figure 61c). However, this microgel did not show the colloidal stability over time. Increasing of the HLB leads to decreasing of the particle size down to 80 nm with high stability. The minimal size of the microgel particles of R_h ≈160±5 nm is observed at 50:50 vol.% of water-organic mixture (2 mol.% of monomers concentration, 6 wt.% of surfactants, HLB=6). Enrichment by water up to 70 vol.% increases R_h up to 240±3 nm and microgels precipitate (2 mol.% of monomers concentration, 6 wt.% of surfactants, HLB=6).

Table 22 - Parameters of AAm_{80}-$APTAC_{10}$-$AMPS_{10}$ microgels synthesis at various HLB

HLB	Concentration of monomers, mol·L^{-1}	Water phase 60 vol.%		Organic phase 40 vol.%			Initiator, wt.%
		Monomers, wt.%	Water, wt.%	Isooctane, wt.%	Surfactants, wt.%		
					SPAN80	TWEEN80	
5	2	15	45	34	6		0,1
5.5							
6							
6,5							
7							

The minimal size of the microgel particles of R_h ≈160 nm is observed at 50:50 vol.% of water-organic mixture (2 mol·L^{-1} of monomers concentration, 6 wt.% of surfactants, HLB=6). Enrichment by water up to 70 vol.% increases R_h up to 240 nm and microgels precipitate (Table 23, Figure 61d).

Table 23 - Parameters of AAm_{80}-$APTAC_{10}$-$AMPS_{10}$ microgels synthesis at various water/organic phase ratio

Water/organic phase ratio, vol.%	Concentration of monomers, mol·L^{-1}	HLB	Surfactants, wt.%	Initiator, wt.%
40/60	2	5,5	6	0,1
45/55				
50/50				
55/45				
60/40				
70/30				

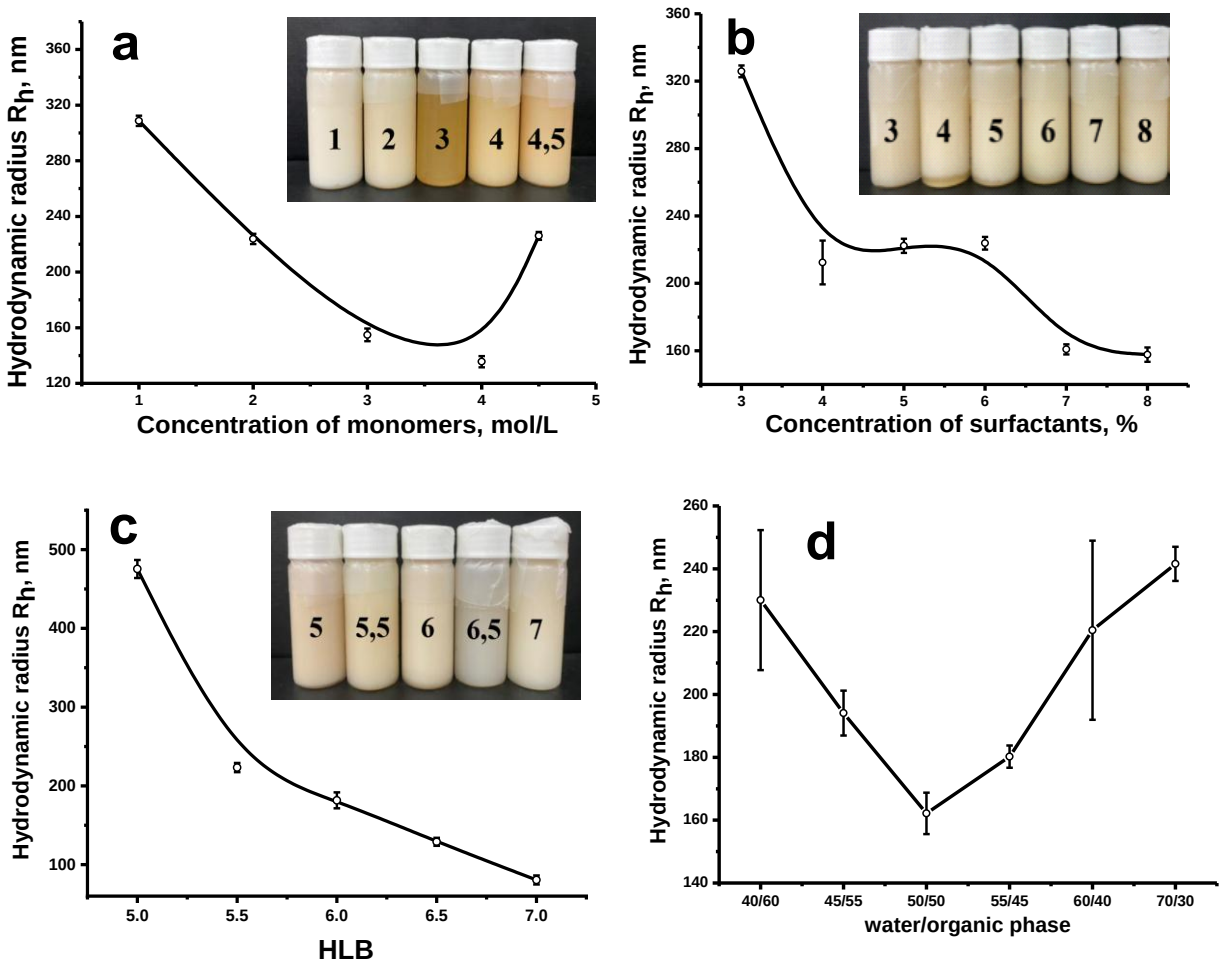

Figure 61 - Mean hydrodynamic radius of microgels from DLS obtained at various monomer concentrations (a), surfactant concentrations (b), HLB values (c) and water/organic phase ratio (d)

For AAm_{80}-$APTAC_{10}$-$AMPS_{10}$ the size distribution of nano- and microgels derived from DLS data and TEM images was compared as a function of monomer concentration at constant surfactant concentration (6 wt.%), HLB = 5.5 and mixture of water:oil = 60:40 vol.% (Figures 62, 63).

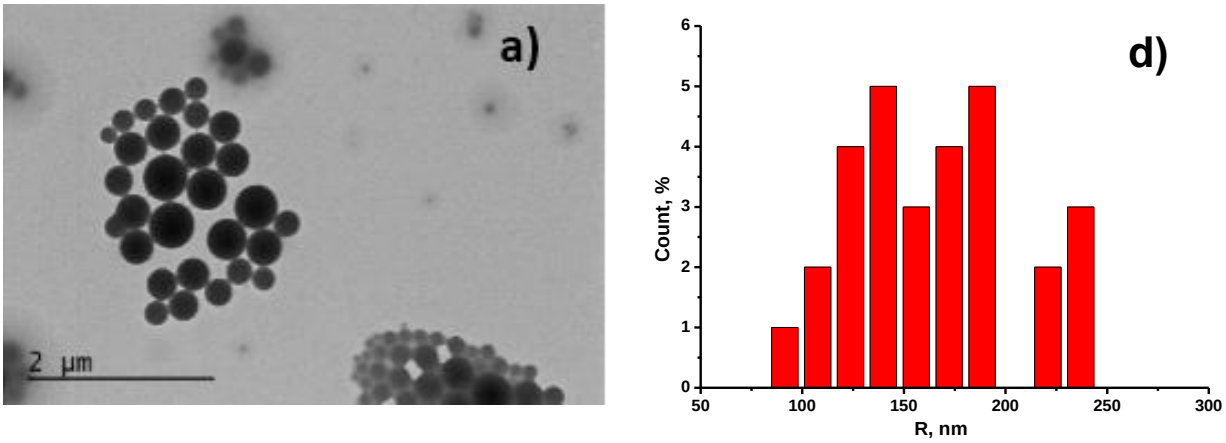

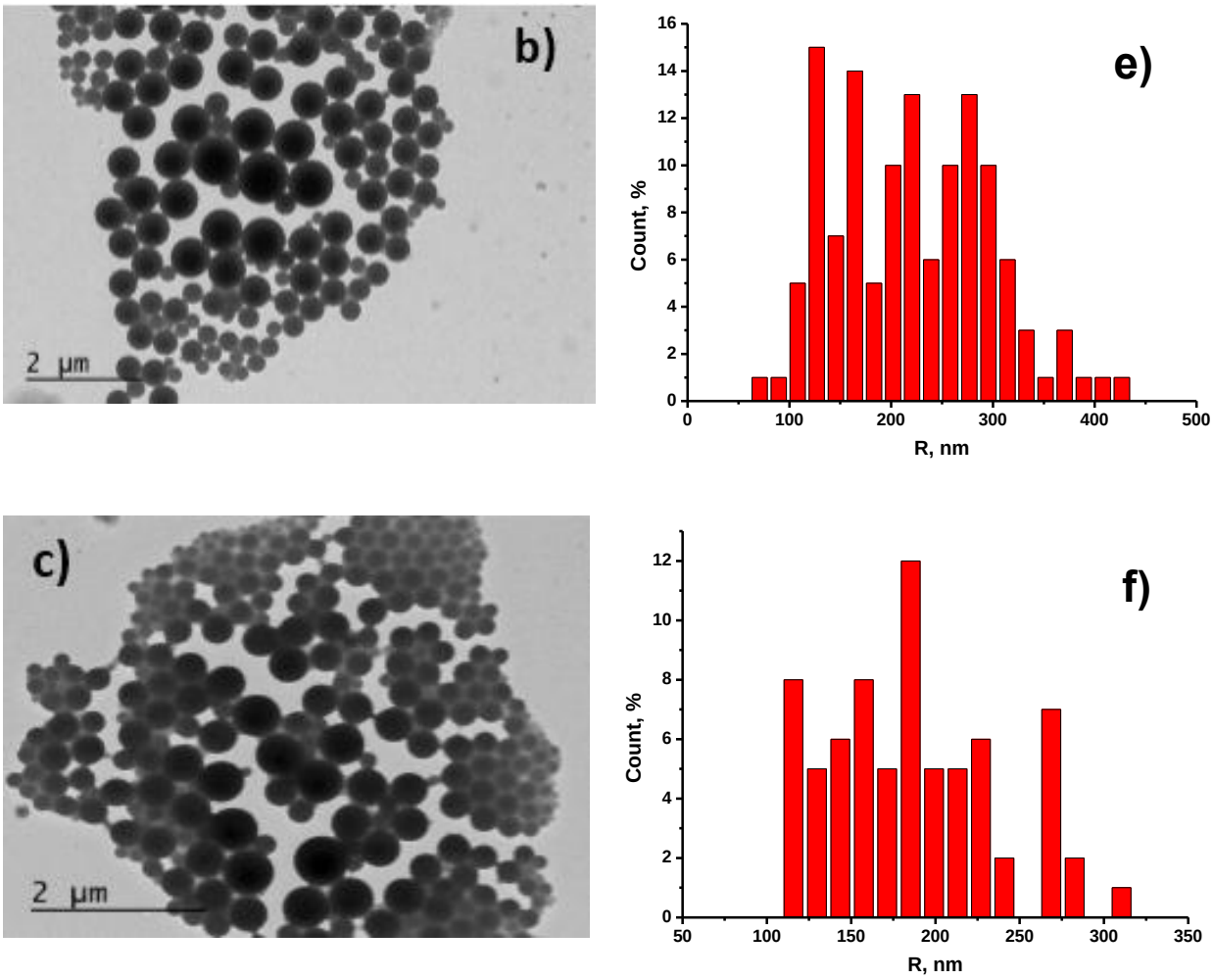

Figure 62 - TEM images (a,b,c) and size distribution histogram (obtained from TEM images) of AAm_{80}-$APTAC_{10}$-$AMPS_{10}$ microgels (d,e,f) at monomer concentration 1 (a, d), 2 (b, e) and 3 mol·L^{-1} (c, f). Surfactant concentration is 6 wt.%, HLB = 5.5 and water:oil = 60:40 vol.%

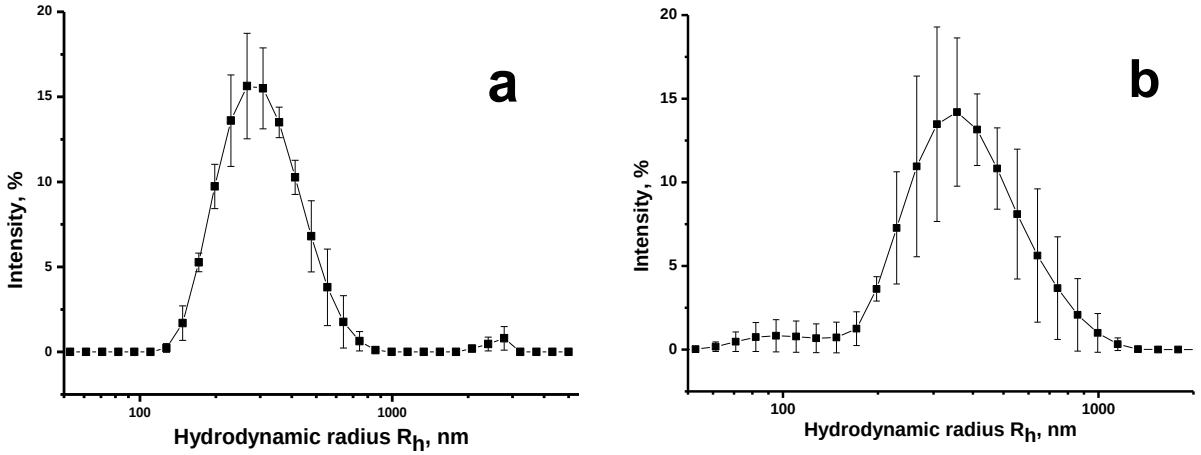

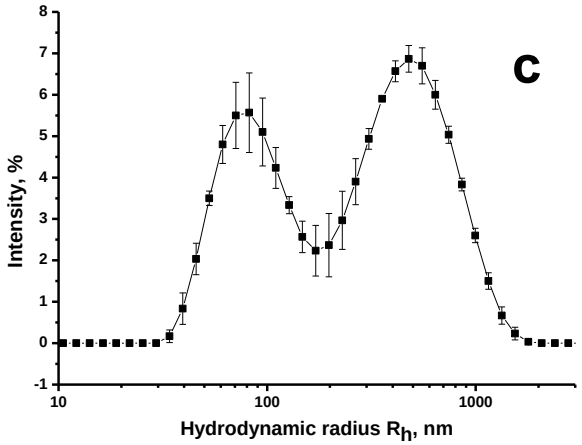

Figure 63 - DLS data of AAm_{80}-$APTAC_{10}$-$AMPS_{10}$ nano- and microgels prepared at monomer concentration 1 (a), 2 (b) and 3 mol·L^{-1} (c). Surfactant concentration is 6 wt.%, HLB = 5.5 and water:oil = 60:40 vol.%

The average hydrodynamic size of nano- and microgels determined by TEM (Figure 62) and DLS (Figure 63) cannot be compared directly because TEM results are related to dried samples (anhydrous state) while DLS data represent the hydrated states of particles that are definitely bigger than TEM image. Moreover, TEM technique deals with limited number of particles per unit area. Therefore, the number of counted particles does not reflect the real picture. It is well-known that DLS technique measures the hydrodynamic diameter of the hydrated particles and is more sensitive to size of particles rather than number of particles. The bigger size of particles according to DLS data may be the result of interparticle aggregation. The size distribution of nano- and microgels prepared at monomer concentration of 3 mol·L^{-1} is bimodal and consists of nanogels (R_h ~ 70-80 nm) and microgels (R_h ~ 500 nm). The latter probably belong to aggregated nanoparticles. Monomodal size distribution is observed for nano- and microgels prepared at lower concentrations of monomers [129].

Increasing of the concentration of monomers, the ratio of water/organic phase and surfactant concentration leads to increasing of the dynamic viscosities of AAm_{80}-$APTAC_{10}$-$AMPS_{10}$ microgels (Figures 64, a-c). However increasing of HLB value from 5 to 5.5 sharply decreases the dynamic viscosity of AAm_{80}-$APTAC_{10}$-$AMPS_{10}$ microgel (Figure 64, d). Therefore, by changing the concentration of monomers, the ratio of water/organic phases, the concentration of surfactants and HLB parameters, it is possible to regulate the average hydrodynamic size as well as the dynamic viscosity of AAm_{80}-$APTAC_{10}$-$AMPS_{10}$ microgels in a wide range to apply them further for enhanced oil recovery.

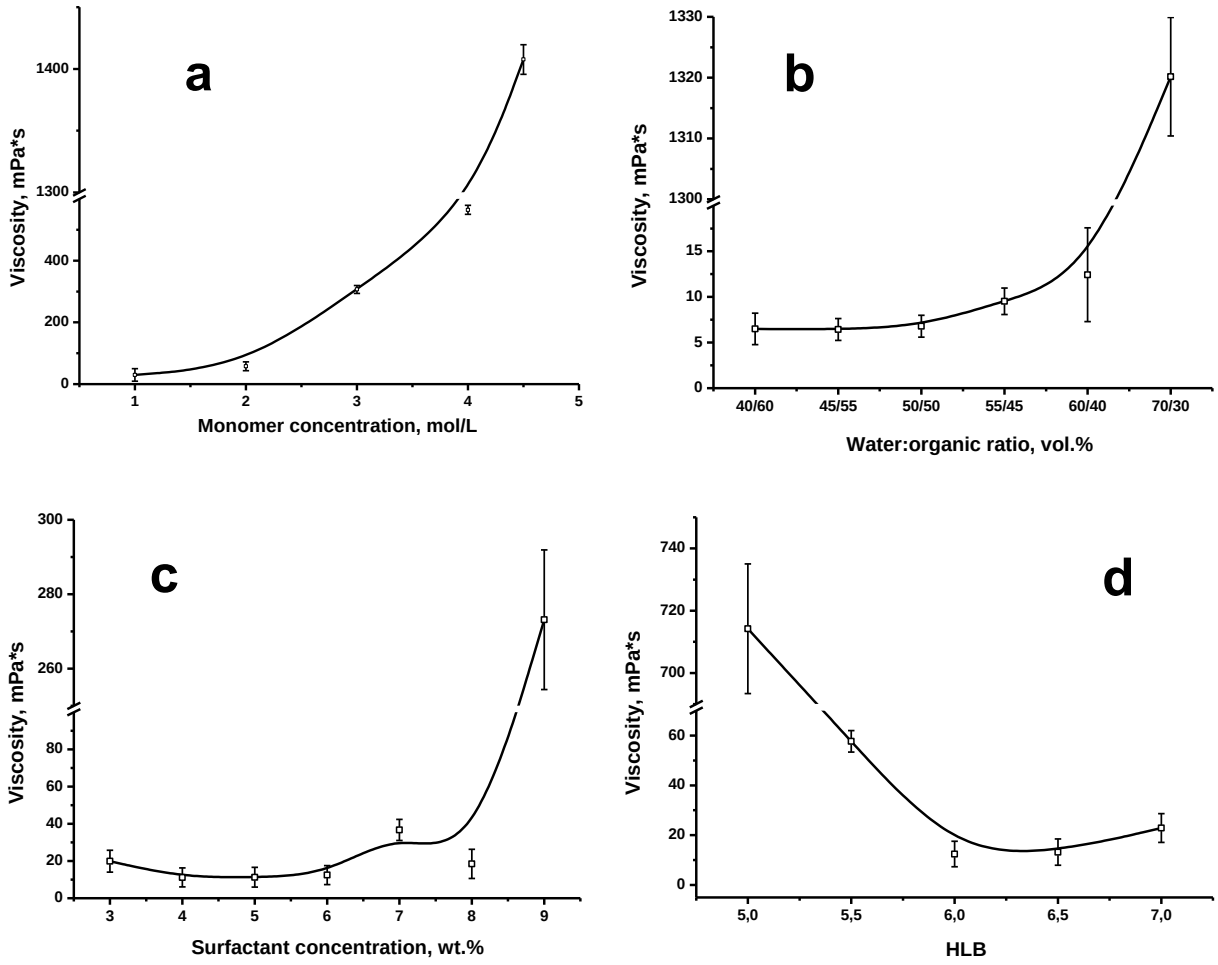

Figure 64 - Influence of monomer concentration (a), ratio of water/organic phase (b), surfactant concentration (c) and HLB (d) on the dynamic viscosity of AAm_{80}-$APTAC_{10}$-$AMPS_{10}$ microgels

3.5.1 Studying the thermal stability and salt resistance of polyampholyte microgels based on AAm-APTAC-AMPS and conducting core-flooding experiments to evaluate the applicability of microgels for oil recovery in a model oil reservoir

The results of thermogravimetric and differential thermal analysis of polyampholyte microgels are shown in Figures 65a and 65b. Dried microgel samples show a 5% weight loss associated with the removal of residual moisture in the region of ~100°C. The beginning of thermal decomposition of microgels is observed at 270°C. Complete thermal decomposition of AAm-APTAC-AMPS microgels occurs in the temperature range between 438 and 445°C. The obtained results indicate that microgels based on AAm-APTAC-AMPS have high thermal stability and can be used for injection into oil reservoirs with formation temperatures up to 200°C [129].

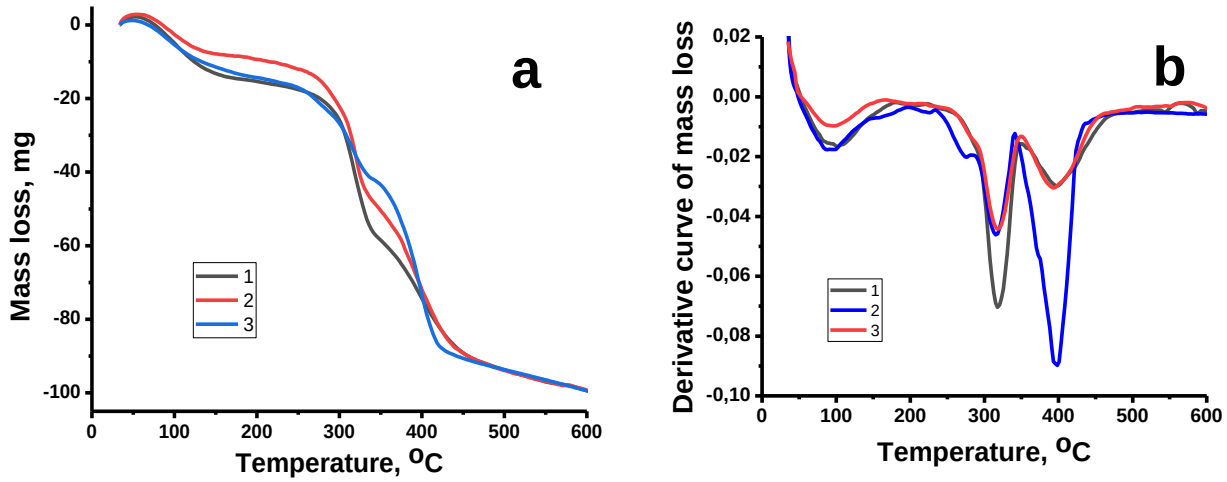

Figure 65 - Integral (a) and differential (b) curves of thermal decomposition of AAm_{70}-$APTAC_{15}$-$AMPS_{15}$ (1), AAm_{80}-$APTAC_{10}$-$AMPS_{10}$ (2) and AAm_{90}-$APTAC_5$-$AMPS_5$ (3) microgels

The swelling capacity of AAm_{80}-$APTAC_{10}$-$AMPS_{10}$ microgels upon salt addition was evaluated. In the range of 0.1-4.0 M NaCl the average hydrodynamic size of microgel particles R_h and dynamic viscosity linearly increases due to "antipolyelectrolyte" effect (Figure 66). In 4.0 M NaCl the R_h of microgel particles and the dynamic viscosity increases 2.5-2.7 times compared to 0.1 M NaCl. The ability of polyampholyte microgels to swell and be effective viscosity enhancers in high-salinity and high-temperature reservoirs may play a crucial role in oil recovery.

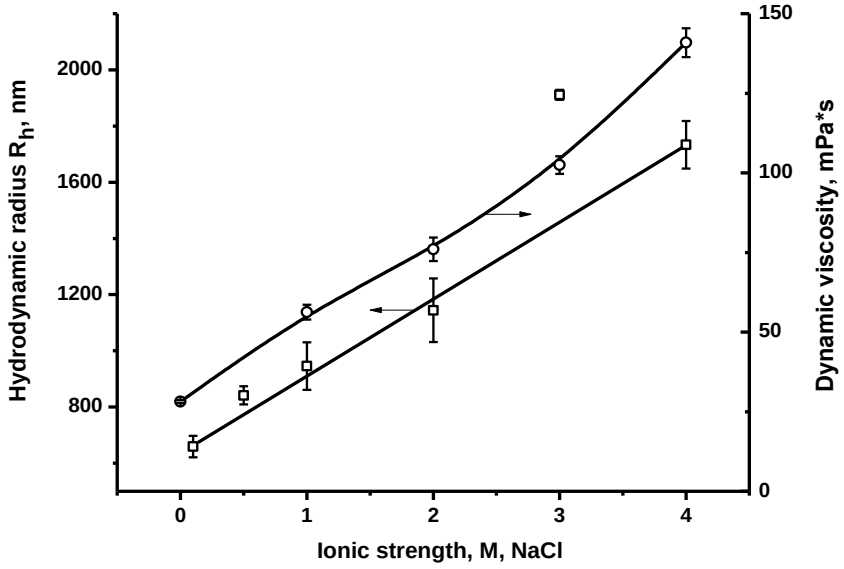

Figure 66 - Dynamic viscosity (1) and average hydrodynamic size (2) of AAm_{80}-$APTAC_{10}$-$AMPS_{10}$ mircogel in saline water

When injecting microgels into oil reservoirs, it is necessary to find out the possibility of penetration of microparticles into the micropores of the rock. If

microgels get stuck in pores, their injection can lead to the rock permeability damage and/or formation hydraulic fracturing.

In our experiments the 2.500 ppm AAm_{80}-$APTAC_{10}$-$AMPS_{10}$ microgel suspension in 136 $g \cdot L^{-1}$ brine was injected into the sandstone core sample equipped with two pressure measurement taps for experiments (Figure 67).

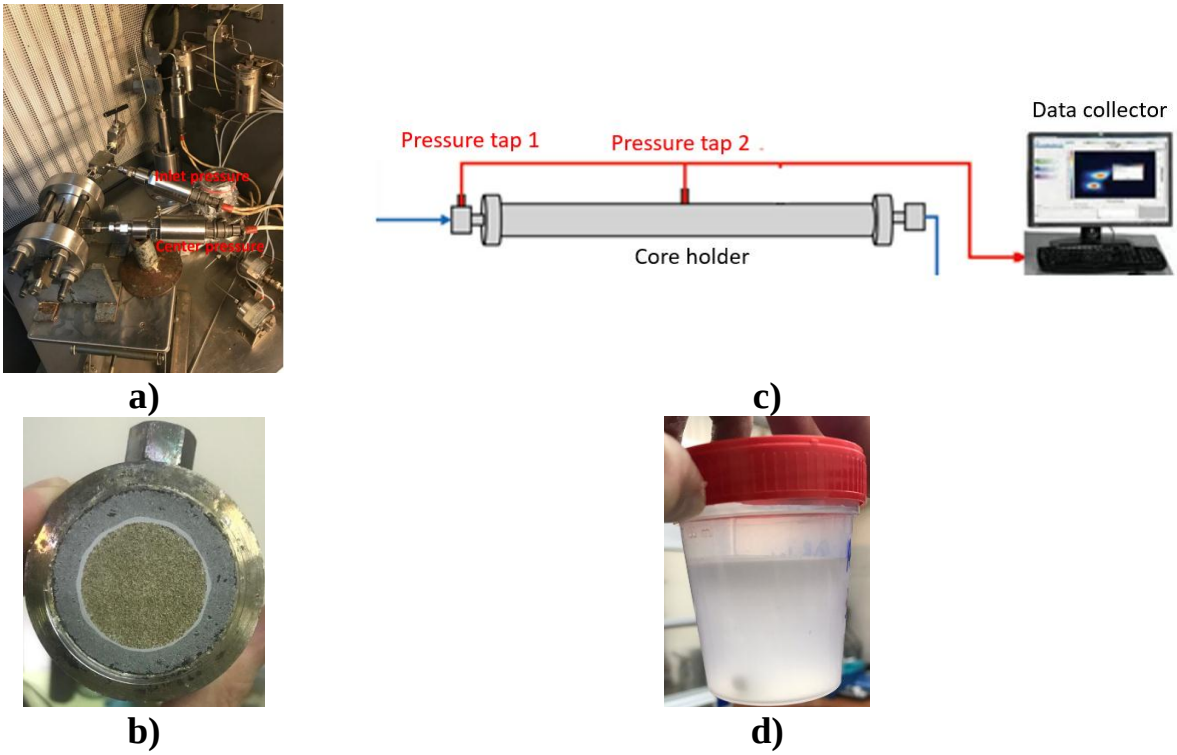

Figure 67 - Core holder (model) equipped with 2 pressure sensors (a); core face (b); layout of core holder connected to a personal computer (c) and microgel particles dissolved in 136 $g \cdot L^{-1}$ brine (d)

Figures 68 (a-c) show pressure readings taken during the injection of brine and microgel suspension into the core. During the injection of water (Figure 68a) the pressure values at the inlet and center of the core stabilized at the level of 0.324 and 0.067 MPa, respectively. The following injection of the microgel suspension did not cause progressive plugging of the core which is evident from stable pressure values shown in Figure 68b. During this stage the pressure values at the inlet and center of the core stabilized at the level of 0.545 and 0.097 MPa, respectively. These values are notably higher than those registered during the water flooding. This is explained by the retention of microgels in the porous media of the core. The following post-flush was also characterized by relatively high pressure values – 0.621 and 0.095 MPa (Figure 68c). Of note is that no sudden falls in pressure were observed during this stage of the experiment, this indicates that the tested microgel is capable of relatively long-lasting permeability reduction in the core.

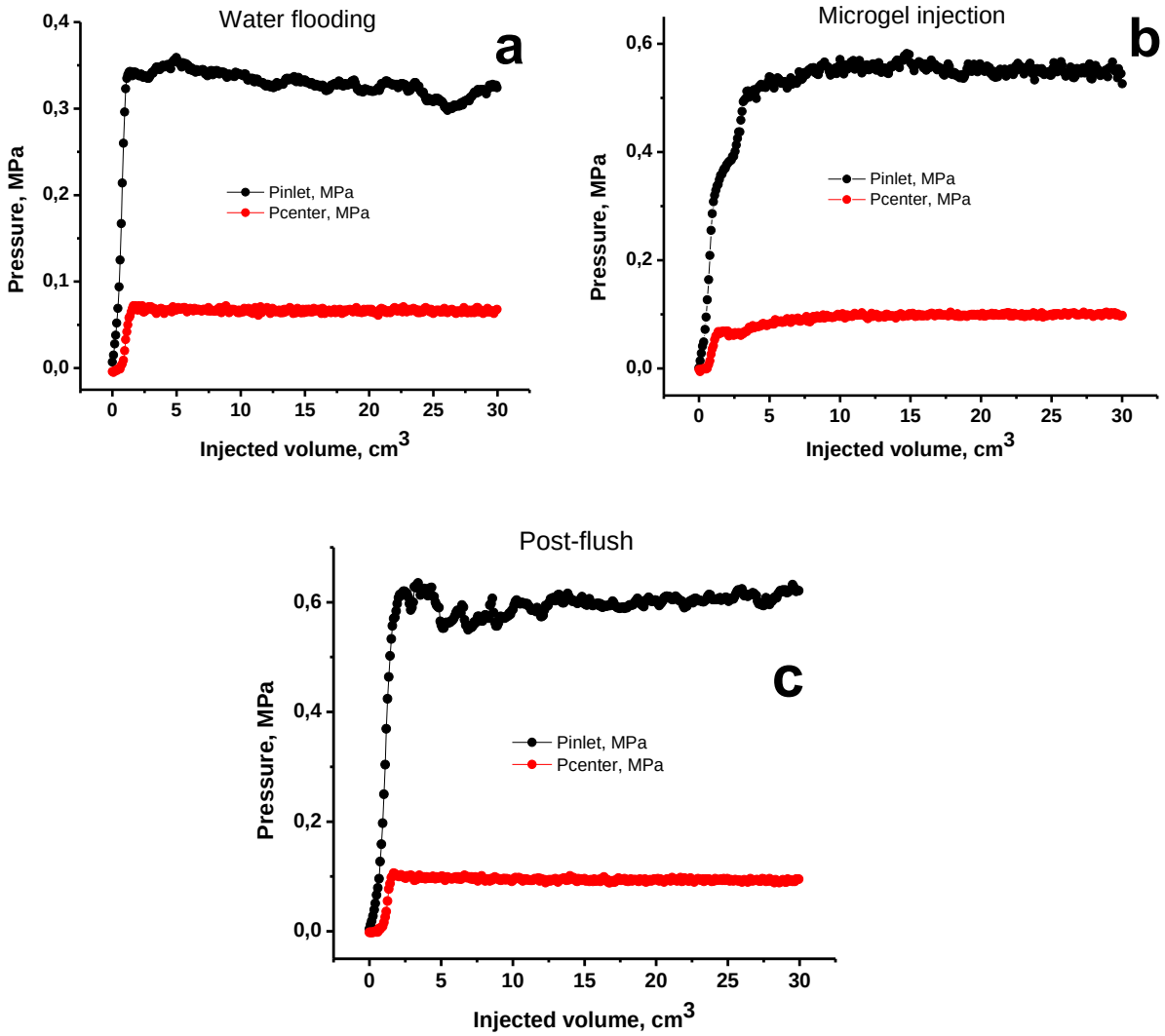

Figure 68 - Pressure readings at the inlet and center of the core during: oil displacement with brine (water flooding) (a); injection of 2,500 ppm microgel (b); post-flush with 136 g·L^{-1} brine (c)

Table 24 shows stabilized pressure readings, which were used to calculate the resistance and residual resistance factors. Of note is that in spite of the fact that the first half of the core was 3.8 times less permeable than the second, which is indicated by 3.8 times higher pressure drop for the first half of the core, the microgel penetrated the porous media without progressive plugging.

Table 24 - Stabilized pressure readings observed during water flooding, microgel injection and post-flush

Water flooding		Microgel injection		Post-flush	
P inlet, MPa	P center, MPa	P inlet, MPa	P center, MPa	P inlet, MPa	P center, MPa
0.324	0.067	0.545	0.097	0.621	0.095

Figure 69 shows the results of resistance and residual resistance factors calculated for different parts of the core. It is remarkable that RRF for the first part of the core was notably higher than RF. This may be explained by the swelling of the microgels during the shut-in period.

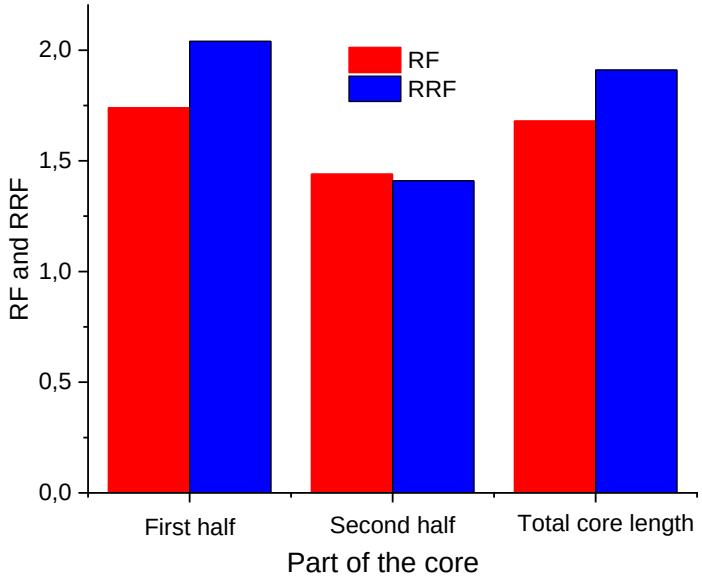

Figure 69 - The values of resistance (RF) and residual resistance (RRF) factors calculated for different parts of core samples

It should be noted that for the 1st half of the core RRF was higher than RF. This may be explained by the swelling of the microgels during 24 h aging period (Step 6). For the second part of the core RF and RRF were almost equal. This result can be explained by stabilization of microgel particles in brine solution and reduction of the permeability [129].

4 Technological part

4.1 Thermo- and salt-responsive polyampholyte microgels based on AAm-APTAC-AMPS for enhanced oil recovery

As mentioned earlier in the previous section, microgels containing hydrophilic groups, including new ones obtained on the basis of AAm-APTAC-AMPS, can be used as thickening agents due to the ability to form non-Newtonian liquids and improve rheological properties. Due to their superior ability to control the injectivity profile, the property of disproportionately reducing the permeability of oil wells and the ease of their preparation, polymer gels are widely used in mature reservoirs [143].

In high-temperature (≥ 90°C) and high-salinity oil reservoirs, the use of polyacrylamide-based thickening agents presents several problems, including chemical and thermal degradation, high degrees of hydrolysis and polymer precipitation, ultimately resulting in a loss of viscosity [144, 145]. Incorporating ionic groups into polymer materials enhances their resistance to salt, imparts greater solution stability and increases their resilience to high temperatures [146].

Numerous polymer gel systems have been developed to address challenges posed by diverse reservoir conditions, including temperature variations, ionic composition and pH levels of formation water, the presence of carbon dioxide or hydrogen sulfide, as well as the adsorption of chemicals onto reservoir rocks [112].

The main methods for obtaining microgels used to enhance oil recovery include the synthesis of bulk gels followed by mechanical grinding, precipitation polymerization, and reverse emulsion polymerization. The most widely adopted method is reverse emulsion polymerization, as it allows for the production of particles in various sizes and offers numerous modifications [105].

The crucial aspect of emulsion polymerization lies in maintaining the polymerization process within a confined space, the size of which is determined by the desired end product. These confined spaces, often referred to as micro or nanoreactors, are typically created using either the oil-in-water (direct) or water-in-oil (reverse) methods. The formation of micelles is a direct outcome of the surfactant's presence at the oil/water interface [61].

Cross-linked polyampholyte microgels, composed of anionic (sodium 2-acrylamido-2-methylpropanesulfonate, AMPS), cationic (3-acrylamidopropyltrimethylammonium chloride, APTAC) and hydrophilic (acrylamide, AAm) monomers, obtained through inverse emulsion polymerization, have shown promise as effective thickening agents in high-temperature and high-salinity tanks. Polyampholyte microgels exhibit conformational and volume-phase transitions in response to varying salt concentrations, solvent properties and interactions with surfactants. The incorporation of a hydrophilic monomer (acrylamide) into highly charged polyampholyte microgels can enhance their thermal stability and resistance to salts, making them suitable for use in oil reservoirs characterized by elevated temperatures and salinity levels.

During the research work, polyampholyte microgels of various compositions were synthesized: [AAm]-[APTAC]-[AMPS] = 90-5-5; 80-10-10; 70-15-15 mol.%. The properties and characteristics of the obtained samples were studied using various physicochemical methods of analysis. Based on the data obtained, a microgel with the composition [AAm]-[APTAC]-[AMPS] = 80-10-10 mol.% was chosen as the optimal object of study for use in experiments on cores and a physical model of the reservoir to assess the oil-displacing (oil-producing) capacity under reservoir conditions.

4.2 Technological scheme for preparing polyampholyte microgels based on AAm-APTAC-AMPS

The production process of polyampholyte microgels based on AAm-APTAC-AMPS by inverse emulsion polymerization is sequential and consists of the following stages: 1) mixing the components of the aqueous phase; 2) mixing the components of the oil phase; 3) homogenization of the aqueous and oil phases to obtain an emulsion; 4) polymerization of the emulsion with the addition of an initiator to obtain the finished microgel.

For emulsion polymerization, stirrers, which can be anchor or frame, play an important role. Industrial emulsion polymerization processes are typically carried out in standard glass-lined, ideal-mix reactors with the reaction mixture heated.

Figure 70 shows a technological scheme for preparing polyampholyte microgels based on AAm-APTAC-AMPS. The technological process begins with the preparation of aqueous and oil phases, the formulation of which is selected taking into account production requirements and scale (Table 25).

Table 25 – Recipe for producing microgel AAm_{80}-$APTAC_{10}$-$AMPS_{10}$ by inverse emulsion polymerization

Component		Quantity, mass%	Functional purpose of components
Technical	Chemical		
Comonomer	AAm	6.62	Main components of water phase
Comonomer	APTAC	3.2	
Comonomer	AMPS	5.34	
Crosslinking agent	MBAA	0.18	
Water	H_2O	44.55	
Surfactant	TWEEN80	1.1	Main components of oil phase
Surfactant	SPAN80	4.89	
Oil	i-C_8	33.95	
Initiator	APS	0.14	Starting the polymerization process
	Total:	100	

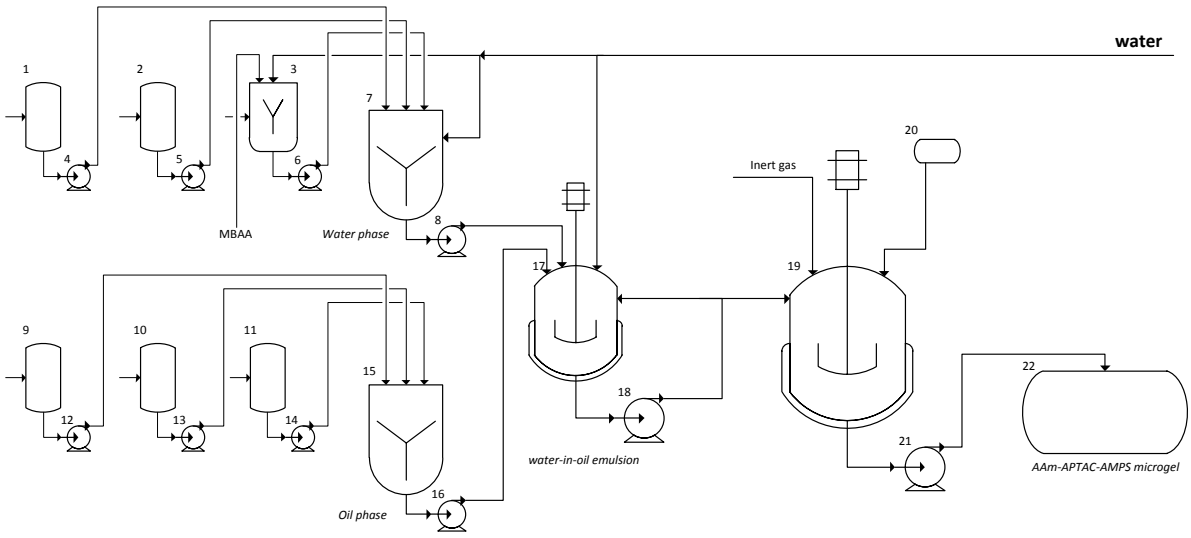

1 – reservoir for APTAC; 2 – reservoir for AMPS; 3 – reservoir with a stirrer for dissolving AAm and MBAA; 9, 10, 11 – reservoirss for isooctane, SPAN80 and TWEEN80, respectively; 7 – apparatus for preparing the aqueous phase; 15 – apparatus for preparing the oil phase; 17 – homogenizer; 19 - polymerization reactor; 20 – container for a mixture of initiators; 22 – container for obtained microgel; 4,5,6,8,12,13,14,16,18,21 – pumps.

Figure 70 - Technological scheme for preparing polyampholyte microgels based on AAm-APTAC-AMPS

APTAC, AMPS, AAm and MBAA are supplied from reservoirs 1, 2 and 3, respectively, to an aqueous phase preparation apparatus 7 equipped with a stirrer. Isooctane, SPAN80 and TWEEN80 are supplied from reservoirs 9, 10 and 11, respectively, to an oil phase preparation apparatus 15 equipped with a stirrer. To prepare a water-in-oil emulsion, the aqueous phase from apparatus 7 and the oil phase from apparatus 15 enter homogenizer 17, where they are mixed at a speed of 10 thousand rpm. Next, the resulting emulsion is sent to the polymerization reactor 19, where a mixture of initiators is supplied from container 20 and the polymerization reaction occurs at 80°C. Finally, the obtained microgel based on AAm-APTAC-AMPS is collected in container 22.

4.3 Mass balance for the inverse emulsion polymerization process to produce microgel based on AAm-APTAC-AMPS

In the production of AAm-APTAC-AMPS microgel via inverse emulsion polymerization, a mass balance is crucial to ensure accurate measurements and efficient resource utilization. This balance helps determine the quantities of each component required and produced during the process (Table 26).

The frequency of the emulsion polymerization process dictates the number of working days per year, as outlined below:

$$D = 365 - (R+W),$$

where D is the number of working days per year; R is the number of days per year allocated for major and other types of repairs; W - the number of holidays and weekends in a year.

Table 26 – Mass balance of the inverse emulsion polymerization process for the production of microgel AAm_{80}-$APTAC_{10}$-$AMPS_{10}$

Component	Income, kg/day	Losses, kg/day	Expenditure, kg/day
AAm	66.2	1.4	64.8
APTAC	32	0.6	31.4
AMPS	53.4	1.2	52.3
MBAA	1.8	0.04	1.76
H_2O	445.5	8.9	436.6
TWEEN80	11	0.2	10.8
SPAN80	48.9	1	47.9
i-C_8	339.5	6.8	332.7
APS	1.4	0.03	1.37
Total:	1000	20.2	979.8

The components consumption coefficients for producing 1000 kg of AAm-APTAC-AMPS microgel are listed in Table 27.

Table 27 - Components consumption coefficients for producing 1000 kg of AAm-APTAC-AMPS microgel

Component	Component consumption	
	Quantity per 1000 kg	Quantity, mass%
AAm	66.2	6.62
APTAC	32	3.2
AMPS	53.4	5.34
MBAA	1.8	0.18
H_2O	445.5	44.55
TWEEN80	11	1.1
SPAN80	48.9	4.89
i-C_8	339.5	33.95
APS	1.4	0.14
Total:	1000	100
Losses:	20.2	2.02
Yield:	979.8	97.98

CONCLUSION

The conducted studies and the obtained scientific results enable to formulate the following conclusions:

1 The samples of polyampholyte nanogels based on NIPAM-APTAC-AMPS of various compositions, specifically 90:5:5; 90:2.5:7.5 and 90:7.5:2.5 mol.%, were obtained via free-radical polymerization method in the presence of a cross-linking agent.

2 The composition of polyampholyte nanogels was determined by FTIR, ^{1}H NMR spectroscopy, and elemental analysis. The surface morphology was studied using SEM. The method of dynamic light scattering and zeta potential was used to determine the average hydrodynamic radius and zeta potential of amphoteric macromolecules. Thermal stability was studied by TGA and DTA methods.

3 The influence of temperature on the volume phase behavior of nanogels depending on the ionic strength of the solution was studied. It was shown that the volume phase transition temperature of the $NIPAM_{90}$-$APTAC_5$-$AMPS_5$ nanogel decreases from 47.8 to 38.3°C in the range of ionic strength of the solution μ = 0.1-1 M NaCl. The volume phase transition temperature of the $NIPAM_{90}$-$APTAC_{2.5}$-$AMPS_{7.5}$ nanogel in the range of ionic strength of the solution μ = 0.01-1 M NaCl decreases from 42 to 33°C. The volume phase transition temperature of the $NIPAM_{90}$-$APTAC_{7.5}$-$AMPS_{2.5}$ nanogel in the range of ionic strength of the solution μ = 0.001-1 M NaCl decreases from 45 to 33.5°C.

4 The linear NIPAM-APTAC-AMPS polyampholytes with an excess of positive (APTAC) or negative (AMPS) monomers form equimolar complex 1:1 with anionic dye – methyl orange (MO) and cationic dye – methylene blue (MB) that served as model drugs. For this reason, further study of the dyes release from the volume of the NIPAM-APTAC-AMPS nanogels was carried out for equimolar nanogel-dye compositions found for linear polyampholytes.

5 The release kinetics of dye molecules from the matrix of nanogels was studied at various ionic strengths of the solution. It has been shown that the diffusion rate of a free dye through a semipermeable membrane is much higher than from a nanogel matrix. This is explained by the formation of complexes between nanogels and dyes, which keeps dye ions in the volume and/or on the surface of nanogels. It is noted that the diffusion of the dyes themselves through the dialysis membrane is a function of the ionic strength of the solution. The release of dyes from the matrix of nanogels was carried out by controlling the ionic strength of the solution.

7 Using inverse emulsion polymerization in the presence of a cross-linking agent, prototypes of polyampholyte microgels based on AAm-APTAC-AMPS of various compositions 90:5:5, 80:10:10 and 70:15:15 mol.% were obtained. The influence of the concentration of monomers and surfactants, HLB and the ratio of water/oil phases on the average hydrodynamic dimensions of microgels was studied.

8 The structure and composition of polyampholyte microgels were established by FTIR spectroscopy and TEM, thermal stability was studied by TGA and DTA.

9 In order to assess the applicability of the synthesized microgels for oil recovery, tests were carried out on cores simulating the conditions of a model oil reservoir.

The results obtained indicate that the suspension of microgels does not clog the micropores of the rock and can be used to extract oil.

Assessment of the completeness of task fulfillment. The goal set in the dissertation work has been achieved and all tasks have been successfully completed: thermo- and salt-responsive polyampholyte nano- and microgels have been synthesized in conjunction with hydrophobic/hydrophilic monomers and studied for potential use in the development of prolonged-action pharmaceuticals and in the field of oil production.

Development of recommendations and initial data for specific utilization of the results. The conducted research, formulated conclusions and recommendations can be applied to integrate them into the production of new thermo- and salt-responsive polymers, which have potential applications as injectable drug carriers tailored to the patient's body temperature with controlled release kinetics. Additionally, they can be used as thickening agents in reservoirs with high temperature and salinity levels.

Assessment of the technical and economic efficiency of implementation. The polyampholyte nano- and microgels obtained via free-radical and emulsion polymerization serve as stimuli-responsive systems with controlled conformational, physico-chemical and physico-mechanical properties. The incorporation of hydrophobic monomer (N-isopropylacrylamide) into highly charged polyampholyte nanogels promotes the self-organization of macromolecular chains through the formation of micellar structures, facilitating the immobilization of poorly water-soluble (lipophilic) pharmaceuticals with subsequent release upon changes in the external environment parameters. Conversely, the inclusion of hydrophilic monomer (acrylamide) into highly charged polyampholyte microgels may enhance the thermal stability of the microgels and their resistance to salts in conditions of an oil reservoir with high temperature and salinity.

Assessment of the scientific level of the conducted research in comparison with the best achievements in the field. In the dissertation work, for the first time, thermo- and salt-responsive highly charged polyampholyte nano- and microgels from anionic, actionic, hydrophilic and hydrophobic monomers have been obtained, which are new objects of research and can be used for the controlled release of drugs in medicine and as reagents for leveling the injectivity profile of petroleum products in oil production. The obtained results can expand fundamental knowledge about synthetic polyampholytes, in particular, when modeling the behavior of proteins and nucleic acids using their synthetic analogs, enzymatic catalysis, "molecular recognition", self-assembly.

REFERENCES

1 Kudaibergenov S.E. Recent advances in the study of synthetic polyampholytes in solutions // Advances in Polymer Science. - 1999. - P. 115-197. doi.10.1007/3-540-68384-4_3

2 Lowe A.B., McCormick C.L. Synthesis and solution properties of zwitterionic polymers // Chemical Reviews. - 2002. - Vol.102, №11. - P. 4177-4189. doi.10.1021/cr020371t

3 Kudaibergenov S.E. Polyampholytes:Synthesis, Characterization and Application. - New York: Springer, 2002. - 220 p.

4 Laschewsky A. Structures and Synthesis of Zwitterionic Polymers // Polymers. - 2014. - Vol.**6**, №5. - P. 1544-1601. doi.10.25932/publishup-47616

5 He X.Y., Zhou W.R., Xu X.J., Yang W. Preparation and Application of Zwitterionic Polymers // Progress in Chemistry. - 2013. - Vol.**25**, №6. - P. 1023-1030.

6 Bernards M., He Y. Polyampholyte polymers as a versatile zwitterionic biomaterial platform // Journal of Biomaterials Science-Polymer Edition. - 2014. - Vol.25, №14-15. - P. 1479-1488. doi.10.1080/09205063.2014.938976

7 Kudaibergenov S.E., Nuraje N., Khutoryanskiy V.V. Amphoteric nano-, micro-, and macrogels, membranes, and thin films // Soft Matter. - 2012. - Vol.8, №36. - P. 9302-9321. doi.10.1039/c2sm25766a

8 Dai C.L., Xu Z., Wu Y., Zou C., Wu X., Wang T., Guo X., Zhao M. Design and Study of a Novel Thermal-Resistant and Shear-Stable Amphoteric Polyacrylamide in High-Salinity Solution // Polymers. -2017. -Vol.**9**, №7. - 296. doi.10.3390/polym9070296

9 Sun T.L., Luo F., Hong W., Cui K., Huang Y., Zhang, H. J., King D.R., Kurokawa T., Nakajima T., Gong J.P. Bulk Energy Dissipation Mechanism for the Fracture of Tough and Self-Healing Hydrogels // Macromolecules. - 2017. - Vol.**50**, №7. - P. 2923-2931. doi.10.1021/acs.macromol.7b00162

10 Ihsan B.A., Sun T.L., Kurokawa T., Karobi S.N., Nakajima T., Nonoyama T., Roy C.K., Luo F., Gong J.P. Self-Healing Behaviors of Tough Polyampholyte Hydrogels // Macromolecules. - 2016. - Vol.49, №11. - P. 4245-4252. doi.10.1021/acs.macromol.6b00437

11 Sponchioni M., Capasso Palmiero U., Manfredini N., Moscatelli D. RAFT copolymerization of oppositely charged monomers and its use to tailor the composition of nonfouling polyampholytes with an UCST behaviour // Reaction Chemistry & Engineering. - 2019. - Vol.4, №2. - P. 436-446. doi.10.1039/c8re00221e

12 Nakahata R., Yusa S. Preparation of Water-Soluble Polyion Complex (PIC) Micelles Covered with Amphoteric Random Copolymer Shells with Pendant Sulfonate and Quaternary Amino Groups // Polymers. - 2018. - Vol.10, №2. - 205. doi.10.3390/polym10020205

13 Sharker K.K., Ohara Y., Shigeta Y., Ozoe S., Yusa S. Upper Critical Solution Temperature (UCST) Behavior of Polystyrene-Based Polyampholytes in

Aqueous Solution // Polymers. - 2019. - Vol.11, №2. - 265. doi.10.3390/polym11020265

14 Rabiee A., Ershad-Langroudi A., Jamshidi H. Polyacrylamide-based polyampholytes and their applications // Reviews in Chemical Engineering. - 2014. - Vol.30, №5. - P. 501-519. doi.10.1515/revce-2014-0004

15 Mumick P.S., Welch P.M., Salazar L.C., McCormick C.L. *Water-soluble copolymers. 56. Structure and solvation effects of polyampholytes in drag reduction* // Macromolecules. - 1994. - Vol.27, №2. - P. 323-331. doi.10.1021/ma00080a003

16 Sun T.L., Kurokawa T., Kuroda S., Ihsan A. B., Akasaki T., Sato K., Anamul Haque Md., Nakajima T., Gong J.P. Physical hydrogels composed of polyampholytes demonstrate high toughness and viscoelasticity // Nature Materials. - 2013. - Vol.12, №10. - P. 932-937. doi.10.1038/nmat3713

17 Charaya H., Li X., Jen N., Chung H.-J. Specific Ion Effects in Polyampholyte Hydrogels Dialyzed in Aqueous Electrolytic Solutions // Langmuir. - 2019. - Vol.35, №5. - P. 1526-1533. doi.10.1021/acs.langmuir.8b02281

18 Zhang Y.C., Liao J., Wang T., Sun W., Tong Z. Polyampholyte Hydrogels with pH Modulated Shape Memory and Spontaneous Actuation // Advanced Functional Materials. - 2018. - Vol.28, №18. - 1707245. doi.10.1002/adfm.201707245

19 Tae G.P., Hoffman A.S. Preparation of large, uniform size temperature-sensitive hydrogel beads // Journal of Polymer Science Part a-Polymer Chemistry. - 1992. - Vol.30, №3. - P. 505-507. doi.10.1002/pola.1992.080300318

20 McNaught A.D., Wilkinson A. Compendium of chemical terminology:IUPAC recommendations. - Oxford: Blackwell Science, 1997. - 450 p.

21 Aleman J., Chadwick A.V., He J., Hess M., Horie K., Jones R.G., Kratochvil P., Meisel I., Mita I., Moad G., Penczek S., Stepto R.F.T. Definitions of terms relating to the structure and processing of sols, gels, networks, and inorganic-organic hybrid materials (IUPAC Recommendations 2007) // Pure and Applied Chemistry. - 2007. - Vol.79, №10. - P. 1801-1829. doi.10.1351/pac200779101801

22 Plamper F.A., Richtering W. Functional Microgels and Microgel Systems // Accounts of Chemical Research. - 2017. - Vol.50, №2. - P. 131-140. doi.10.1021/acs.accounts.6b00544

23 Pelton R. Temperature-sensitive aqueous microgels // Advances in Colloid and Interface Science. - 2000. - Vol.85, №1. - P. 1-33. doi. 10.1016/s0001-8686(99)00023-8

24 Keidel R., Ghavami A., Lugo D.M., Lotze G., Virtanen O., Beumers P., Pedersen J.S., Bardow A., Winkler R.G., Richtering W. Time-resolved structural evolution during the collapse of responsive hydrogels: The microgel-to-particle transition // Science Advances. - 2018. - Vol.4, №4. doi.10.1126/sciadv.aao7086

25 Brijitta J., Tata B.V.R., Joshi R.G., Kaliyappan T. Random hcp and fcc structures in thermoresponsive microgel crystals // Journal of Chemical Physics. - 2009. - Vol.131, №7. - 074904. doi.10.1063/1.3210765

26 Rauh A., Carl N., Schweins R., Karg M. Role of Absorbing Nanocrystal Cores in Soft Photonic Crystals: A Spectroscopy and SANS Study // Langmuir. - 2018. - Vol.34, №3. - P. 854-867. doi.10.1021/acs.langmuir.7b01595

27 Destribats M., Lapeyre V., Wolfs M., Sellier E., Leal-Calderon F., Ravaine V., Schmitt V. Soft microgels as Pickering emulsion stabilisers: role of particle deformability // Soft Matter. - 2011. - Vol.**7**, №17. - P. 7689-7698. doi.10.1039/c1sm05240c

28 Scotti A., Bochenek S., Brugnoni M., Fernandez-Rodriguez M.A., Schulte M.F., Houston J.E., Gelissen A.P.H., Potemkin I.I., Isa L., Richtering W. Exploring the colloid-to-polymer transition for ultra-low crosslinked microgels from three to two dimensions // Nature Communications. - 2019. - Vol.10, №1. - 1418. doi.10.1038/s41467-019-09227-5

29 Ogawa Y., Ogawa K., Kokufuta E. Swelling-shrinking behavior of a polyampholyte gel composed of positively charged networks with immobilized polyanions // Langmuir. - 2004. - Vol.20, №7. - P. 2546-2552. doi.10.1021/la0347408

30 Fernandez-Nieves A., Marquez M. Electrophoresis of ionic microgel particles: From charged hard spheres to polyelectrolyte-like behavior // Journal of Chemical Physics. - 2005. - Vol.122, №8. - 084702. doi.10.1063/1.1844392

31 Dai S., Ravi P., Tam K.C. pH-Responsive polymers: synthesis, properties and applications // Soft Matter. - 2008. - Vol.4, №3. - P. 435-449. doi.10.1039/b714741d

32 Sahiner N., Ozay O., Aktas N., Blake D.A., John V.T. Arsenic (V) removal with modifiable bulk and nano p(4-vinylpyridine)-based hydrogels: The effect of hydrogel sizes and quarternization agents // Desalination. - 2011. - Vol.279, №1-3. - P. 344-352. doi.10.1016/j.desal.2011.06.028

33 Jiang M., Jiang M., Li M., Xiang M., Zhou H.Interpolymer complexation and miscibility enhancement by hydrogen bonding // Advances in Polymer Science. - 1999. - Vol.146. - P. 121-196. doi. 10.1007/3-540-49424-3_3

34 Coats J.P., Cochereau R., Dinu I.A., Messmer D., Sciortino F., Palivan C.G. Trends in the Synthesis of Polymer Nano- and Microscale Materials for Bio-Related Applications // Macromolecular Bioscience. - 2023. - Vol.23, №8. doi. 10.1002/mabi.202200474

35 Huang J., Wu X.Y. Effects of pH, salt, surfactant and composition on phase transition of poly(NIPAm/MAA) nanoparticles // Journal of Polymer Science Part a-Polymer Chemistry. - 1999. - Vol.37, №14. - P. 2667-2676.

36 Richtering W., Pich A. The special behaviours of responsive core-shell nanogels // Soft Matter. - 2012. - Vol.8, №45. - P. 11423-11430. doi.10.1039/c2sm26424b

37 Ni H., Kawaguchi H., Endo T. Preparation of amphoteric microgels of poly(acrylamide/methacrylic acid/dimethylamino ethylene methacrylate) with a novel pH-volume transition // Macromolecules. - 2007. - Vol.40, №17. - P. 6370-6376. doi.10.1021/ma070358g

38 Thies S., Simon P., Zelenina I., Mertens L., Pich A. In Situ Growth and Size Regulation of Single Gold Nanoparticles in Composite Microgels // Small. - 2018. - Vol.14, №51. - 1803589. doi.10.1002/smll.201803589

39 Suzuki D., Horigome K., Kureha T., Matsui S., Watanabe T. Polymeric hydrogel microspheres: design, synthesis, characterization, assembly and applications // Polymer Journal. - 2017. - Vol.49, №10. - P. 695-702. doi.10.1038/pj.2017.39

40 Sanson N., Rieger J. Synthesis of nanogels/microgels by conventional and controlled radical crosslinking copolymerization // Polymer Chemistry. - 2010. - Vol.1, №7. - P. 965-977. doi.10.1039/c0py00010h

41 Aseyev V., Tenhu H., Winnik F.M. Non-ionic Thermoresponsive Polymers in Water // Advanced Polymer Science. - 2011. - Vol.242. - P. 29-89. doi.10.1007/12_2010_57

42 Ito D., Kubota K. Solution properties and thermal behavior of Poly(N-n-propylacrylamide) in water // Macromolecules. - 1997. - Vol.30, №25. - P. 7828-7834. doi.10.1021/ma971005s

43 Lanzalaco S., Armelin E. Poly(N-isopropylacrylamide) and Copolymers: A Review on Recent Progresses in Biomedical Applications. Gels. - 2017. - Vol.3, №4. - 36. doi.10.3390/gels3040036

44 Taylor M.J., Tomlins P., Sahota T.S. Thermoresponsive Gels // Gels. - 2017. - Vol.3, №1. - 4. doi.10.3390/gels3010004

45 Boutris C., Chatzi E.G., Kiparissides C. Characterization of the LCST behaviour of aqueous poly(N-isopropylacrylamide) solutions by thermal and cloud point techniques // Polymer. - 1997. - Vol.38, №10. - P. 2567-2570. doi.10.1016/s0032-3861(97)01024-0

46 Lin S.Y., Chen K.S., Run-Chu L. Drying methods affecting the particle sizes, phase transition, deswelling/reswelling processes and morphology of poly(N-isopropylacrylamide) microgel beads // Polymer. - 1999. - Vol.40, №23. - P. 6307-6312. doi.10.1016/s0032-3861(98)00872-6

47 Liu Y.L., Xing L., Zhang Q., Mu Q., Liu P., Chen K., Zhang X., Wang K., Wei Y. Thermo- and salt-responsive poly(NIPAm-co-AAc-Brij-58) microgels: adjustable size, stability under salt stimulus, and rapid protein adsorption/desorption // Colloid and Polymer Science. - 2016. - Vol.294, №3. - P. 617-628. doi.10.1007/s00396-015-3819-x

48 Truzzolillo D., Sennato S., Sarti S., Casciardi S., Bazzoni C., Bordi F. Overcharging and reentrant condensation of thermoresponsive ionic microgels // Soft Matter. - 2018. - Vol.14, №20. - P. 4110-4125. doi.10.1039/c7sm02357j

49 Saha P., Ganguly R., Li X., Das R., Singha N.K., Pich A. Zwitterionic Nanogels and Microgels: An Overview on Their Synthesis and Applications // Macromolecular Rapid Communications. - 2021. - Vol.42, №13. - 2100112. doi.10.1002/marc.202100112

50 Fernandez-Lopez C., Perez-Balado C., Perez-Juste J., Pastoriza-Santos I., de Lera A.R., Liz-Marzan L.M. A general LbL strategy for the growth of pNIPAM

microgels on Au nanoparticles with arbitrary shapes // Soft Matter. - 2012. - Vol.8, №15. - P. 4165-4170. doi.10.1039/c1sm06396k

51 Ahiabu A., Serpe M.J. Rapidly Responding pH- and Temperature-Responsive Poly (N-Isopropylacrylamide)-Based Microgels and Assemblies // Acs Omega. - 2017. - Vol.2, №5. - P. 1769-1777. doi.10.1021/acsomega.7b00103

52 Ozbas Z., Ozkahraman B., Ozturk A.B. Controlled release profile of 5-fluorouracil loaded P(AAM-co-NVP-co-DEAEMA) microgel prepared via free radical precipitation polymerization // Polymer Bulletin. - 2018. - Vol.75, №7. - P. 3053-3067. doi.10.1007/s00289-017-2202-0

53 Muratalin M., Luckham P.F., Esimova A., Aidarova S., Mutaliyeva B., Madybekova G., Sharipova A., Issayeva A. Study of N-isopropylacrylamide-based microgel particles as a potential drug delivery agents // Colloids and Surfaces a-Physicochemical and Engineering Aspects. - 2017. - Vol.532. - P. 8-17. doi.10.1016/j.colsurfa.2017.07.075

54 Karg M., Pich, A., Hellweg, T., Hoare, T., Lyon, L. A., Crassous, J. J., Suzuki D., Gumerov R.A., Schneider S., Potemkin I.I., Richtering W. Nanogels and Microgels: From Model Colloids to Applications, Recent Developments, and Future Trends // Langmuir. - 2019. - Vol.35, №19. - P. 6231-6255. doi.10.1021/acs.langmuir.8b04304

55 Wei Y.-Y., Liu Z., Luo F., Zhang L., Wang W., Ju X.-J., Xie R., Chu L.-Y. A Novel Poly(N-Isopropylacrylamide-co-acryloylamidobenzo-12-crown-4) Microgel with Rapid Stimuli-Responsiveness for Molecule-Specific Adsorption of γ-Cyclodextrin // Macromolecular Chemistry and Physics. - 2017. - Vol.218, №20. - 1700216. doi.10.1002/macp.201700216

56 Parkatzidis K., Wang H.S., Truong N.P., Anastasaki A. Recent Developments and Future Challenges in Controlled Radical Polymerization: A 2020 Update // Chem. - 2020. - Vol.6, №7. - P. 1575-1588. doi.10.1016/j.chempr.2020.06.014

57 Etchenausia L., Deniau E., Brulet A., Forcada J., Save M. Cationic Thermoresponsive Poly(N-vinylcaprolactam) Microgels Synthesized by Emulsion Polymerization Using a Reactive Cationic Macro-RAFT Agent // Macromolecules. - 2018. - Vol.51, №7. - P. 2551-2563. doi.10.1021/acs.macromol.8b00155

58 Pioge S., Tran T.N., McKenzie T.G., Pascual S., Ashokkumar M., Fontaine L., Qiao G. Sono-RAFT Polymerization-Induced Self-Assembly in Aqueous Dispersion: Synthesis of LCST-type Thermosensitive Nanogels // Macromolecule. - 2018. - Vol.51, №21. - P. 8862-8869. doi.10.1021/acs.macromol.8b01606

59 Cors M., Wrede O., Genix A.-C., Anselmetti D., Oberdisse J., Hellweg T. Core-Shell Microgel-Based Surface Coatings with Linear Thermoresponse // Langmuir. - 2017. - Vol.33, №27. - P. 6804-6811. doi.10.1021/acs.langmuir.7b01199

60 Brugnoni M., Scotti A., Rudov A.A., Gelissen A.P.H., Caumanns T., Radulescu A., Eckert T., Pich A., Potemkin I.I., Richtering W. Swelling of a Responsive Network within Different Constraints in Multi-Thermosensitive

Microgels // Macromolecules. - 2018. - Vol.51, №7. - P. 2662-2671. doi.10.1021/acs.macromol.7b02722

61 Sjoblom J., Lindberg R., Friberg S.E. Microemulsions - Phase equilibria characterization, structures, applications and chemical reactions // Advances in Colloid and Interface Science. - 1996. - Vol.65. - P. 125-287. doi.10.1016/0001-8686(96)00293-x

62 Gupta A., Eral H.B., Hatton T.A., Doyle P.S. Nanoemulsions: formation, properties and applications // Soft Matter. - 2016. - Vol.12, №11. - P. 2826-2841. doi.10.1039/c5sm02958a

63 Wik J., Bansal K.K., Assmuth T., Rosling A., Rosenholm J.M. Facile methodology of nanoemulsion preparation using oily polymer for the delivery of poorly soluble drugs // Drug Delivery and Translational Research. - 2020. - Vol.10, №5. - P. 1228-1240. doi.10.1007/s13346-019-00703-5

64 Ulanski P., Rosiak J.M. Encyclopedia of Nanoscience and Nanotechnology. Polymeric nano/microgels. - Stevenson Ranch, CA, USA:American Scientific Publishers, 2004. - P. 845–871.

65 Antonietti M., Landfester K. Polyreactions in miniemulsions // Progress in Polymer Science. - 2002. - Vol.27, №4. - P. 689-757. doi.10.1016/S0079-6700(01)00051-X

66 Dyab A.K.F., Atta A.M. Microgel-stabilised non-aqueous emulsions // Rsc Advances. - 2013. - Vol.3, №48. - P. 25662-25665. doi.10.1039/C3RA45263H

67 Urakami H., Hentschel J., Seetho K., Zeng H., Chawla K., Guan Z. Surfactant-Free Synthesis of Biodegradable, Biocompatible, and Stimuli-Responsive Cationic Nanogel Particles // Biomacromolecules. - 2013. - Vol.14, №10. - P. 3682-3688. doi.10.1021/bm401039r

68 Sobhanimatin M.B., Pourmahdian S. Study on the inverse emulsion copolymerization of microgels based on acrylamide/2-acrylamido-2-methylpropane sulfonic acid // Iranian Polymer Journal. - 2016. - Vol.25, №5. - P. 405-413. doi.10.1007/s13726-016-0432-x

69 Ramli R.A., Hashim S., Laftah W.A. Synthesis, characterization, and morphology study of poly(acrylamide-co-acrylic acid)-grafted-poly(styrene-co-methyl methacrylate) "raspberry"-shape like structure microgels by pre-emulsified semi-batch emulsion polymerization // Journal of Colloid and Interface Science. - 2013. - Vol.391. - P. 86-94. doi.10.1016/j.jcis.2012.09.047

70 Shen Y.H., Zhang X., Lu J., Zhang A., Chen K., Li X. Effect of chemical composition on properties of pH-responsive poly(acrylamide-co-acrylic acid) microgels prepared by inverse microemulsion polymerization // Colloids and Surfaces a-Physicochemical and Engineering Aspects. - 2009. - Vol.350, №1-3. - P. 87-90. doi.10.1016/j.colsurfa.2009.09.009

71 Echeverria C., Lopez D., Mijangos C. UCST Responsive Microgels of Poly(acrylamide-acrylic acid) Copolymers: Structure and Viscoelastic Properties // Macromolecules. - 2009. - Vol.42, №22. - P. 9118-9123. doi.10.1021/ma901316k

72 Echeverria C., Peppas N.A., Mijangos C. Novel strategy for the determination of UCST-like microgels network structure: effect on swelling

behavior and rheology // Soft Matter. - 2012. - Vol.8, №2. - P. 337-346. doi.10.1039/c1sm06489d

73 Hajighasem A., Kabiri K. Novel crosslinking method for preparation of acrylic thickener microgels through inverse emulsion polymerization // Iranian Polymer Journal. - 2015. - Vol.24, №12. - P. 1049-1056. doi.10.1007/s13726-015-0392-6

74 Landfester K., Pawelzik U., Antonietti M. Polydimethylsiloxane latexes and copolymers by polymerization and polyaddition in miniemulsion // Polymer. - 2005. - Vol.46, №23. - P. 9892-9898. doi.10.1016/j.polymer.2005.07.080

75 Deen G.R., Alsted T., Richtering W., Pedersen J.S. Synthesis and characterization of nanogels of poly(N-isopropylacrylamide) by a combination of light and small-angle X-ray scattering // Physical Chemistry Chemical Physics. - 2011. - Vol.13, №8. - P. 3108-3114. doi.10.1039/c0cp01359e

76 Braun O., Selb J., Candau F. Synthesis in microemulsion and characterization of stimuli-responsive polyelectrolytes and polyampholytes based on N-isopropylacrylamide // Polymer. - 2001. - Vol.42, №21. - P. 8499-8510. doi.10.1016/s0032-3861(01)00445-1

77 Tan B.H., Ravi P., Tam K.C. Synthesis and characterization of novel pH-responsive polyampholyte microgels // Macromolecular Rapid Communications. - 2006. - Vol.27, №7. - P. 522-528. doi.10.1002/marc.200500830

78 Chen H.B., Kelley M., Guo C., Yarger J.L., Dai L.L. Adsorption and release of surfactant into and from multifunctional zwitterionic poly(NIPAm-co-DMAPMA-co-AAc) microgel particles // Journal of Colloid and Interface Science. - 2015. - Vol.449. - P. 332-340. doi.10.1016/j.jcis.2015.01.064

79 Richtering W., Potemkin I.I., Rudov A.A., Sellge G., Trautwein C. Could multiresponsive hollow shell-shell nanocontainers offer an improved strategy for drug delivery? // Nanomedicine. - 2016. - Vol.11, №22. - P. 2879-2883. doi. 10.2217/nnm-2016-0327

80 Van Gheluwe L., Chourpa I., Gaigne C., Munnier E. Polymer-Based Smart Drug Delivery Systems for Skin Application and Demonstration of Stimuli-Responsiveness // Polymers. - 2021. - Vol.13, №8. - 1285. doi.10.3390/polym13081285

81 Goncalves C., Pereira P., Gama M. Self-Assembled Hydrogel Nanoparticles for Drug Delivery Applications // Materials. - 2010. - Vol.3, №2. - P. 1420-1460. doi.10.3390/ma3021420

82 Kendre P.N., Satav T.S. Current trends and concepts in the design and development of nanogel carrier systems // Polymer Bulletin. - 2019. - Vol.76, №3. - P. 1595-1617. doi.10.1007/s00289-018-2430-y

83 Farhana Sultana, Manirujjaman, Imran-Ul-Haque Md., Arafat M., Sharmin S. An Overview of Nanogel Drug Delivery System // Journal of Applied Pharmaceutical Science. - 2013. - Vol.3. - P. S95-S105. doi. 10.7324/JAPS.2013.38.S15

84 Dromi S., Frenkel V., Luk A., Traughber B., Angstadt M., Bur M., Poff J., Xie J., Libutti S.K., Li K.C.P., Wood B.J. Pulsed-high intensity focused ultrasound

and low temperature sensitive liposomes for enhanced targeted drug delivery and antitumor effect // Clinical Cancer Research. - 2007. - Vol.13, №9. - P. 2722-2727. doi.10.1158/1078-0432.ccr-06-2443

85 Jhaveri A., Deshpande P., Torchilin V. Stimuli-sensitive nanopreparations for combination cancer therapy // Journal of Controlled Release. - 2014. - Vol.190. - P. 352-370. doi.10.1016/j.jconrel.2014.05.002

86 Matsumoto K., Kimura S., Itai S., Kondo H., Iwao Y. In vivo temperature-sensitive drug release system trigged by cooling using low-melting-point microcrystalline wax // Journal of Controlled Release. - 2019. - Vol.303. - P. 281-288. doi.10.1016/j.jconrel.2019.04.029

87 Roy D., Brooks W.L.A., Sumerlin B.S. New directions in thermoresponsive polymers // Chemical Society Reviews. - 2013. - Vol.42, №17. - P. 7214-7243. doi.10.1039/C3CS35499G

88 McMasters J., Poh S., Lin J.B., Panitch A. Delivery of anti-inflammatory peptides from hollow PEGylated poly (NIPAM) nanoparticles reduces inflammation in an ex vivo osteoarthritis model // Journal of Controlled Release. - 2017. - Vol.258. - P. 161-170. doi.10.1016/j.jconrel.2017.05.008

89 Shiotani A., Mori T., Niidome T., Niidome Y., Katayama Y. Stable incorporation of gold nanorods into N-isopropylacrylamide hydrogels and their rapid shrinkage induced by near-infrared laser irradiation // Langmuir. - 2007. - Vol.23, №7. - P. 4012-4018. doi.10.1021/la0627967

90 Gerecke, C., Edlich, A., Giulbudagian, M., Schumacher, F., Zhang, N., Said, A., Yealland G., Lohan S.B., Neumann F., Meinke M.C., Ma N., Calderon M., Hedtrich S., Schafer-Korting M., Kleuser B. Biocompatibility and characterization of polyglycerol-based thermoresponsive nanogels designed as novel drug-delivery systems and their intracellular localization in keratinocytes // Nanotoxicology. - 2017. - Vol.11, №2. - P. 267-277. doi.10.1080/17435390.2017.1292371

91 Michalek J., Pradny M., Dusek K., Duskova-Smrckova M. Hydrogels in biology and medicine // Advances in Medicine and Biology. - 2010. - Vol.2, №2. - P. 1-55.

92 Li Z.Q., Guo X., Matsushita S., Guan J. Differentiation of cardiosphere-derived cells into a mature cardiac lineage using biodegradable poly(N-isopropylacrylamide) hydrogels // Biomaterials. - 2011. - Vol.32, №12. - P. 3220-3232. doi.10.1016/j.biomaterials.2011.050

93 Qian Q.Q., Niu S., Williams G.R., Wu J., Zhang X., Zhu L.-M. Peptide functionalized dual-responsive chitosan nanoparticles for controlled drug delivery to breast cancer cells // Colloids and Surfaces a-Physicochemical and Engineering Aspects. - 2019. - Vol.564. - P. 122-130. doi.10.1016/j.colsurfa.2018.12.026

94 Dadfar S.M.R., Pourmahdian S., Tehranchi M.M., Dadfar S.M. Novel dual-responsive semi-interpenetrating polymer network hydrogels for controlled release of anticancer drugs // Journal of Biomedical Materials Research Part A. - 2019. - Vol.107, №10. - P. 2327-2339. doi. 10.1002/jbm.a.36741

95 Abu Samah N.H., Heard C.M. Enhanced in vitro transdermal delivery of caffeine using a temperature- and pH-sensitive nanogel, poly(NIPAM-co-AAc) //

International Journal of Pharmaceutics. - 2013. - Vol.453, №2. - P. 630-640. doi.10.1016/j.ijpharm.2013.05.042

96 Sharma A., Raghunathan K., Solhaug H., Antony J., Stenvik J., Nilsen A.M., Einarsrud M.-A., Bandyopadhyay S. Modulating acrylic acid content of nanogels for drug delivery & biocompatibility studies // Journal of Colloid and Interface Science. - 2022. - Vol.607. - P. 76-88. doi.10.1016/j.jcis.2021.07.139

97 Garbern J.C., Hoffman A.S., Stayton P.S. Injectable pH- and Temperature-Responsive Poly(N-isopropylacrylamide-co-propylacrylic acid) Copolymers for Delivery of Angiogenic Growth Factors // Biomacromolecules. - 2010. - Vol.11, №7. - P. 1833-1839. doi.10.1021/bm100318z

98 Cheng R., Meng F., Deng C., Klok H.-A., Zhong Z. Dual and multi-stimuli responsive polymeric nanoparticles for programmed site-specific drug delivery // Biomaterials. - 2013. - Vol.34, №14. - P. 3647-3657. doi.10.1016/j.biomaterials.2013.084

99 Argentiere S., Blasi L., Morello G., Gigli G. A Novel pH-Responsive Nanogel for the Controlled Uptake and Release of Hydrophobic and Cationic Solutes // Journal of Physical Chemistry C. - 2011. - Vol.115, №33. - P. 16347-16353. doi.10.1021/jp204954a

100 Li W., Guo Q., Zhao H., Zhang L., Li J., Gao J., Qian W., Li B., Chen H., Wang H., Dai J., Guo Y. Novel dual-control poly(N-isopropylacrylamide-co-chlorophyllin) nanogels for improving drug release // Nanomedicine. - 2012. - Vol.7, №3. - P. 383-392. doi.10.2217/nnm.11.100

101 Yang Y., Peng W., Zhang H., Wang H., He X. The oil/water interfacial behavior of microgels used for enhancing oil recovery: A comparative study on microgel powder and microgel emulsion // Colloids and Surfaces a-Physicochemical and Engineering Aspects. - 2022. - Vol. 632. - 127731. doi.10.1016/j.colsurfa.2021.127731

102 Yao C.J., Lei G., Li L., Gao X. Selectivity of Pore-Scale Elastic Microspheres as a Novel Profile Control and Oil Displacement Agent // Energy & Fuels. - 2012. - Vol.26, №8. - P. 5092-5101. doi.10.1021/ef300689c

103 Rozhkova Y.A., Burin D.A., Galkin S.V., Yang H. Review of Microgels for Enhanced Oil Recovery: Properties and Cases of Application. Gels. - 2022. - Vol.8, №2. - 112. doi.10.3390/gels8020112

104 Es-Haghi H., Bouhendi H., Bagheri Marandi G., Zohurian-Mehr M.J., Kabiri K. An investigation into novel multifunctional cross-linkers effect on microgel prepared by precipitation polymerization // Reactive & Functional Polymers. - 2013. - Vol.73, №3. - P. 524-530. doi.10.1016/j.reactfunctpolym.2012.11.006

105 Hamzah Y.B., Hashim S., Rahman W.A. Synthesis of polymeric nano/microgels: a review // Journal of Polymer Research. - 2017. - Vol.24, №9. - 134. doi.10.1007/s10965-017-1281-9

106 Pich A., Richtering W. Microgels by Precipitation Polymerization: Synthesis, Characterization, and Functionalization // Chemical Design of Responsive Microgels. - 2010. - Vol.234. - P. 1-37. doi.10.1007/12_2010_70

107 Tauer K., Hernandez H., Kozempel S., Lazareva O., Nazaran P. Towards a consistent mechanism of emulsion polymerization - new experimental details // Colloid and Polymer Science. - 2008. - Vol.286, №5. - P. 499-515. doi.10.1007/s00396-007-1797-3

108 Kang W.L., Hu L.-L., Zhang X.-F., Yang R.-M., Fan H.-M., Geng, J. Preparation and performance of fluorescent polyacrylamide microspheres as a profile control and tracer agent // Petroleum Science. - 2015. - Vol.12, №3. - P. 483-491. doi.10.1007/s12182-015-0042-9

109 Chen L.W., Yang B.Z., Wu M.L. Synthesis and kinetics of microgel in inverse emulsion polymerization of acrylamide // Progress in Organic Coatings. - 1997. - Vol.31, №4. - P. 393-399. doi. 10.1016/s0300-9440(97)00100-8

110 Yao C., Lei G., Gao X., Li L. Controllable preparation, rheology, and plugging property of micron-grade polyacrylamide microspheres as a novel profile control and flooding agent // Journal of Applied Polymer Science. - 2013. - Vol.130, №2. - P. 1124-1130. doi.10.1002/app.39283

111 Xiong B.Y., Xiong B., Loss R.D., Shields D., Pawlik T., Hochreiter R., Zydney A.L., Kumar M. Polyacrylamide degradation and its implications in environmental systems // Npj Clean Water. - 2018. - Vol.1. - 17. doi.10.1038/s41545-018-0016-8

112 Bai B.J., Zhou J., Yin M.F. A comprehensive review of polyacrylamide polymer gels for conformance control // Petroleum Exploration and Development. - 2015. - Vol.42, №4. - P. 525-532. doi.10.1016/s1876-3804(15)30045-8

113 Wang L., Zhang G., Ge J., Li G., Zhang J., Ding B. Preparation of Microgel Nanospheres and Their Application in EOR. Proceedings of International Oil and Gas Conference and Exhibition in China: Beijing, China, 2010. doi.10.2523/130357-ms

114 Wang B., Lin M., Guo J., Wang D., Xu F., Li M. Plugging properties and profile control effects of crosslinked polyacrylamide microspheres // Journal of Applied Polymer Science. - 2016. - Vol.133, №30. doi.10.1002/app.43666

115 Liu J.C., Almakimi A., Wei M., Bai B., Hussein I.A. A comprehensive review of experimental evaluation methods and results of polymer micro/nanogels for enhanced oil recovery and reduced water production // Fuel. - 2022. - Vol.324. - 124664. doi. 10.1016/j.fuel.2022.124664

116 Yang H., Kang W., Tang X., Gao Y., Zhu Z., Wang P., Zhang X. Gel kinetic characteristics and creep behavior of polymer microspheres based on bulk gel // Journal of Dispersion Science and Technology. - 2018. - Vol.39, №12. - P. 1808-1819. doi. 10.1080/01932691.2018.1462192

117 Yang H., Shao S., Zhu T., Chen C., Liu S., Zhou B., Hou X., Zhang Y., Kang W. Shear resistance performance of low elastic polymer microspheres used for conformance control treatment // Journal of Industrial and Engineering Chemistry. - 2019. - Vol.79. - P. 295-306. doi/10.1016/j.jiec.2019.07.005

118 Yang H., Zhou B., Zhu T., Wang P., Zhang X., Wang T., Wu F., Zhang L., Kang W., Ketova Y.A., Galkine S.V. Conformance control mechanism of low

elastic polymer microspheres in porous medium // Journal of Petroleum Science and Engineering. - 2021. - Vol.196. - 107708. doi.10.1016/j.petrol.2020.107708

119 Mohammadi M.S., Sahraei E., Bayati B. Synthesis optimization and characterization of high molecular weight polymeric nanoparticles as EOR agent for harsh condition reservoirs // Journal of Polymer Research. - 2020. - Vol.27, №2. doi.10.1007/s10965-020-2017-9

120 Durmaz S., Okay O. Acrylamide/2-acrylamido-2-methylpropane sulfonic acid sodium salt-based hydrogels: synthesis and characterization // Polymer. - 2000. - Vol.41, №10. - P. 3693-3704. doi.10.1016/s0032-3861(99)00558-3

121 Yu X., Pu W., Chen D., Zhang J., Zhou F., Zhang R., Gu S. Degradable cross-linked polymeric microsphere for enhanced oil recovery applications // Rsc Advances. - 2015. - Vol.**5**, №77. - P. 62752-62762. doi.10.1039/c5ra05366h

122 Yang H., Hu L., Chen C., Zhao H., Wang P., Zhu T., Wang T., Zhang L., Fan H., Kang W. Influence mechanism of fluorescent monomer on the performance of polymer microspheres // Journal of Molecular Liquids. - 2020. - Vol.308. - 113081. doi.10.1016/j.molliq.2020.113081

123 Yang H., Hu L., Tang X., Gao Y., Shao S., Zhang X., Wang P., Zhu Z., Kang W. Preparation of a fluorescent polymer microsphere and stability evaluation of its profile control system by a fluorescence stability index // Colloids and Surfaces a-Physicochemical and Engineering Aspects. - 2018. - Vol.558. - P. 512-519. doi.10.1016/j.colsurfa.2018.09.019

124 Ashrafizadeh M., Chiu Tam K., Javadi A., Abdollahi M., Sadeghnejad S., Bahramian A. Synthesis and physicochemical properties of dual-responsive acrylic acid/butyl acrylate cross-linked nanogel systems // Journal of Colloid and Interface Science. - 2019. - Vol.556. - P. 313-323. doi.10.1016/j.jcis.2019.08.066

125 Teimouri A., Sadeghnejad S., Dehaghani A.H.S. Investigation of acid pre-flushing and pH-sensitive microgel injection in fractured carbonate rocks for conformance control purposes // Oil & Gas Science and Technology. - 2020. - Vol.75. - 52. doi.10.2516/ogst/2020048

126 Ayazbayeva A.Ye., Shakhvorostov A.V., Seilkhanov T.M., Aseyev V.O., Kudaibergenov S.E. Synthesis and characterization of novel thermo- and salt-sensitive amphoteric terpolymers based on acrylamide derivatives // Bulletin of the University of Karaganda – Chemistry. - 2021. - Vol.104, №4. - P.12-20. doi. 10.31489/2021Ch4/9-20

127 Ayazbayeva A.Ye., Shakhvorostov A.V., Kudaibergenov S.E. Temperature and Salt Responsivity of Anionic, Cationic and Amphoteric Nanogels Based on N-Isopropylacrylamide, 2-Acrylamido-2-Methyl-1-Propanesulfonic Acid Sodium Salt and (3-Acrylamidopropyl) Trimethylammonium Chloride // Bulletin of the University of Karaganda – Chemistry. — 2022. - Vol.108, №4. - P. 14-24. doi.10.31489/2022Ch4/4-22-15

128 Ayazbayeva A.Y., Shakhvorostov A.V., Gussenov I.S., Seilkhanov T.M., Aseyev V.O., Kudaibergenov S.E. Temperature and Salt Responsive Amphoteric Nanogels Based on N-Isopropylacrylamide, 2-Acrylamido-2-methyl-1-

propanesulfonic Acid Sodium Salt and (3-Acrylamidopropyl) Trimethylammonium Chloride // Nanomaterials — 2022. — Vol.12. — 2343. doi.10.3390/nano12142343

129 Ayazbayeva A., Baddam V., Shakhvorostov A., Gussenov I., Asetev V., Yermagambetov M., Kudaibergenov S. Amphoteric nano- and microgels with acrylamide backbone for potential application in oil recovery // Polymers for advanced technologies. - 2023. doi.10.1002/pat.6182

130 Ayazbayeva A.Ye., Nauryzova S.Z., Aseyev V.O., Shakhvorostov A.V. Immobilization of Methyl Orange and Methylene Blue within the Matrix of Charge-Imbalanced Amphoteric Nanogels and Study of Dye Release Kinetics as a Function of Temperature and Ionic Strength // Bulletin of the University of Karaganda-Chemistry. - 2022.- Vol.107, №3. - P. 127-140. doi.10.31489/2022Ch3/3-22-4

131 Seright R.S. How Much Polymer Should Be Injected During a Polymer Flood? Review of Previous and Current Practices // Spe Journal. - 2017. - Vol.22, №1. - P. 1-18. doi.10.2118/179543-pa

132 Aseyev V.O., Tenhu H., Winnik F.M. Temperature dependence of the colloidal stability of neutral amphiphilic polymers in water // Advanced Polymer Science. - 2006. - Vol.196. - P. 1-85. doi.10.1007/12_052

133 Pat.№7008 Kazakhstan. C08F 8/00 B82B 1/00. Polyampholytic nanogel for thermo- and salt-sensitive materials (options) and method for production thereof / S. Kudaibergenov, A.V. Shakhvorostov, A.Ye.Ayazbayeva, G.M. Kudaibergenova; applicant and patentee Institute of Polymer Materials and Technology. 09.11.2021

134 Ru G., Wang N., Huang S., Feng J., ^{1}H HRMAS NMR Study on Phase Transition of Poly(N-isopropylacrylamide) Gels with and without Grafted Comb-Type Chains // Macromolecules. - 2009. - Vol.42, №6. - P. 2074-2078. doi.10.1021/ma802780d

135 Mori H., Endo T. Amino-Acid-Based Block Copolymers by RAFT Polymerization // Macromolecular Rapid Communications. - 2012. - Vol.33, №13. - P. 1090-1107. doi.10.1002/marc.201100887

136 Sun S., Tang H., Wu P., Wan X. Supramolecular self-assembly nature of a novel thermotropic liquid crystalline polymer containing no conventional mesogens // Physical Chemistry Chemical Physics. - 2009. - Vol.11, №42. - P. 9861-9870. doi.10.1039/b909914j

137 Lovett J.R., Derry M.J., Yang P., Hatton F.L., Warren N.J., Fowler P.W., Armes S.P. Can percolation theory explain the gelation behavior of diblock copolymer worms? // Chemical Science. - 2018. - Vol.9, №35. - P. 7138-7144. doi.10.1039/c8sc02406e

138 Ritger P.L., Peppas N.A. A simple equation for description of solute release II. Fickian and anomalous release from swellable devices // Journal of Controlled Release. - 1987. - Vol.5, №1. - P. 37-42. doi.10.1016/0168-3659(87)90035-6

139 Chandrasekaran A.R., Jia C.Y., Theng C.S., Muniandy T., Muralidharan S., Sokkalingam D.A. Invitro studies and evaluation of metformin marketed tablets-

Malaysia // Journal of Applied Pharmaceutical Science. - 2011. - Vol.1, №5. - P. 214-217.

140 Pat.№8346 Kazakhstan. Polyampholite microgel for production of a thickening agent / S. Kudaibergenov, A.V. Shakhvorostov, A.Ye.Ayazbayeva; applicant and patentee Institute of Polymer Materials and Technology. 28.07.2023

141 Nechaev A.I., Voronina N.S., Valtsifer V.A., Strelnikov V.N. Stability of the dispersed system in inverse emulsion polymerization of ionic acrylate monomers // Colloid and Polymer Science. - 2021. - Vol.299, №7. - P. 1127-1138. doi.10.1007/s00396-021-04832-7

142 Fu Z., Liu M., Xu J., Wang Q., Fan Z. Stabilization of water-in-octane nano-emulsion. Part I: Stabilized by mixed surfactant systems // Fuel. - 2010. - Vol.89, №10. - P. 2838-2843. doi. 10.1016/j.fuel.2010.05.031

143 Salehi M.B., Moghadam A.M., Jarrahian K. Effect of Network Parameters of Preformed Particle Gel on Structural Strength for Water Management // Spe Production & Operations. - 2020. - Vol.35, №2. - P. 362-372. doi.10.2118/193631-ms

144 Seright R.S., Lane R.H., Sydansk R.D. A strategy for attacking excess water production // Spe Production & Facilities. - 2003. - Vol.18, №3. - P. 158-169. doi.10.2118/84966-pa

145 Al-Muntasheri G.A., Nasr-Ei-Din H.A., Hussein I.A. A rheological investigation of a high temperature organic gel used for water shut-off treatments // Journal of Petroleum Science and Engineering. - 2007. - Vol.59, №1-2. - P. 73-83. doi.10.1016/j.petrol.2007.02.010

146 Peng B., Peng S., Long B., Miao Y., Guo W.-Y. Properties of High-Temperature-Resistant Drilling Fluids Incorporating Acrylamide/(Acrylic Acid)/(2-Acrylamido-2-Methyl-1-Propane Sulfonic Acid) Terpolymer and Aluminum Citrate as Filtration Control Agents // Journal of Vinyl & Additive Technology. - 2010. - Vol.16, №1. - P. 84-89. doi.10.1002/vnl.20199